OCEANOGRAPHIC BASIS FOR MANAGING THE EFFECTS OF NOXIOUS PHYTOPLANKTON BLOOMS ON CAGE SALMON AQUACULTURE

by

Alejandro Clément

Special Project
submitted to:

Marine Resource Management Program

College of Oceanography

Oregon State University

December 1988

In partial fulfillment
of the requirements for
degree

Master of Science

TO THE ALACALUFES AND HAIDA NATIVE TRIBES

ACKNOWLEDGEMENTS

I would like to thank my adviser Dr. Fred J. Smith for his continuous understanding, support and friendship.

I send my special thanks to Dr. Steve Neshyba who taught me more than oceanography. His thoughtful guidance was a great experience for me. I am sure it will have a constructive influence on my future years as a professional of the sea and as a man. I will always remember him and his family.

I would like to express my gratitude to the faculty of the College of Oceanography, especially, James Good, Jefferson Gonor, Ted Strub, Pat Wheeler, William Quinn, Murray Levine, Fred Prahl, Bob Collier, Mark Abbott, Adriana Huyer and Bob Smith.

I would like to thank Kathryn Howd and friends of the MRM program and College of Oceanography for their patience and understanding during my Corvallis life.

I also acknowledge the team and students who work in the digital image processing lab (College of Oceanography) for their technical help and to Rodrigo Nuñez for its helpful suggestions on computer problems.

I am grateful to my home-institution (Instituto Profesional de Osorno, Chile) that gave this opportunity and financial support as well as Oregon State University and partially the Tinker Foundation.

Finally, I would like to thank my girlfriend Sonia Eller for her support during our stay in this great town, state and country.

CONTENTS

ACRONYMS

ADEOS: Advanced Earth Observing Satellite
AVHRR: Advanced Very High Resolution Radiometer
B.C.: British Columbia
CZCS: Coastal Zone Color Scanner
DOP: Dissolved Organic Pigments
HRV: High-resolution-visible
IHA: Institúto Hidrográfico de la Armada
IR: Infra Red
MCDW: Monthly Climatic Data for the World
MESSR: Multi-spectral Electronic Self-scanning Radiometer
MODIS-n: Moderate-Resolution Imaging Spectrometer
MOS-n: Marine Observation Satellite
MSR: Microwave Scanning Radiometer
MSS: Multispectral Scanner
NASA: National Aeronautics and Space Administration
NOAA: National Oceanic and Atmospheric Administration
OCI: Ocean Color Imager
OCTS: Ocean Color and Temperature Sensor
OSU: Oregon State University
PNIS: Pacific Northwest Inland System
SAIC: Sistema de Aguas Interiores de Chiloé
Sea-WiFS: Sea Wide Field Sensor
SOI: Southern Oscillation Index
SPOT-n: Systeme Probatoire d`Observation de la Terre
SST: Sea Surface Temperature
TIR: Thermal Infra-Red
TM: Thematic Mapper
UBC: University of British Columbia.
VTIR: Visible of Thermal Infrared Radiometer
WCTS: West Coast Time Series

OCEANOGRAPHIC BASIS FOR MANAGING THE EFFECTS OF NOXIOUS PHYTOPLANKTON BLOOMS ON CAGE SALMON AQUACULTURE

1. INTRODUCTION

Marine resources of fjords and estuaries such as living wild stocks and fish, shellfish, and seaweed aquaculture products; tourism, recreation and transportation are important to the economy of coastal regions of the world. At least, it has been the major factor in the local economic growth of Southern Chile.

In Chile, neither general nor specific management plans have been developed by government agencies and no concern about environmental issues has been shown. The private sector in Southern Chile has been achieving a tremendous growth with no government control.

The project presented here emphasizes a specific biological problem affecting the salmon cage culture with the final goal being to propose a realistic management strategy for fjordic estuaries worldwide.

Cage salmon farming is carried out in three mainly temperate regions of the world 1) Northwestern Europe 2) Northwestern North America and 3) Southern Chile. These regions have been seriously affected by noxious phytoplankton blooms, with cumulative economic losses greater than $ 13 million since 1986. In general, a noxious phytoplankton bloom is represented by a high mono-specific biomass within the phytoplankton ecological community causing deleterious effects and kills, usually in

vertebrates due to physical damage, toxins and/or dissolved oxygen depletion.

The Chilean fjord region is one of the largest fjord regions and pristine aquatic systems in the world. It thus has a substantial and great potential for aquaculture development. This region has an eminent economic importance in the development of Southern Chile, generating jobs, and raising partially the income of the local people because they are working for enterprises which export high market value goods. Despite the high degree of exploitation of the marine resources during the last decades and large fisheries and aquaculture investments (more than $ 60 million, belonging significantly to multinationals), the government has been passive, mostly as an observer. Hence, no overall management policy has been addressed, and none is likely in the near future due to the current free enterprise economic policy. Thus, the government applies only certain rules and regulations (Méndez, 1988), and therefore, the private sector should be involved and also responsible for future management plans. Results of upcoming democratic elections might have a control over aquaculture management, but eventually it would occur in the next 3 to 4 years.

The scientific information of the region is very scarce which makes difficult the task of developing adequate management policies. The scarce available oceanographic and meteorological information as recently been summarized by Clément et al (1988). Some of this data will be presented in later sections.

The geomorphological similarities of the fjords systems throughout the world is very interesting (Norway, North America, Chile, Fig. 1). The differences include some specific oceanographic parameters (Freeland et al 1980), but most of the differences are socio-cultural.

From a salmon aquaculture approach, the Norwegian government in the early 70's began an intense program raising Atlantic salmon (Salmo salar) with excellent results and with an expansion today to the Eastern Pacific Fjords (North America and South America). Afterward, in the early 80's, local and multinational enterprises initiated the same salmon aquaculture development raising Atlantic salmon in Scotland and Pacific salmon (Onchorhyncus spp. coho and chinook) in British Columbia (Canada), Puget Sound (Washington) and Southern Chile, and recently also Atlantic salmon in these Eastern Pacific Fjords (Fig. 2). Thus, the "salmon rush" is covering many inlets/fjords and estuaries in various regions of the world, including, Japan, eastern coast of North America, Ireland, Faroe Island (Denmark), Sweden, etc. Around a twenty percent net profit from this business is the reason for the expansion of the industry worldwide.

STATEMENT OF THE PROBLEM:

Phytoplankton blooms and/or red tides cause serious economic losses in the marine fish-farming industry worldwide. Therefore, more research on phytoplankton and their effects on fish cage culture, as well as on mitigation techniques are needed.

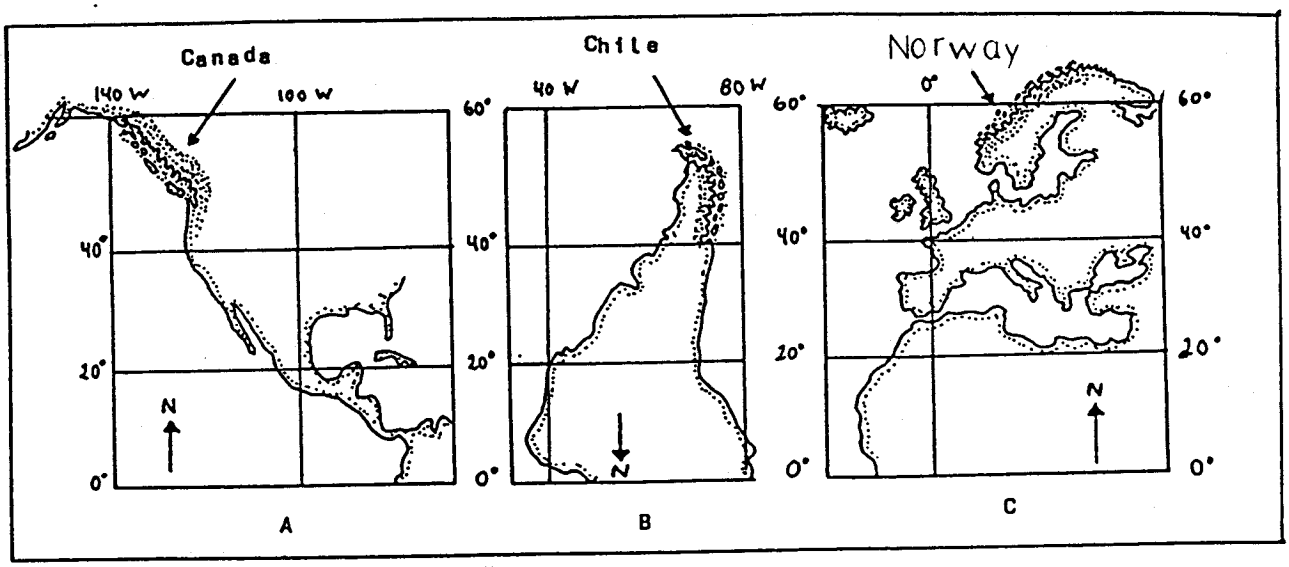

(From Vidal and Andrade, 1984).

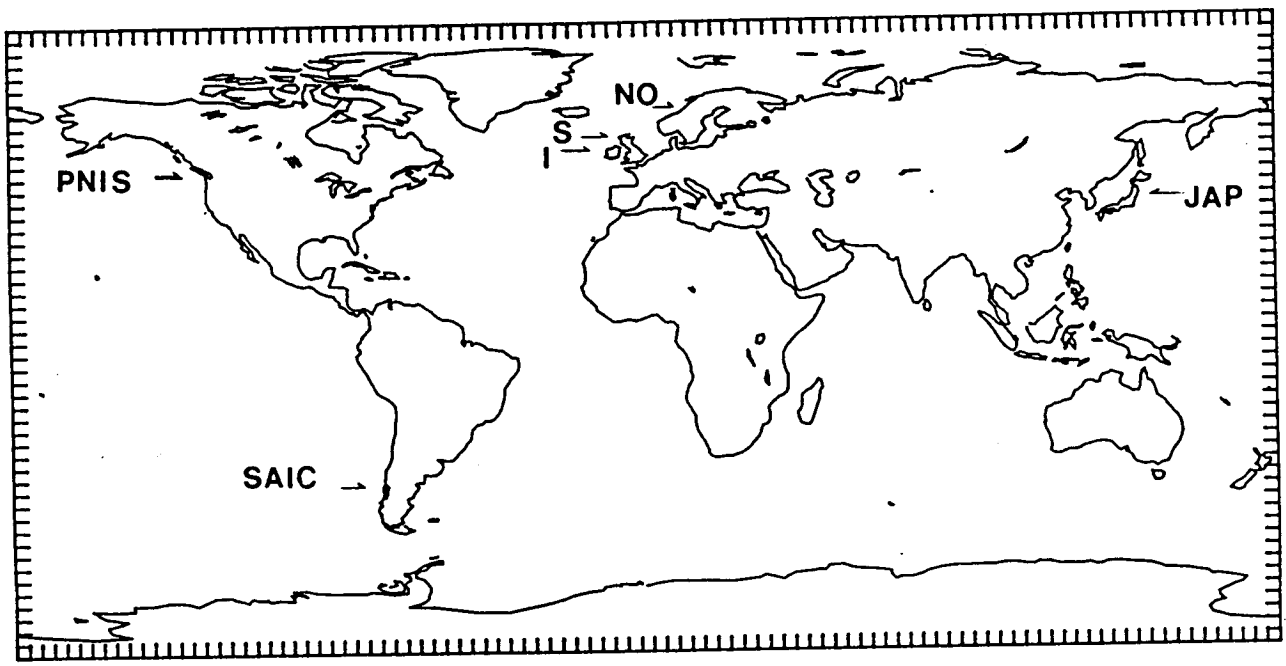

FIG. 1 STUDY AREA MAPS. A, B, AND C ARE MAJOR FJORD REGIONS OF THE WORLD. D: GEOGRAPHIC DISTRIBUTION OF MAJOR CAGE SALMON FARMS WORLDWIDE.

I: Ireland, JAP: Japan, NO: Norway, PNIS: Pacific Northwest Inland System, SAIC: Sistema de Aguas Interiores de Chiloé (Chile), S: Scotland

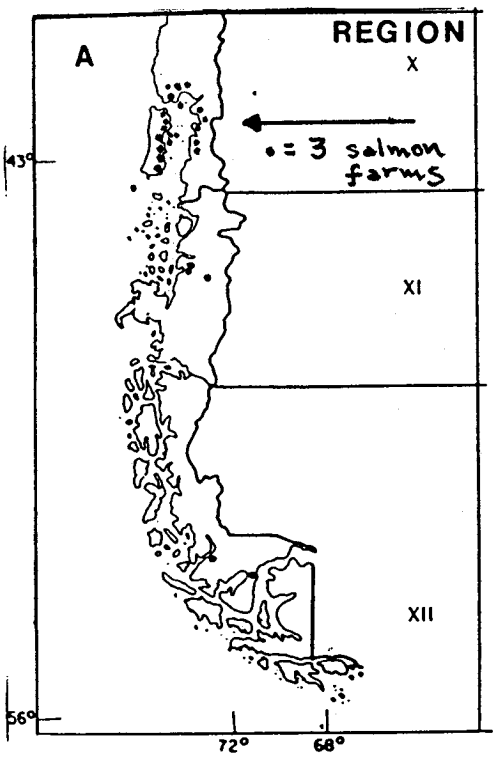

B
DISTRIBUTION OF OPERATING FARMS IN BRITISH COLUMBIA

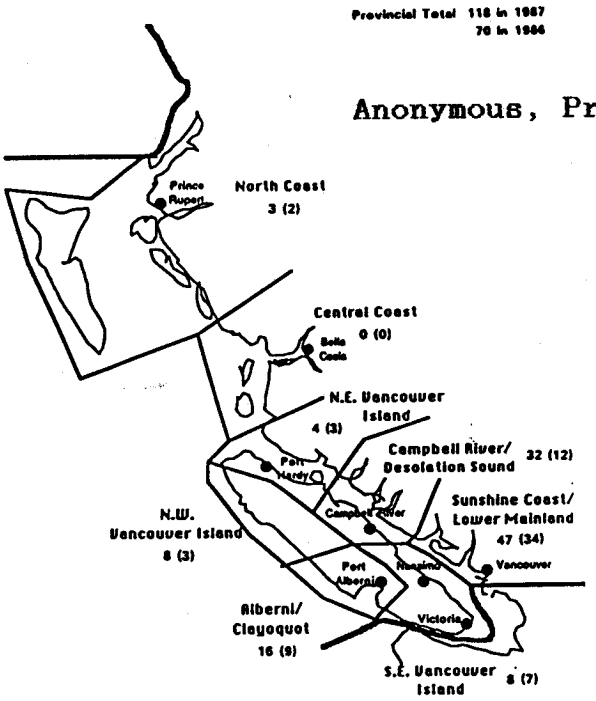

Up to November 30, 1987. Numbers in parentheses were the farms operating up to October 30, 1986.

Anonymous, Prov. of B.C.

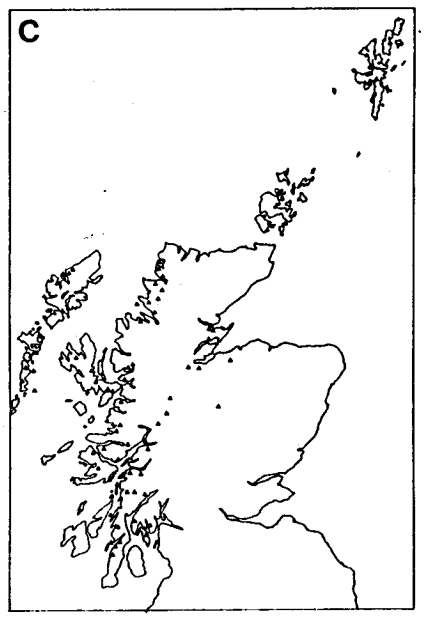

In: Beveridge, 1987

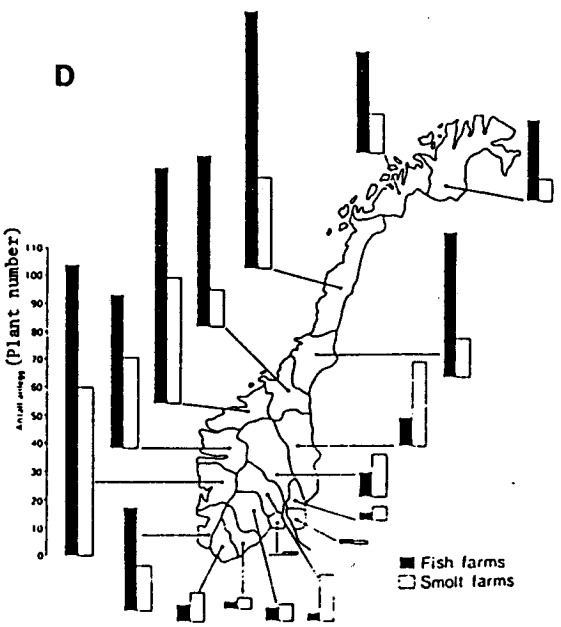

In: Lavin and Anderson, 1986.

FIG. 2. WORLD FJORDIC ESTUARIES DISTRIBUTION OF MAJOR SALMON FARMS.

A) CHILE B) CANADA (B.C.) C) SCOTLAND AND D) NORWAY.

Despite the fact that Chile is one of the world leaders in cage salmon production, the available information regarding biological and physical processes in the sea-farm environments are scarce.

Hence, I have addressed the problem in three main parts; first, describing the available oceanographic data set, second, evaluating the application of satellite imagery, and third, proposing a management strategy for the problem. Consequently the objectives are as follows:

General Objective:

Improve management decisions in cases of phytoplankton blooms affecting the cage salmon industry.

Specific Objectives:

a) To develop, collect and evaluate data on key oceanographic and meteorological factors causing plankton blooms in the Chilean inland marine waters.

b) To determine the utility of remote sensing, specifically satellite imaging to detect the presence of phytoplankton blooms in inland marine waters where salmon cage culture predominates.

c) To propose an efficient and realistic management strategy for dealing with noxious phytoplankton blooms.

2. GENERAL OCEANOGRAPHY OF INLAND GULF-ESTUARY TYPE SYSTEM

The inland marine systems [hereafter; Sistema de Aguas Interiores de Chiloé (SAIC) and Pacific Northwest Inland System (PNIS)] of interest are outlined in Fig. 3. The oceanographic description will focus upon the SAIC (Fig. 4).

Beginning with the Boca del Guafo, the Golfo Corcovado extends inland about 100 km, turning northward around Isla Chiloé for an additional 100 km to a quasi-barrier of small islands, that have been called the Apiao-Desertores Constriction (Clément et al 1988). Beyond this constriction is the Golfo de Ancud, connected with Corcovado mainly through the Canal Apiao and Canal Desertores. Extending still further northward is Seno Reloncavi, connected to Golfo de Ancud by the narrow strait Paso Queullin.

In all, the SAIC extends some 250 km inland from Isla Guafo, with a typical width of 30-40 km, and a depth along its central axis that ranges around 100 to 350 m.

2.1. CIRCULATION

2.1.1. Tide-driven:

Typical of inland marine waters with broad connection to the open seas, the Chilean SAIC circulation is driven mainly by tides. Fig. 4 shows the maximum tide ranges at several locations in the SAIC. These vary from a maximum of 7 m at Quemchi to a bit over 2.3 m at Isla Guafo.

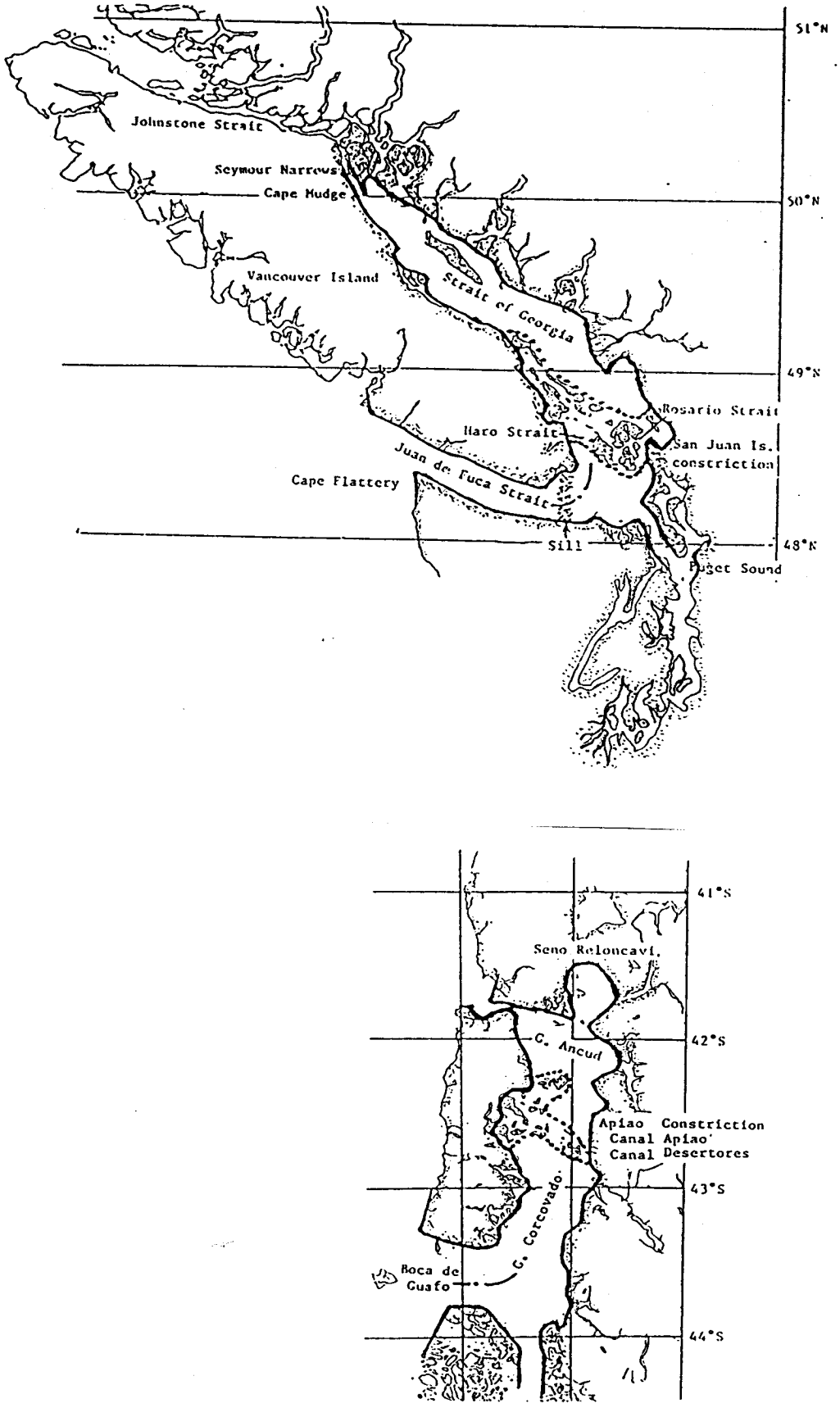

FIG. 3 GEOGRAPHY OF THE PACIFIC NORTHWEST INLAND SYSTEM (PNIS) AND THE SISTEMA DE AGUAS INTERIORES DE CHILOE (SAIC)

If one estimates crudely the average depth of the SAIC at 200 m, and its average maximum tide ranges at 4 m, then the daily volume of tidal prism is 2% of the total volume. Clearly, major circulation is tidally driven.

The narrow strait between Chiloé and the mainland, Canal de Chacao, sustains the strongest tidal current. Referring to Fig. 4, note that the maximum tide range at Ancud is 2.5 m, whereas at station Roca Remolinos just inside the Canal de Chacao, the tide range is over 5 m. This means that the difference in level of water surface between these two stations, separated by ≈40 km, can be quite large. For example, assuming that both stations reach high tide at the same time, the height difference reaches as much as 1.2 m. But sea level differences along Canal de Chacao can be higher, if the times of highest tides are out-of-phase along the strait axis.

The principal tide wave travels along the Chilean coast from north to south. Using the shallow water wave estimate (vel.=$\sqrt{gd}$, d= water depth, ≈ 200 m), the time of travel for a tide wave that appears first at the ocean entrance at Boca del Guafo, then travels east around southern Isla Chiloé and then north to Canal de Chacao, is about 1.6 hours. Even this rough estimate correlates well with the difference in time of high tides, at Bahía Ancud versus Roca Remolinos, from Chilean tide tables about a hour (IHA, 1988). This time difference to extreme tide mark results in a maximum sea level difference of about 2 m along the Canal de Chacao over a distance of about 40 Km; tide currents

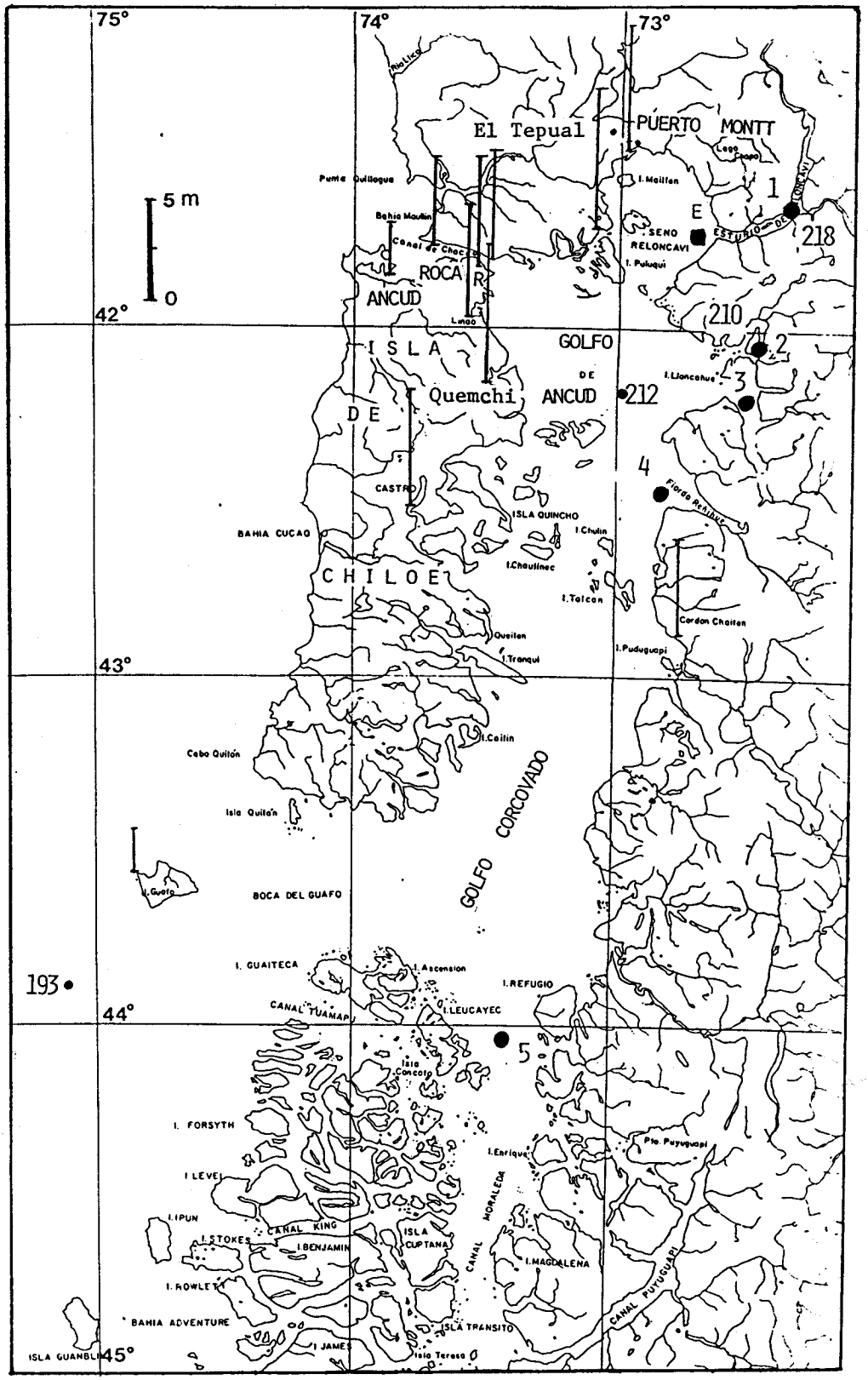

FIG. 4 MAP OF THE SISTEMA DE AGUAS INTERIORES DE CHILOE (SAIC) MAXIMUM TIDE RANGES ARE SHOWN FOR SOME STATIONS. ALSO SHOWN ARE THE LOCATIONS OF THE HUDSON EXP. STATIONS.

through this strait reach 6-9 knots.

No published data on the magnitude of tide currents in the main bodies of water, Golfo de Ancud and Golfo Corcovado have been reported. However, we can make an analogy with tidal currents in the Juan de Fuca Strait, on the west coast of North America. Both the geometry and bathymetry of the Fuca strait is similar to the SAIC, and the spring tide range of 2.5 m at Cape Flattery (British Columbia), the entrance to Juan de Fuca strait (Thomson, 1981) is the same as at Isla Guafo at the entrance to Corcovado. By analogy, one can expect tide currents along the axis of Corcovado-Ancud of 1.5 to 2.5 knots on large spring tides. Other analogous oceanographic and remote sensing data between the SAIC and PNIS will be shown in later sections.

2.1.2. Wind-driven currents:

Surface winds have two main impacts on surface layers of inland water systems:

a) Set-up. This is a consequence of the Ekman effect, in which the friction drag of wind over water pushes a wedge of surface water against a shore. If the bottom is deeper than the local stratification, then the wedge will accumulate against the shoreline to the **left** of the direction of the forcing wind (Southern Hemisphere). For example, the January 1949 density profile in Seno Reloncavi (Fig. 5) shows the surface layer only about 10 m thick; the stratification barrier to vertical mixing is very strong at this depth, and prevents the energy of the wind from

FIG. 5. SEASONAL VARIATION OF VERTICAL DENSITY STRUCTURE IN SENO RELONCAVI DURING 1949 YEAR. (LUND EXP. DATA)

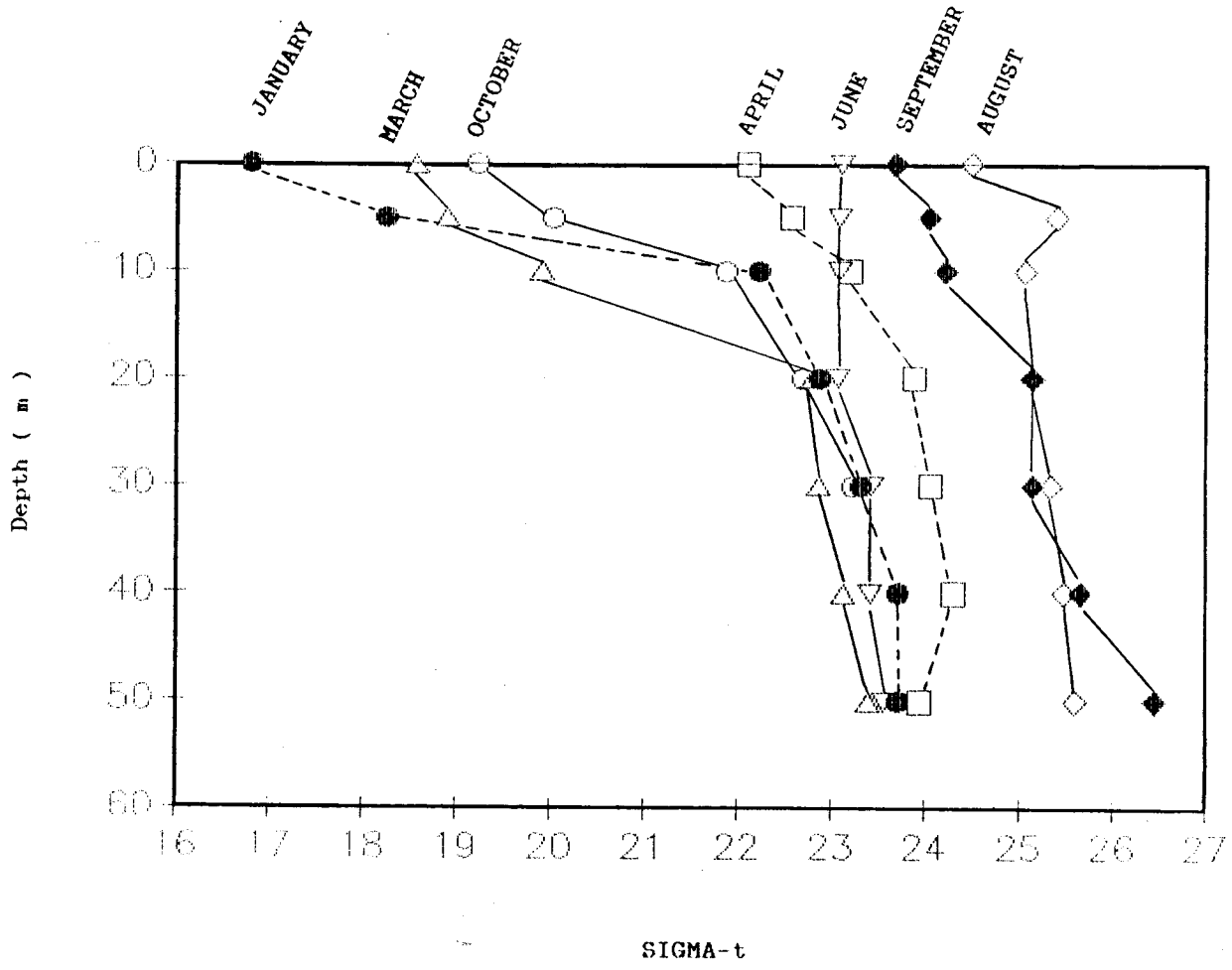

reaching to greater depths. In this case, summer 1949, prevailing south wind would push surface layer water against the west shore of the Seno. Furthermore, all of the fluid that enters into the wedge would be surface layer water, above the 10 m level. If bottom depth is very shallow, as in the case of the Isla Chiloé estuaries, and less than the pycnocline, then the setup will wedge against the downwind shore.

For the **salmon cage industry**, this Ekman setup effect can be the cause of problems of drifting surface contaminants from the open Golfo de Ancud or Corcovado into the inlets along the Chiloé or Andes shores. Plankton blooms occur in patches within the surface layer, above the pycnocline, hence, such patches are transported with the surface water, i.e., toward shore.

b) Wind-drift currents. In the typical weather cycle, or event, normally 4 to 6 days long, the setup effect occurs quite fast, within one inertial period (for the SAIC at 42° S, this is 18 hours). Thereafter, the direction of the movement of surface layer fluid changes to the downwind direction.

Wind field data for the SAIC, Figs. 8-12, show that the dominant wind directions are north and south, along the axis of the SAIC. With the major part of the SAIC well-stratified, typical of inland marine waters receiving river runoff, the Ekman drift will move surface waters against the

eastern shore of Isla Chiloé, during summer (December) when 56% of the winds blow toward the north, and against the Andes shore during winter (July) when 71% of wind directions are toward the south (Fig. 11). For wind systems associated with strong storms, lasting several days, and with a wind direction oriented along a channel, one expects wind drift currents to reach speeds up to 3% of wind speed; for a steady wind of 10 m/sec, this reaches up to 0.5 knot, and can even compete with tidal currents.

Thus, given a tide current of amplitude 1.5 knots along the Corcovado-Ancud axis, a wind-drift current of 0.5 knot during winter can reduce the flood tide current to 1 knot at the surface, and increase ebb tide to 2 knots. Wind currents rarely reach to depths more than about 20 m, about the depth of the well-mixed surface layer.

2.2. STRATIFICATION

2.2.1. Density Stratification and Plankton:

In general, both solar heating and freshwater runoff tend to increase vertical density stratification. In contrast, the insertion of turbulent kinetic energy into the same water column will tend to reduce its density stratification by vertically mixing. Major sources of such turbulent mixing energy are tide forces, mainly at semi-diurnal frequency (12.42 h), and winds with variability of order of days. Between the two forcing factors, tide and wind, most shallow estuaries react more

strongly to even moderate tides than to local winds.

It is important to know how density stratification changes within the SAIC (mainly due to freshwater runoff), because of the well-known relationship between changes in the physical condition and the phytoplankton response to it elsewhere (Sverdrup, 1953, Pingree, et al 1978, Townsend and Spinrad, 1986, Malone et al 1988). The dramatic variation in phytoplankton density and patchiness, seen in the recent spring (Sept. 1988) event, demonstrates clearly the need to know the patterns of time-space scales of both the physical/chemical character of the surface layer, and the biological response of plankton.

In part, plankton response to physical conditions reflects changes in the inputs of organic and inorganic nutrients which are mixed into the surface layer from deeper waters, or from riverine inflow. Whether or not a phytoplankton bloom occurs depends on many aspects of the dynamic forces that control density stratification.

Farmer and Freeland (1983) pointed out that almost all the fjord processes are time-dependent, mainly the wind effects, tidal currents and freshwater run-off. The strong mixing processes occur in the short term. Crean (1978) using a numerical model showed that both the tides and the tide currents, as well as freshwater runoff, are all important forces in shaping the type of estuarine circulation in the inlets along the coast of British Columbia. These inlets are quite similar to those in the northern part of the Chilean SAIC.

2.2.2. Annual Variability:

The most useful existing data on annual change in density stratification comes from the Lund Expedition data (Brattström, H. and E. Dahl, 1951-52). These hydrographic stations were taken in Seno Reloncavi (see Fig. 4 for location) over a complete annual cycle. Virtually all of the column stability against mixing forces during summertime occurs above the 10 m depth, as noted in profiles for October through April (Fig. 5). The maximum stability number (equivalent aproximation of stability, E) is $\approx 5 \times 10^{-3}$ m^{-1}. Vertical mixing begins to deepen in late fall; the March and April profiles show mixing to 20 m, while the June winter profile has mixing to depths in excess of 30 m, i.e., no stratification remains. Figure 5 also shows the rapid re-stratification that occurs in early spring. The August profile is still relatively well-mixed, but the September profile shows a clear build up of stratification from the surface down to 20 m depth.

2.2.3. Biological Significance for Salmon Cage Culture:

These profiles show the ability of the water column to sustain phytoplankton growth. Under conditions where mixing reaches to large depths, as in June-August period noted in Fig. 5, phytoplankton growth is severely curtailed for two reasons: first, light intensity is low during the winter months, and second, plankters spend relatively more time in the deeper, darker portion of the water column. In spite of the fact that

deep mixing renews the fertility of the water column, all the way to the surface, the system does not yield net production.

As stabilization begins in early spring, e.g., September-October, two factors contribute to the promotion of strong plant growth: i) vertical mixing is restricted, so the plankters are retained, for increasing amounts of time, in the well-lit surface zone, and ii) the increased solar heating, which itself is creating the stability, is also supplying large numbers of photons for the photosynthetic process. Thus, the initial spring reaction of the phytoplankton is an increase in production (Sverdrup, 1953).

Three main factors act to limit heavy spring blooms; (1) grazing pressure by zooplankton, (2) depleted nutrient concentrations in the surface layer and (3) strong wind events or late spring winds. Initially in the spring bloom the concentration of zooplankton or herbivores is limited. Because these small animals have a much longer reproduction cycle than the microalgae on which they graze, (e.g., 2 weeks for a copepod reproduction, compared to 1 day for a diatom reproduction), the initial two weeks of heavy spring blooms is unchecked by the addition of new grazers. Only after new generations of grazers are added to the system can plant production be controlled naturally through grazing pressure (Parsons et al 1977). Depletion of nutrients by growing algas within the stabilized upper column will itself eventually limit further production by plants. In general the thinner the stability layer, the more

rapidly will the available nutrient supply be exhausted. Conditions that promote shallow stable layers are:

(1) relatively high river runoff or winter rains; both reduce the density of the surface layer, hence producing a shallow stability layer.

(2) relatively strong solar insolation; heat energy is absorbed exponentially as irradiance downward into the water column.

(3) relatively weak winds; wind stress serves as a source of vertical mixing energy; high winds produce deep mixing.

In summary, the physical condition of the mixed layer, plus the inputs of organic and inorganic nutrients (from deeper waters and/or from riverine inflow; "new production", see Eppley and Peterson, 1979), allows for development and maintenance of a phytoplankton bloom, as well as its decay, due to nutrient depletion, sinking and zooplankton predation.

3. METHODOLOGY AND SOURCE OF THE DATA

Most of the salmon sea farms are concentrated in the western estuaries of the Seno Reloncavi, Ancud Gulf and Corcovado Gulf, and some farms on the eastern region as the Pichicolo fjord, therefore, the Chilean data (hydrographic and imagery) have been gathered mostly from these fjords and inlets (Fig. 4). Also CZCS data has been selected from areas near the sites of salmon

marine farming in British Columbia (Fig. 7) and Southern Chile.

3.1 Hydrographic and Meteorological Data from Southern Chile:

Data from the time period 1937-1940 came from the Meteorological Station at Puerto Montt, 13 m above sea level (41° 28`S, 72° 56`W). The record of air temperature for the time period of 1940 to 1973, as well as the tide gauge, sea surface temperature (SST) and air temperature at Puerto Montt for different time period (1945-1972, 1984-1986) was provided by the Instituto Higrográfico de la Armada (IHA). The Tepual airport meteorological data set (precipitation and air temperature) of the decade 1977-1987 was obtained as monthly means from the Monthly Climatic Data for the World (MCDW, see references) prepared by NOAA. The SST missing points for the time period 1984-1986 (≈3.3%) were linearly interpolated and a ten day average and standard deviation was compute for each parameter.

The wind data set for the entire 1984 year, 8 values per day, equally spaced, was obtained from the Tepual airport station (41°26`S,73°06`W), located 90 m above sea level station and approximately 12 km from the coast at Puerto Montt, a distance without significant topographic obstacles in between. Short term studies comparing the wind field from El Tepual airport and Tenglo Island, Seno Reloncavi (sea level), have demonstrated that the prevailing wind direction is slightly more frequent at Tenglo Island, particularly for SE-S-SW winds (ICC, 1987). The wind raw data was decomposed in the eastward and northward vectors for velocity and wind stress respectively. Wind

stress is the force per unit area that the wind exerts on the water underneath. It has the same direction as the wind, and its magnitude is proportional to the square of the wind speed. The eastward (τ_x) and northward (τ_y) components of the wind stress were computed from the eastward (u) and northward (v) components of the wind velocity (Pittock et al 1982):

$$\tau_x = \sigma C_D (u^2 + v^2)^{1/2} u \qquad \tau_y = \sigma C_D (u^2 + v^2)^{1/2} v$$

where σ is the density of air, taken to be 0.00125 g cm^{-3}, and C_D is the drag coefficient, taken to be 0.0015.

Some data was acquired from the Lund (Brattström and Dahl, 1951-52) and Hudson (Anon. 1971 and Pickard, 1971) expeditions, the nutrients data was provided by Nelson Silva (Univ. Católica de Valparaiso) and from observations by A. Clément in more recent years.

3.2. Imagery of CZCS

3.2.1. British Columbia CZCS Imagery:

The level 3 data was obtain from Dr. Ted Strub's digital tapes Archives (Inventory of CZCS Chlorophyll Data) which are in two formats: 1) As mosaics and 2) as Tiles, which is a square image (5.12° per side) with a resolution of 100 pixels per degree and 512 x 512 pixel per image (WCTS, 1987). Tiles were used in the present project. The tiles digital tapes were selected based on cloudiness and season of the year to avoid the sunglint effects at mid-latitudes. The tapes were first read on the MICROVAX II/VMS system, selecting the files of interest from

B.C., and then transferred to SUN/UNIX system (directory SUN-TOOLS), which has a digital image processing program (called SHO) in a developing stage as a sub-directory of the SUN-TOOLS. The SHO program, originally on UBC Oceanography's VAX750, was modified to run on SUN color work-station by Bill Meyers and installed at OSU oceanography by Andy Thomas. Using SUN-TOOLS, two steps were carried out before the image was able to display. To decode the data and remove the first 11 headers of the image/file, PAS1.OUT and PAS2.OUT programs were run respectively. Then the files (images) were ready to display using the SHO digital image processing program, on screen of the Helios terminal. To print out black and white copies of the images on a LASERwriter the file/image was run through the PRIMAGE program (Fig. 6) written by Steve Gard. Finally, a quantitative descriptive statistical analysis of the digital counts or pixels' radiance was computed to estimate mean, standard deviation and coefficients of variation of photosynthetic pigment concentrations, for specific boxes within three regions of interest; Queen Charlotte Strait (C), Strait of Georgia (G), and Juan de Fuca Strait (G2). The latter corresponds to the east-end of the strait (Fig. 7). This program was able to read each pixel value and average them out for a specific box (matrix), removed and count the numbers of pixels out of range, such as land, clouds or extremely high radiance values (See Appendix).

3.2.2. Southern Chilean CZCS Imagery:

The Chilean CZCS products were obtain from Dr. Steve

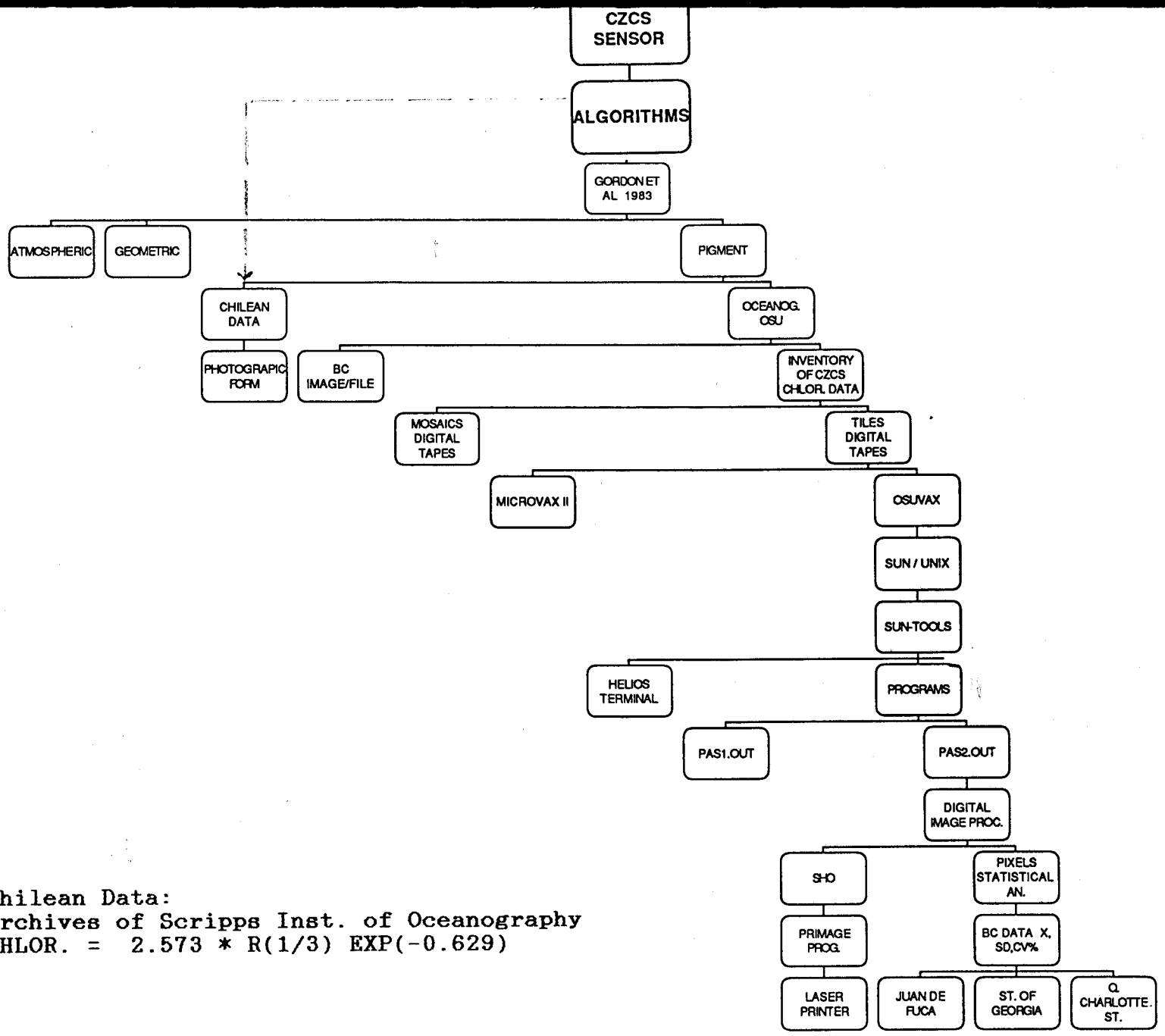

Chilean Data:
Archives of Scripps Inst. of Oceanography
CHLOR. = 2.573 * R(1/3) EXP(-0.629)

FIG. 6. FLOW DIAGRAM OF COMPUTER DIGITAL IMAGE PROCESSING OF CZCS DATA.

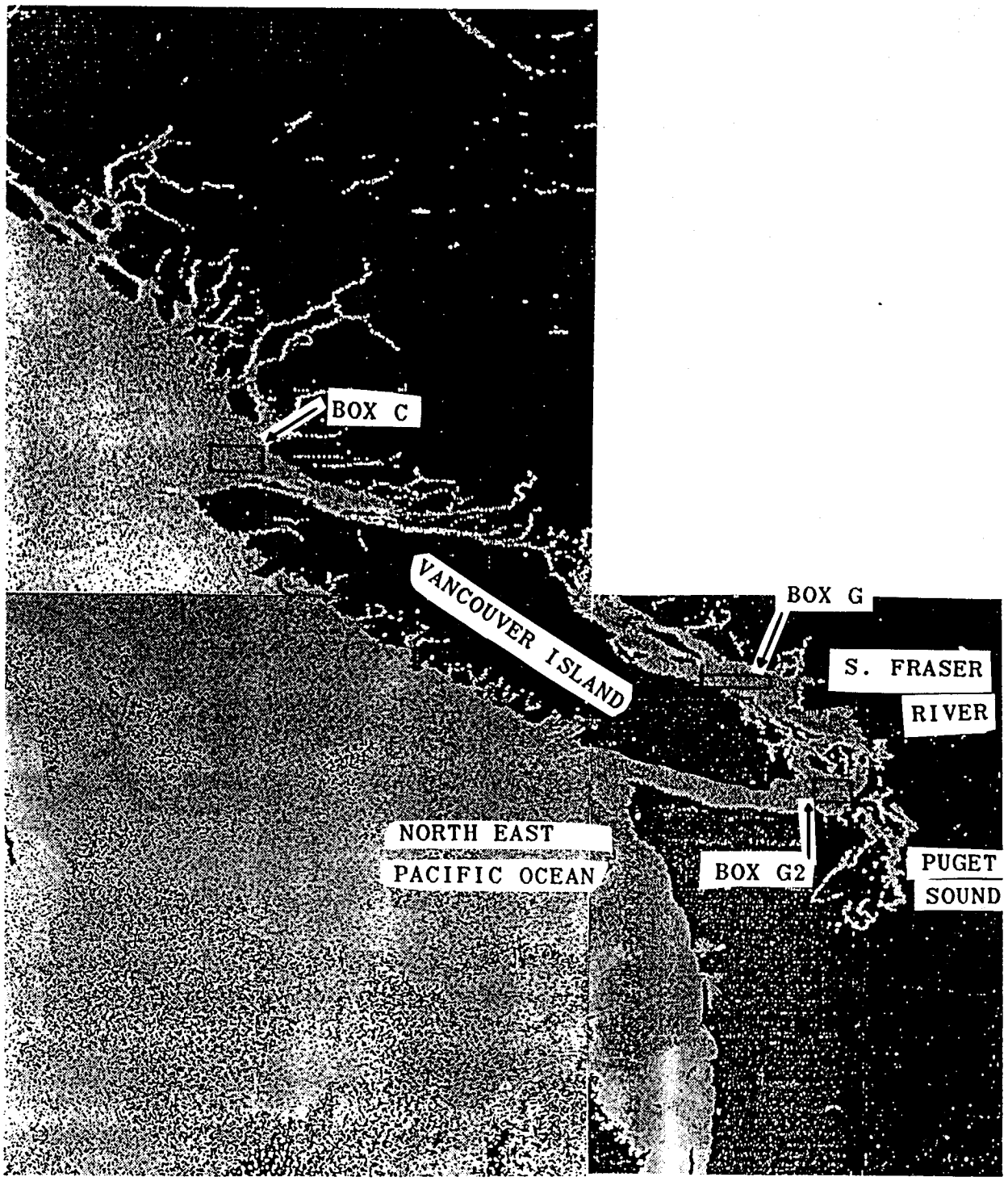

FIG. 7. SELECTED BOXES FROM B.C. IMAGES FOR STATISTICAL ANALYSIS. QUEEN CHARLOTTE STRAIT (C); STRAIT OF GEORGIA (G); JUAN DE FUCA STRAIT (G2).

Neshyba in photographic form. Methodology for these imagery has been described in Uribe and Neshyba (1983) and Espinoza (1984), who studied the phytoplankton pigments off of Chile from 18° to 40° S, using the CZCS. Only a qualitative characterization of the pigments/radiance features was carried out in the present study. In fact, no digital data was available of the pictures, therefore the analysis was just descriptive.

4. RESULTS AND DISCUSSION

4.1. METEOROLOGICAL FACTORS IN THE SAIC.

4.1.1. Winds at Puerto Montt and Isla Guafo:

The average percentage of direction of the winds at Puerto Montt of the December and July 1937-1940 data set, is shown in Fig. 11 a and b. Prevailing winds are 71% from the north, and 11% from the south during July (winter), and 56% from the south and 22% from the north during December (summer). For the same 4-year period, Fig. 12 shows the average number of days per month when wind speed exceeded 36 knots (≈ 66.7 Km/h) at Puerto Montt and Isla Guafo. At both stations, the winter months of June and July each had an average of 3 days with winds in excess of this value, the mid-range of Beaufort Scale 8 winds; Isla Guafo showed similar 3 day high winds during August. This means that P.Montt is subjected to North winds during winter storms at much the same speeds and frequency as is the open coast at Isla Guafo.

Note, however, that the summer time condition for Isla Gaufo is also one of relatively high frequency of strong winds, but

these are summer winds from the south. P.Montt, on the other hand, had no days of such strong winds during the same period. This suggest that P. Montt and Seno Reloncavi are relatively protected against the strongest of the summer south-southwest winds.

It is worth noting that the maximum wind speed measured at Tepual Airport during the 1984 year series of data, Fig. 8, also exceeded the Beaufort 8 scale value 3 times, two days in June and one in August. The August speed maximum measured 90 km/hr at Tepual, is clearly shown in Fig. 8.

The north wind stress (dynes/cm^2) is the most important component with forces higher than 10 dynes/cm^2 as a maximum, with some high values during the beginning of spring and at the end of fall (Fig. 10). The east wind stress is represented in Fig 9. showing values no larger than 3 dynes/cm^2 for the entire 1984 year. The west wind stress (negative values; Fig. 9) is more evident during spring and summer with values no larger than $\approx$ -2.8 dynes/cm^2 (notice different scales).

In summary, magnitude and frequency of the north component of wind stress is an important factor in site selection for cage culture. This is not so much because of setup or wind wave effects, but mainly due to the role of winds in moving surface waters into otherwise protected bays and inlets. Such transports will also distribute contaminants, or phytoplankton blooms, that exist in the surface layer.

FIG. 8 WIND SPEED AT TEPUAL, P.MONTT.

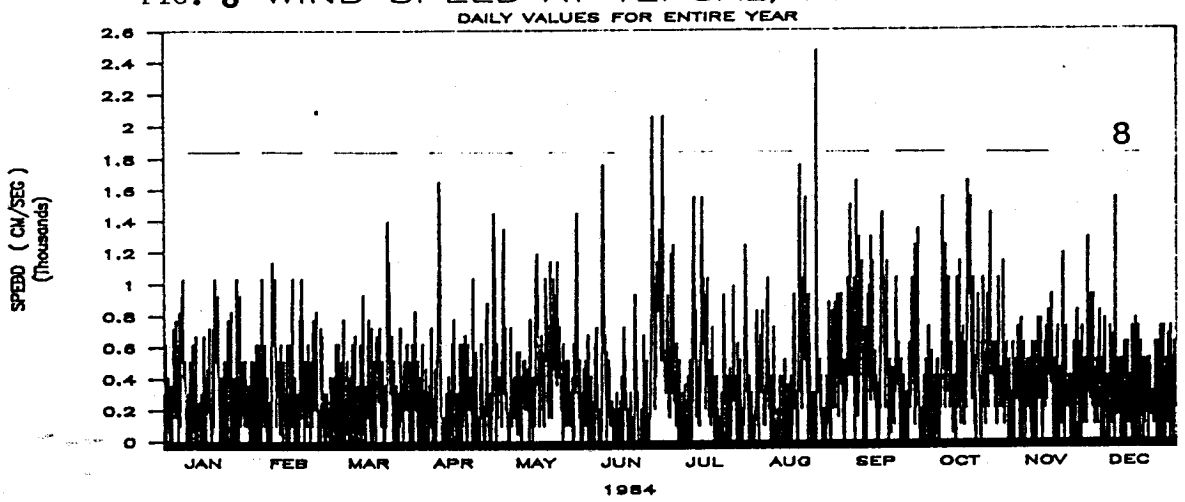

FIG. 9 EAST WIND STRESS AT TEPUAL, P. MONTT.

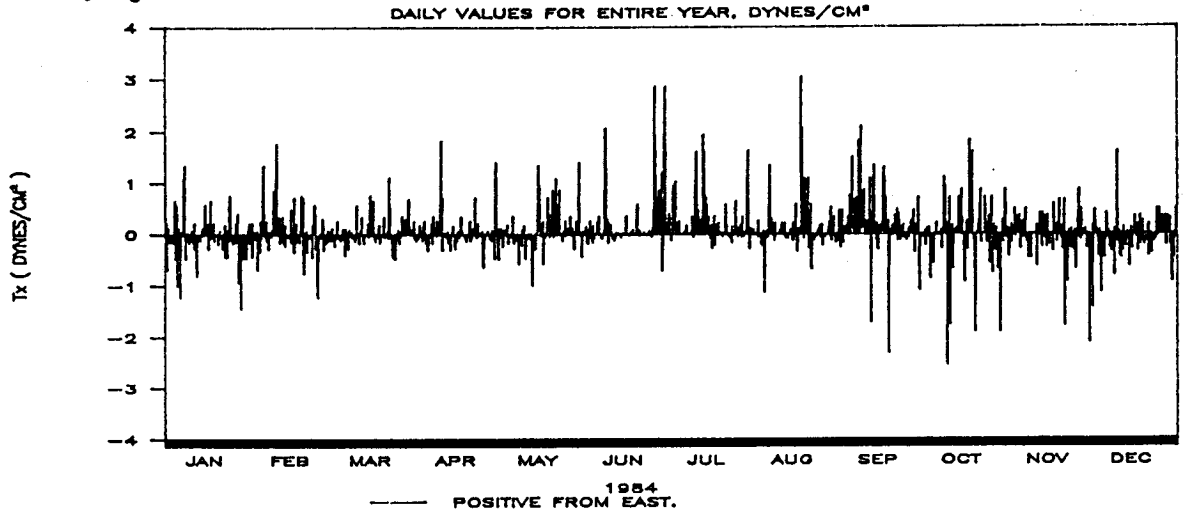

FIG. 10 NORTH WIND STRESS AT TEPUAL, P. MONTT.

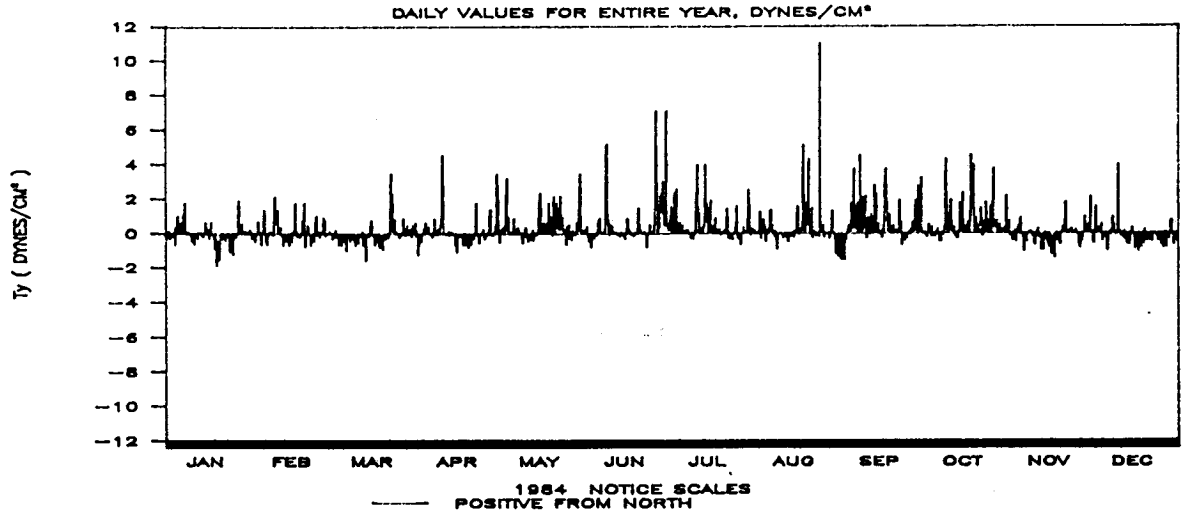

FIG. 11

a

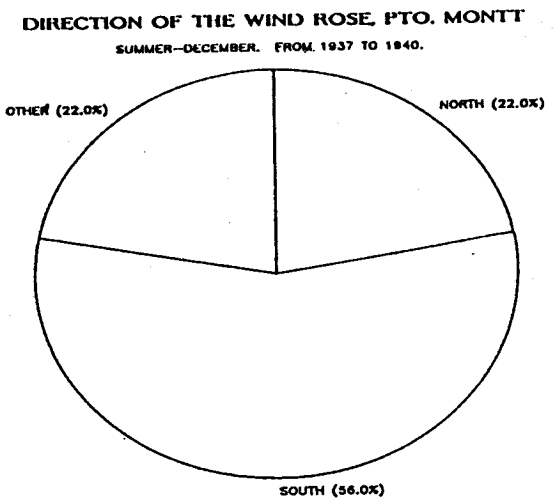

b

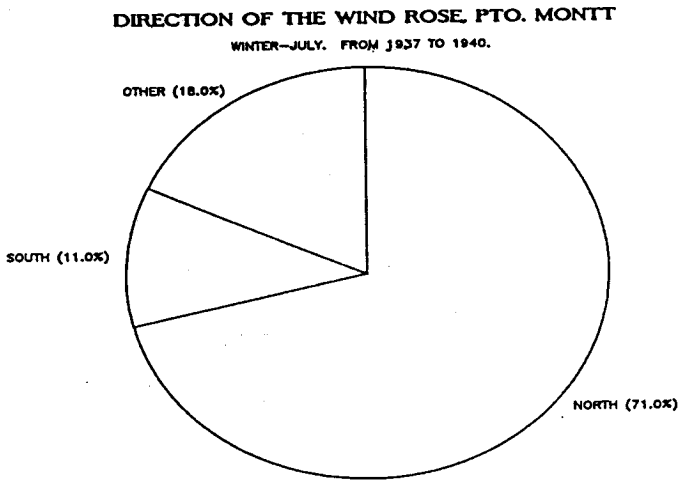

FIG. 12 AVERAGE NUMBER OF DAYS PER MONTH WITH A WIND SPEED LARGER THAN 36 KNOTS (≈ 66.7 km/h) AT SAIC. 1937-1940

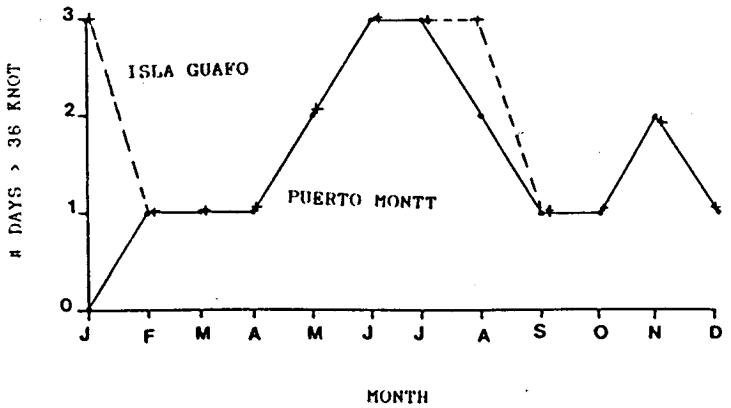

4.1.2. Air temperature at Puerto Montt

Two sets of data have been chosen to develop the variation in air temperature over the SAIC region. The first set, plotted in Fig 13, covers the time period from 1937-1940, and is available with the extreme temperature values recorded during this 4 year period. It shows a typical mid-latitude cycle with the warmest month in January, and with the highest extreme value, 24.5 °C, in the same month. The average coldest month is July, but the lowest extreme value, 0° C, was in June. The post-winter rise in air temperature occurs during the August-September transition.

The second set of air temperature data, Fig. 14, covers a 10-year time period 1977-1987. We chose this decade because of its inclusion of the ENSO (El NiÑO Southern Oscillation) event, itself a 300 year severity event (Quinn W, com per). Here the monthly mean shows a general warming trend up to the summer 1982-1983. The highest monthly mean for the decade was during this same summer, at 15.5 °C. In a coherent manner, the two following winters, 1983 and 1984, produced the coldest monthly mean values of the decade, about 4.6°C.

4.1.3. Precipitation at Puerto Montt:

Comparing the air temperature pattern with monthly total precipitation data, (Fig. 15), one sees clearly that these coldest winter conditions correlate with the lowest winter rainfall. The four-year average of precipitation per month at

FIG. 13 AVERAGE, STANDARD DEVIATION, AND RANGE OF AIR TEMPERATURE. PUERTO MONTT, TIME PERIOD 1937-1940.

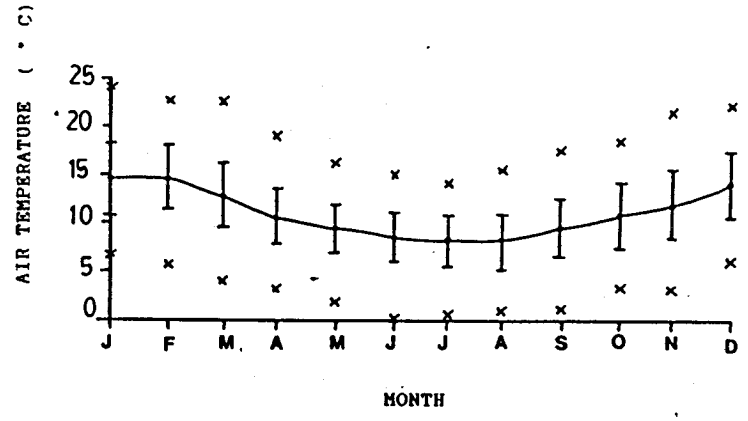

FIG. 14 AIR TEMPERATURE AT TEPUAL, PUERTO MONTT

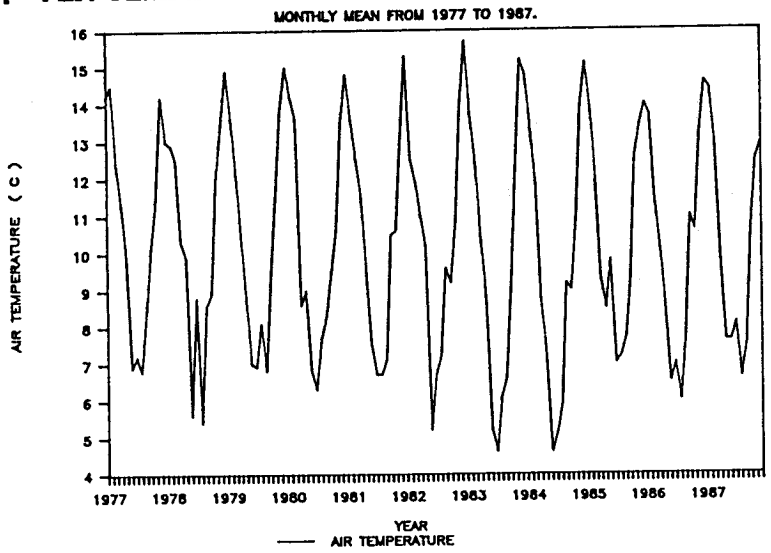

FIG. 15 PRECIPITATION AT PUERTO MONTT, X REGION

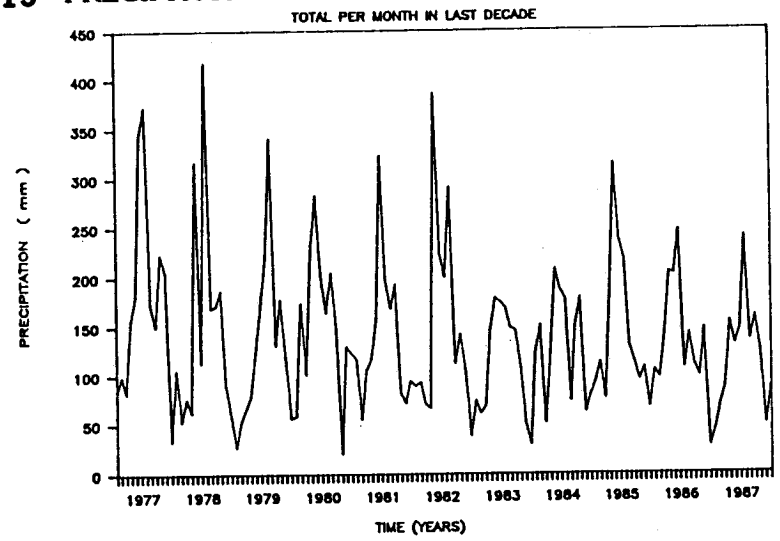

Puerto Montt (Fig. 16) demonstrates the most rainy months and vice versa. Rainfall and river discharge information is very useful to estimate the amount of freshwater input into the inland waters of Chile, a factor that affects the degree of stratification of the water column as well as nutrient inputs from land to the system.

Biological impact of the 1982-1983 event: Beginning early fall 1983, Seno Reloncavi was affected by a strong red tide outbreak which killed wild and "coho" salmon farmed fishes (Lembeye and Campodonico, 1984). The study of physical forces and their anomalies could be an useful index to establish which of the conditions in SAIC causes the red tide events.

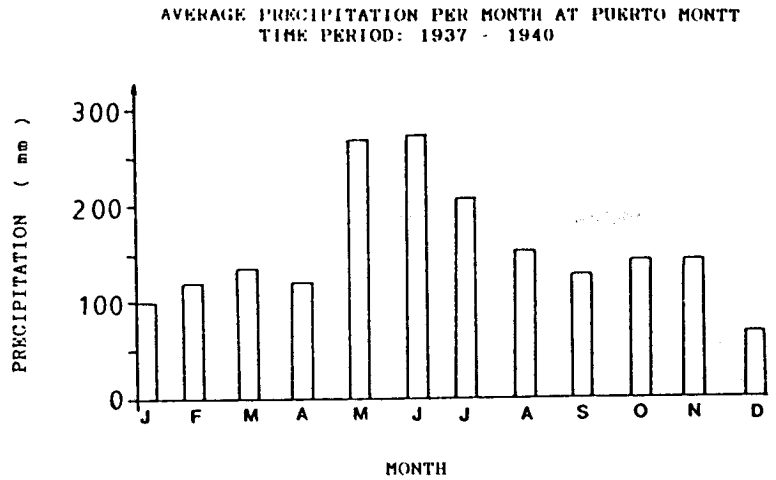

FIG. 16. AVERAGE PRECIPITATION PER MONTH AT PUERTO MONTT. TIME PERIOD 1937-1940.

4.2 OCEANOGRAPHIC FACTORS IN THE SAIC

4.2.1. Sea Surface Temperature (SST).

Figure 17 shows the long-term monthly average of sea surface temperature (SST) at Puerto Montt 1945-1972. Minimum SST occurs in June at about ≈ 10°C, and maximum in January at about 16 °C. From averages, southern Chilean inland waters have an advantage over some other fjordic estuaries with salmon cage culture (Fig 1 and 2), in that winter seasons are not extremely cold; winter minima are not the limiting factor to cage culture here.

However, the relatively high January SST averages do present potential problems because high surface water temperatures are conducive to outbreaks of some bacterial diseases. In Fig. 18 we show the extreme maximum of SST from the 1945-1972 data set. The highest temperature (22°C), occurred in 1951, similar highs were recorded in 1960, 21 °C, and 1968-1969, 20.5 °C. A comparison of ten-day averages of air temperature and SST for 1984-1986, Fig. 19, shows the relationship between these parameters. Correlation is very high, especially during the summer but less in winter. Lower winter correlations probably reflect the fact that North winter winds at P. Montt arrive from the landward direction. Summer winds arrive from sweeping up the axis of the SAIC, and are equilibrated closely to SST.

Possible Biological Consequences:

The plot of standard deviation for the same time period above shows a different pattern for the two summers, 1985 and

FIG. 17. LONG TERM MONTHLY AVERAGE OF SEA SURFACE TEMPERATURE (SST) AT PUERTO MONTT, TIME PERIOD: 1945 - 1972.

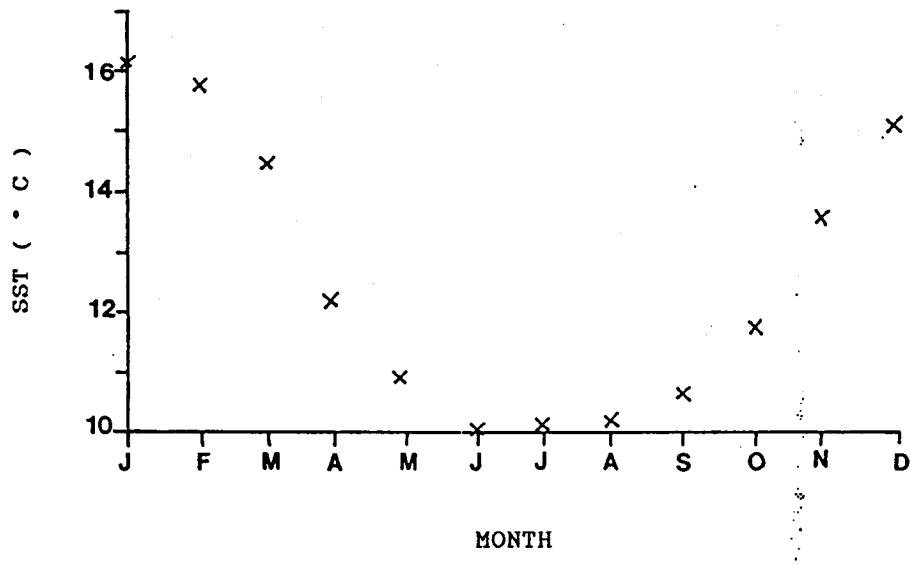

FIG. 18. MAXIMUM SEA SURFACE TEMPERATURE DISTRIBUTION OF JANUARY. PUERTO MONTT. TIME PERIOD; 1945- 1972.

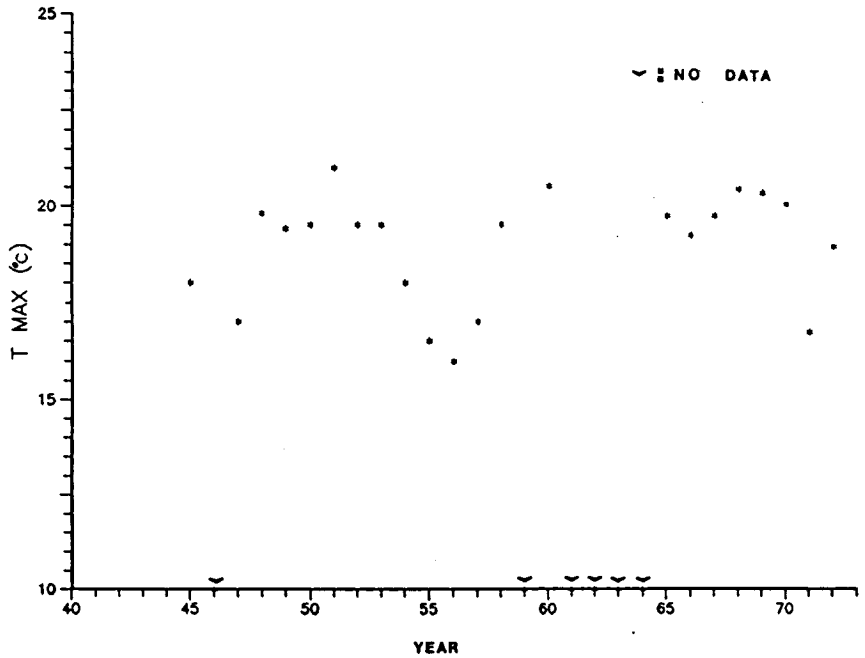

FIG. **19** TEMPERATURES DISTRIBUTION AT P.MONTT

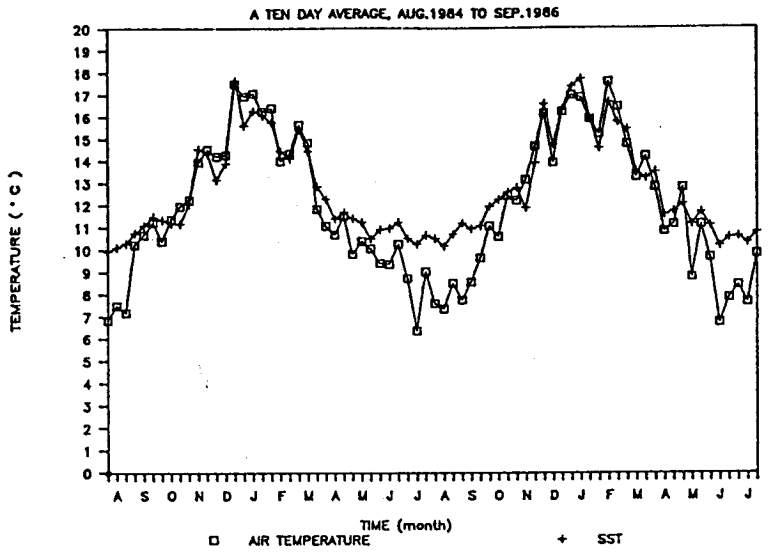

FIG. **20** SST'S STANDARD DEVIATION AT PTO. MONTT

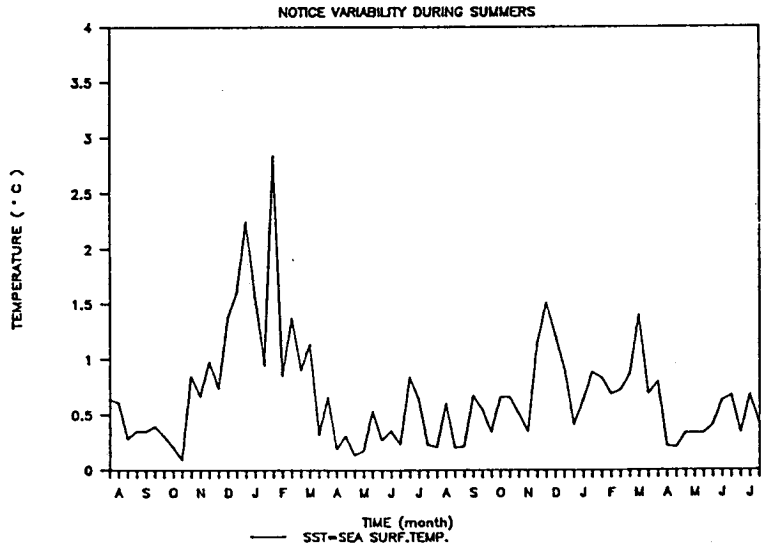

1984 1985 1986

1986 respectively. Variability over the ten day period is much larger for the 1985 summer (Fig. 20), as high as 3°C. This is an extremely large variation, and needs to be studied for cause. It is important to point out that this summer was also quite unusual from a biological standpoint, especially during the summer-fall transition, because a large kill of Chum mackerel (Scomber japonicus) was found in the Reloncavi Fjord (also called Estuary) during February (Clément, 1988) and a nontoxic red tide event occurred during March in the coastal waters of Puerto Montt and Tenglo Channel (Clément and Guzmán, 1988).

4.2.2. Water mass characteristics of the SAIC

Pickard (1971) carried out the only comparative oceanographic survey of inlets and seas within the SAIC, from the vessel Hudson in March, 1970. These data cover one month of sampling. We reproduce here the temperature (T) and salinity (S) data for a number of stations in the Reloncavi-Ancud-Corcovado system; stations locations, Fig. 4, are located in inlets along the length of the SAIC, from Seno Reloncavi (E) to Isla Refugio (5). Figure 21 shows the salinity characteristic of the sample stations at the surface and 20 m depth, respectively, as well as the dissolved oxygen. The comparison illustrates very clearly that the main pynocline stability between the surface and deeper waters lies above 20 m depth. The dashed lines connect S and O_2 values for surface samples at all 5 stations. Note the very low surface salinity at station 1, Reloncavi Estuary, about 16 %., and the increasing surface salinity along the SAIC axis in the

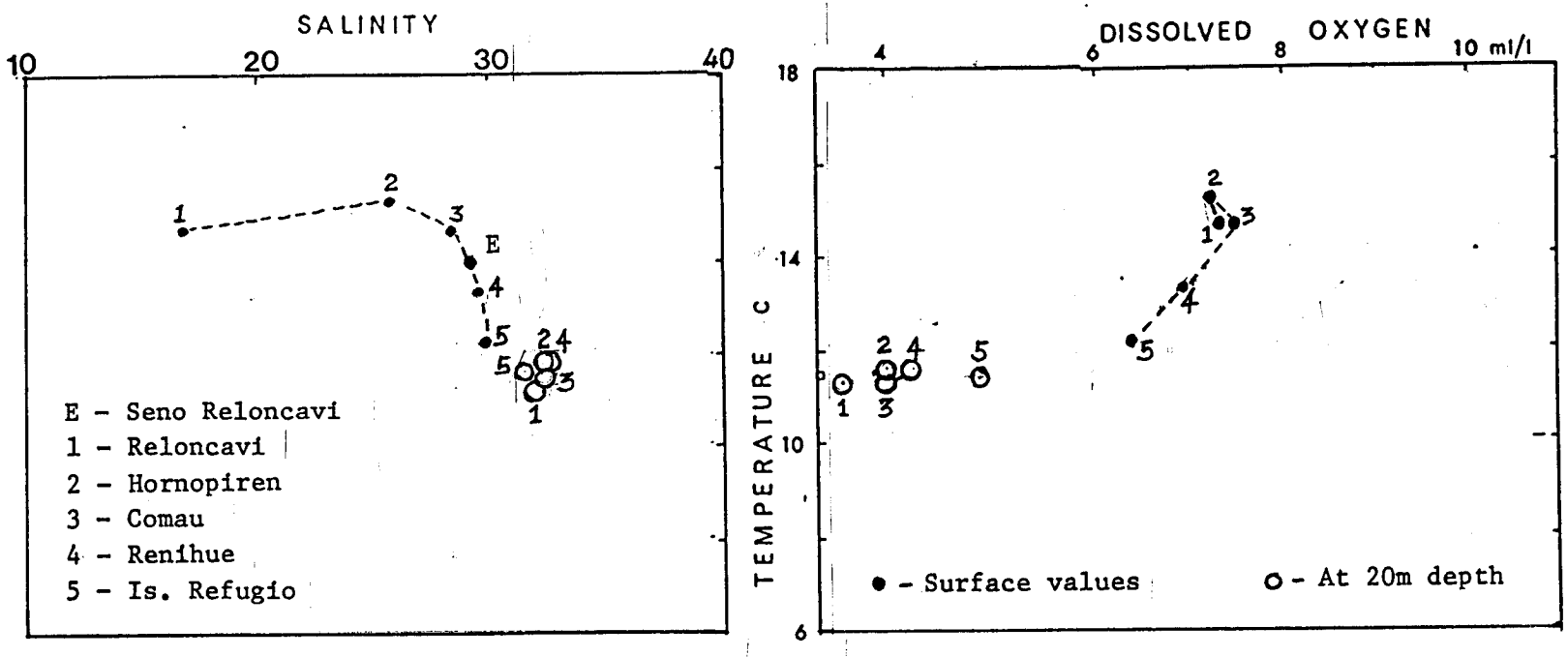

FIG. 21 TEMPERATURE - SALINITY - OXYGEN CONCENTRATIONS AT FIVE STATIONS ALONG INLETS OF THE SISTEMA DE AGUAS INTERIORES CHILE (SAIC), HUDSON EXP. 1970

seaward direction, reaching about 30 %. at station 5. In contrast, the waters at 20 m depth are virtually identical in salinity, 31 %. to 32 %., at all 5 stations including Seno Reloncavi, and demonstrate that the most of the volume of all the SAIC basins are filled with essentially open South Pacific water.

A similar result is seen in the oxygen data. In surface waters, the dissolved oxygen varies between 6 and 8 ml/l. The change in values between stations 1 and 5 are a reflection of the change in saturation point of O_2 with increasing salinity and decreasing temperature. In contrast, O_2 for the 20 m depth level at these stations is much lower, around 4 ml/l. The gradual rise in O_2 from its lowest values at station 1, about 3.5 ml/l, to 4.9 at station 5 probably reflects the higher BOD (biological oxygen demand) in the more inland stations, probably a consequence of the higher input of organic matter in the fjords zone.

4.2.3. **Tides and Sea Level Factors**

4.2.3.1. Tides.

Figure 22 shows the Sept.-Oct. 1979 predicted tide record from Puerto Montt. The 15 day spring-neap tide range cycle is clearly shown. The largest daily tide range in this period occurred Oct. 6, at 7.2 m between high and low tide levels. Tide range on the previous neap range period, Sept.30, was about 2.3 m. This date-cycle has been chosen to explain a southward flow seen in a CZSC image.

This is rather an extreme fluctuation in sea level between successive spring-neap phases, involving about 5 meters of difference in only 7 days. We make the point here to place into perspective that the phenomenal tides of SAIC make virtually all other sea level changes relatively unimportant. For example, a change of 5 m in height of sea surface over a 7-day period is fully equivalent to the maximum "setup" that can be expected in this SAIC due to wind-storm surge phenomena. Further, changes in sea level due to such phenomena as the El Niño, which involves a few centimeters change at the most, or to the seasonal sea level cycle, also measured in centimeters, are of no consequence against the great tide ranges of the SAIC.

4.2.3.2. Tide Currents and Fronts

For the SAIC, with its very high range of tides, tide currents are the main source of turbulent mixing energy to the water column. Because tide waves are very long wavelength waves, tide-generated currents are almost uniform throughout a water column, regardless of bottom depth; of course, the speed of the tide current increases as the bottom shoals. Vertical mixing within the water column occurs in the bottom boundary layer because of friction (Neshyba, com per).

At some critical shoaling depth the tide-mixed layer will begin to interact with the wind-mixed surface layer. Inshore of this depth line mixing occurs from top to bottom; the water column takes an uniform properties, so that the inshore surface

FIG. 22 a) TIDES AT SENO RELONCAVI, 1979

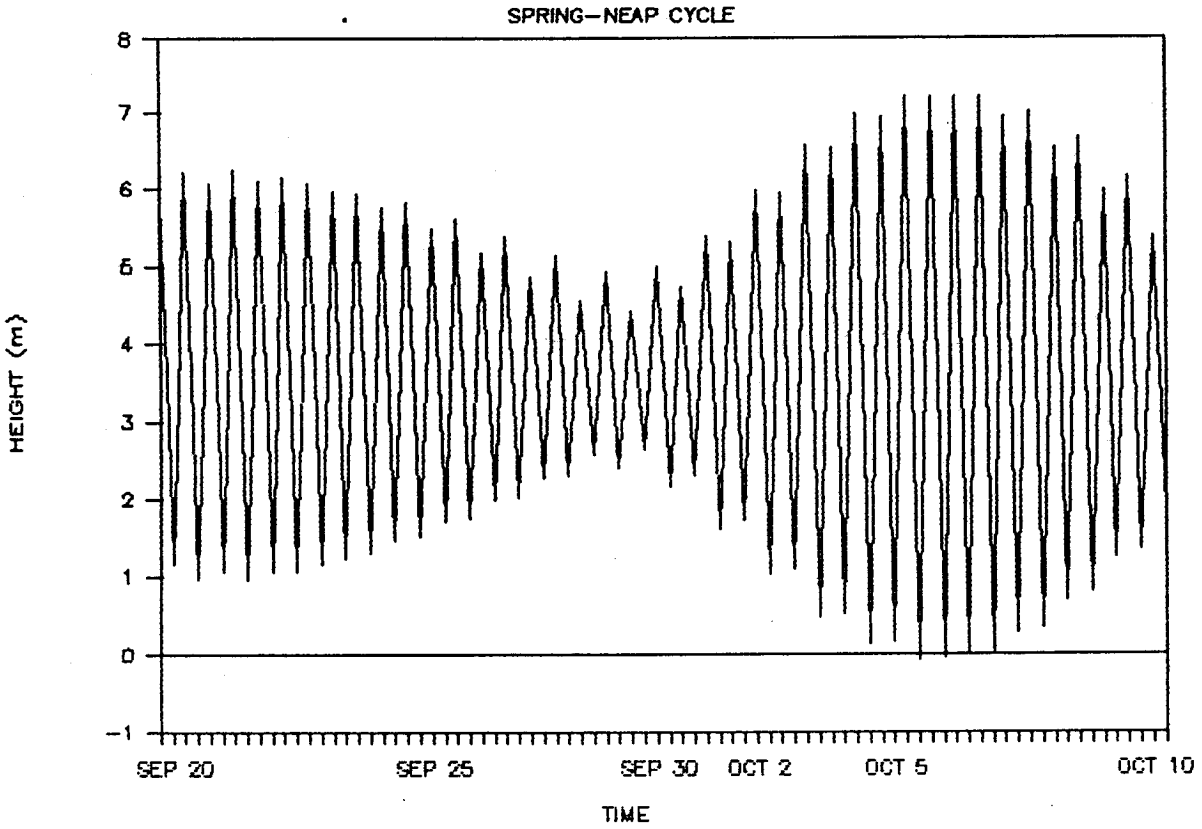

FIG. 22 b) TIDES OF OCTOBER 1 AND 2, 1979

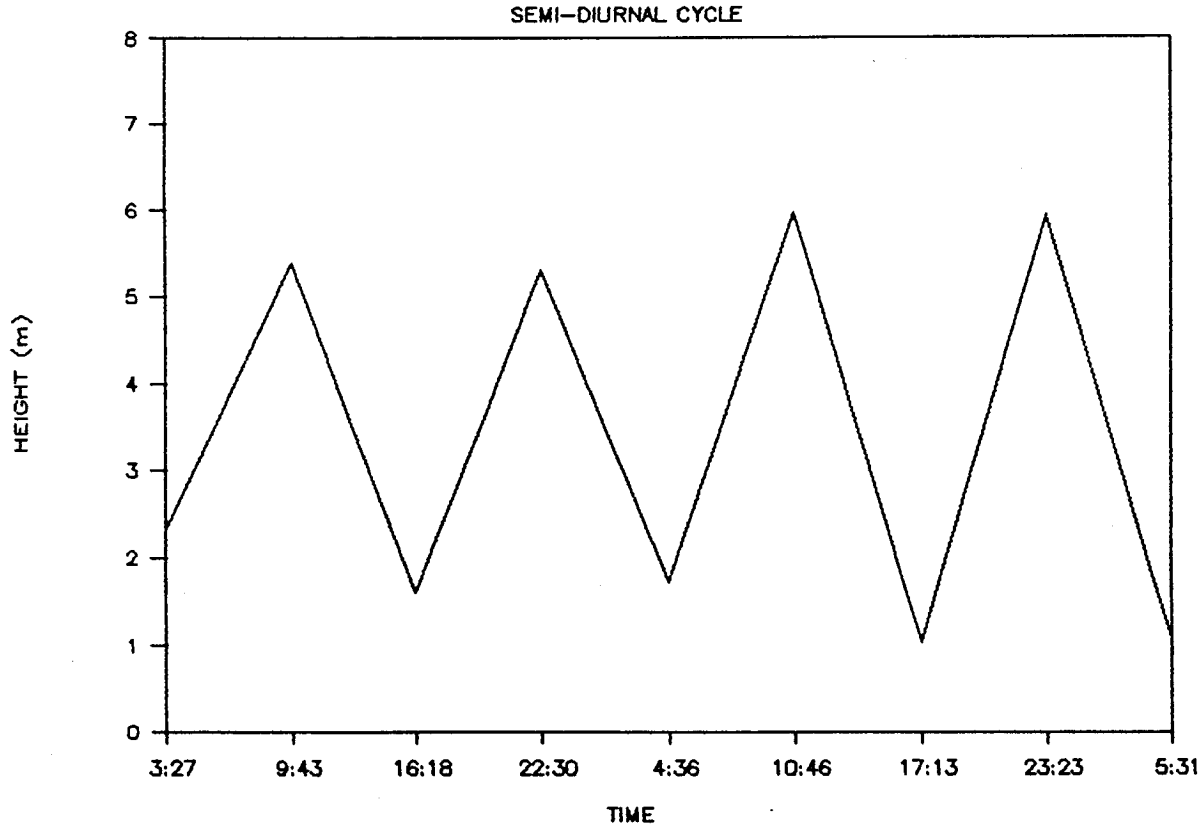

waters drops in temperature as it mixes with cooler bottom layer water. The result is a distinct thermal "front". The actual location of the thermal front and the inshore mixed zone varies widely over space and time. The primary factors that inhibits its formation is the degree of density stratification between the surface layer water and the deeper layer water.

During the fall season, with the drop in solar heating and relative rise in nighttime cooling of surface layer, density differences between surface and lower layer decreases. The wind-mixed layer deepens, especially after fall storms bring stronger winds over the region. The direct result is that the "front" moves offshore, into deeper water. Also, because thermal difference between surface and deeper layers become much smaller during the fall-winter surface cooling, the "mixing front" loses its thermal signature; then, because this is also the season for precipitation, the mixing front may likely take on a salinity "front" characteristic (Neshyba, 1987).

Biological consequences: Pingree et al, (1975) suggested that phytoplankton blooms and particularly red tides events are closely related to frontal boundaries. The conditions for high phytoplankton biomass always accompany the spring processes that promote the thin surface layer, because the prior winter's mixing activity has renewed the nutrients of surface waters. In coastal waters, many phytoplankton species adapt to winter through a benthic resting spore or cyst (Anderson and Keafer, 1985). In shallow waters, these stages return to the water column with the

first rise in light intensity reaching the bottom, and because of the intermixing layers, can rapidly return to the high light intensity surface to begin a new cycle. Typical net phytoplankton species in the SAIC are Nitzschia spp., Thalassiosira spp., Chaetoceros spp., Rhizosolenia spp, S. costatum and among dinoflagellates are Protoperidinium spp., Dinophysis spp., Prorocentrum spp. S. trocoidea (Avaria 1970, Hermosilla 1979, Lembeye and Campódonico 1984, Clément and Guzmán 1988).

4.2.3.3. Speed of the tide wave.

Reference to marine charts of the SAIC provide rough indications of its bottom topography. Depths range upward to about 400 m, with an average around 200 m. As stated in an earlier section of this report, the tide wave requires about 1½ hours to traverse the length of the SAIC. The front of this wave does not proceed as an uniform plane wave, because of the many variations in bottom topography. It is possible to produce a first-order approximation of the progress tide wave across the SAIC using the shallow-water wave equation. We have applied that type of analysis to the Seno Reloncavi, because the entrance to the Seno is so narrow one can treat its tidal excitation as if from a point source, i. e., the Paso Queullin.

Figure 23 shows the propagation of the co-phase contours of a shallow water wave across the Seno. The wave front reaches Puerto Montt about 14 minutes after crossing through Paso

Queullin, and around the same time between Puerto Montt and the mouth of Reloncavi Fjord. Studies of this type have very little application in predicting tide currents, however, because the real currents are complex combinations of wave fronts that are progressive, reflected, or resonant within a sound over the complete tide cycle, not merely the "first" entry wave at the beginning of a cycle. Nevertheless, it illustrates the simple fact that the fastest wave front, and hence the major fraction of tidal transports, occurs along the deepest channels in the SAIC.

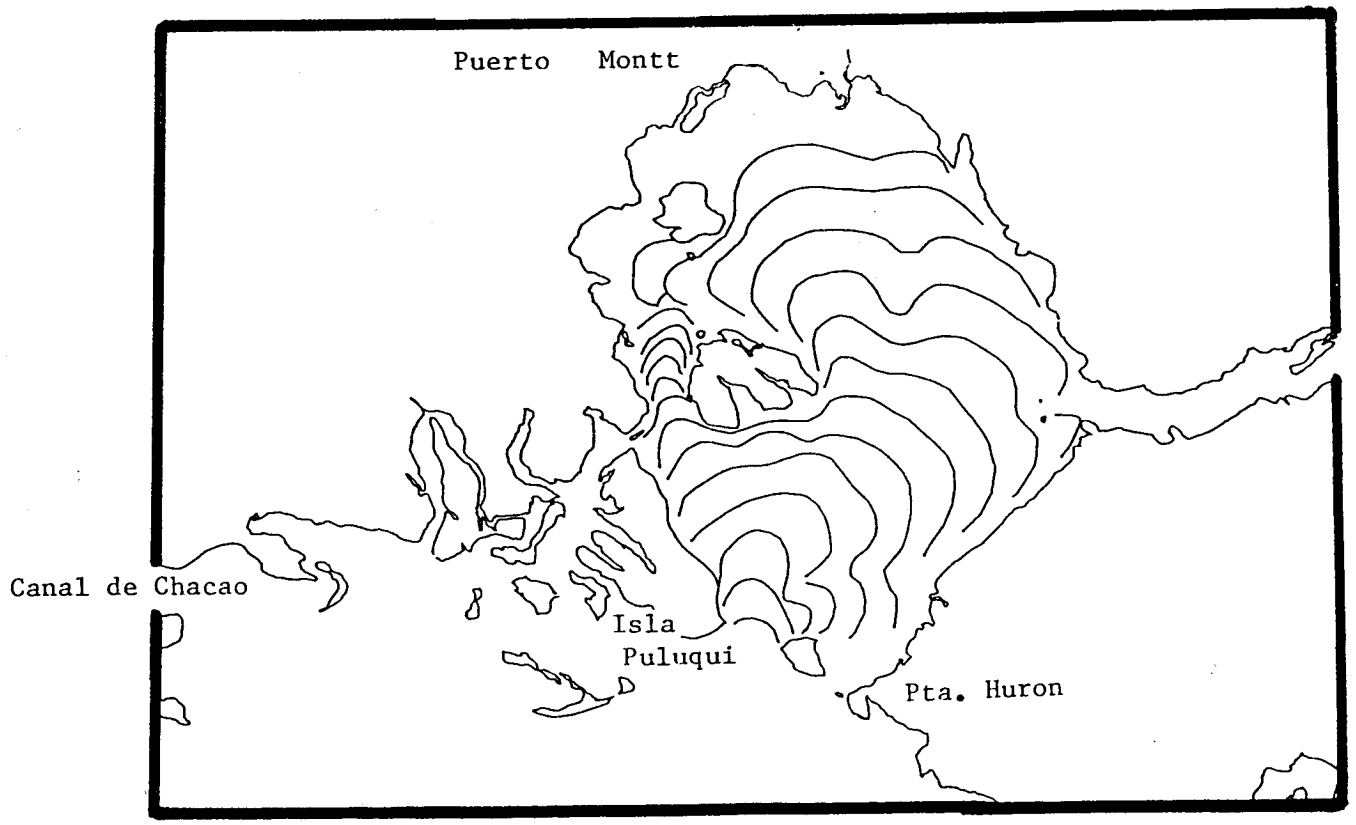

FIG. 23 TIDE WAVE PROPAGATION. CO-PHASE CONTOURS ACROSS THE SENO RELONCAVI.

4.2.3.4. Sea Level Changes in Cage Site Selection

Small variations in monthly sea level do not have large direct effect upon the selection of sites for cage culture (Fig. 24 and 25). Tide currents have much more direct impact on site selection, for reasons of flushing of contaminants, etc., and of the supply of energy for vertical mixing. However, monthly sea level data can reveal clues to circulation pattern within inland waters that short-term current measurements would not. While winds are easily measured, and wind-driven setup calculated from wind stress patterns, only the mean monthly sea level pattern gives a reliable measure of the integrated effect of winds over larger time periods. The thickness of the surface layer limits vertical mixing, for example, can vary over wide limits in response to shifts in wind patterns. And long-term variation in height of the sea surface at the coast entrance to inland waters will also alter the patterns of circulation within the inland regime.

4.2.4 **Phytoplankton cell density and Secchi Disk Depth.**

Clément has reported (Clément and Guzmán, 1988, and unpublished data) simultaneous measurements of Secchi disk depths and density of phytoplankton cells in water samples taken from Canal Tenglo, Puerto Montt, during March 1985, and from Metri, also in Seno Reloncavi, in November 1985 (Fig. 26). The March series of Secchi disc depths was taken during a red tide

FIG. 24 **SEA LEVEL CHANGES AT PUERTO MONTT.**

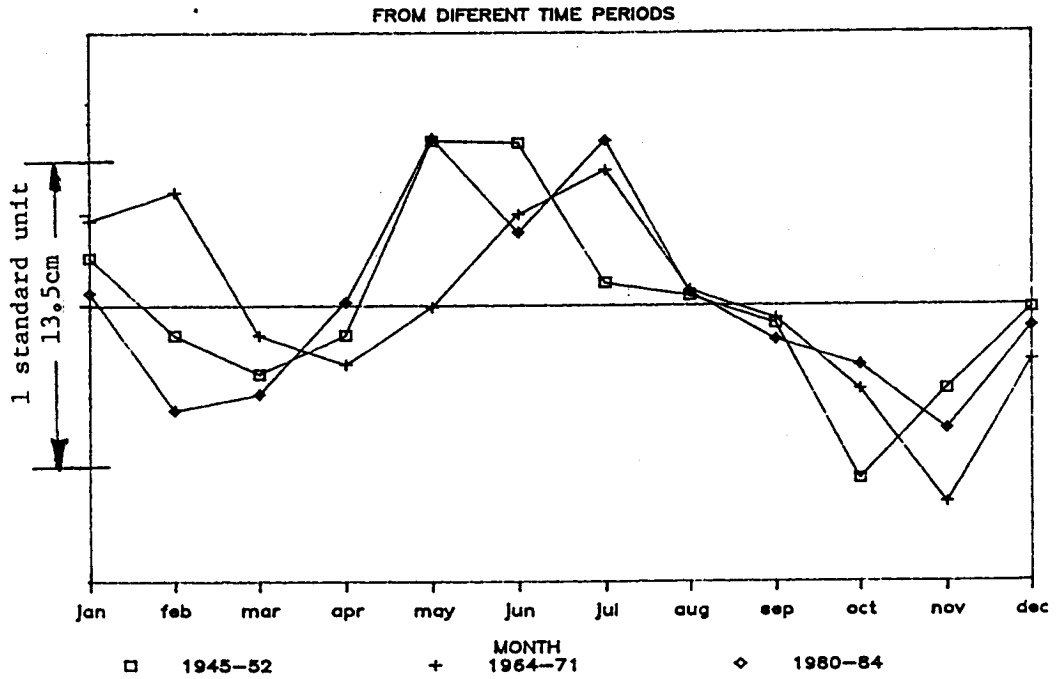

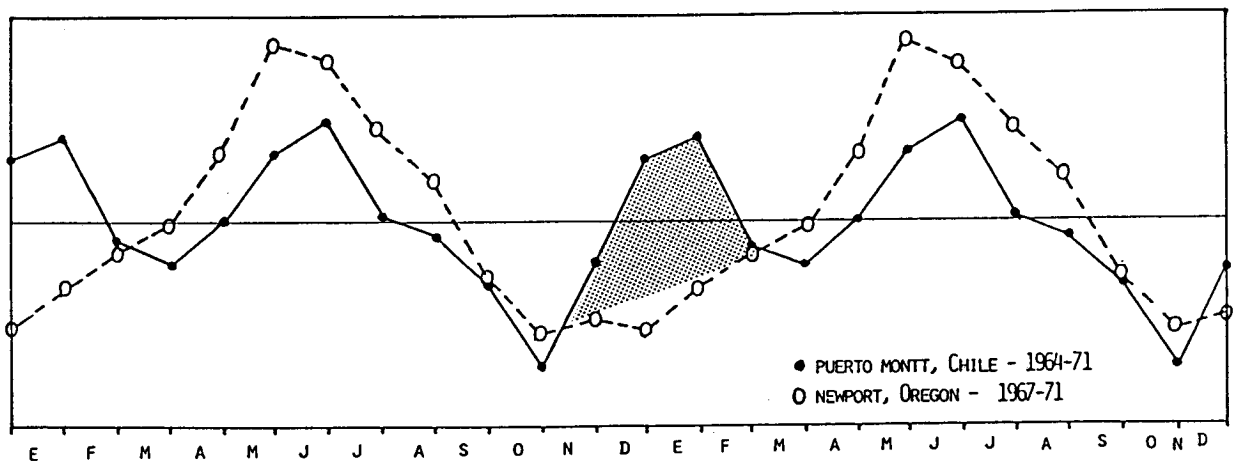

FIG.25 A COMPARISON OF REPEATED ANNUAL CYCLES OF MONTHLY MEAN SEA LEVEL RECORDED AT PUERTO MONTT, CHILE AND AT NEWPORT OREGON; THE OREGON DATA IS SHIFTED SIX MONTHS TO BRING BOREAL-AUSTRAL SEASONS INTO COINCIDENCE AND IS SHOWN AT TWO-THIRDS SCALE.

Oregon Data: Brunson and Elliot, 1974.
Puerto Montt: Clément et al, 1988.

outbreak, over a 5 day period. Samples were taken from within the patch itself as well as outside the patch (as estimated by water color). Figure 26 illustrates one simultaneous Secchi measurement of only 0.5 m depth, together with a phytoplankton cell count of over $13x10^6$ cells per liter from surface water taken at the same time and place. During November 1985, a late spring condition, it shows a Secchi disk depth of 9.5 m together with a corresponding sample cell count of only 35 000 cells per liter.

FIG. **26** SECCHI DISK VARIATION IN SENO RELONCAVI

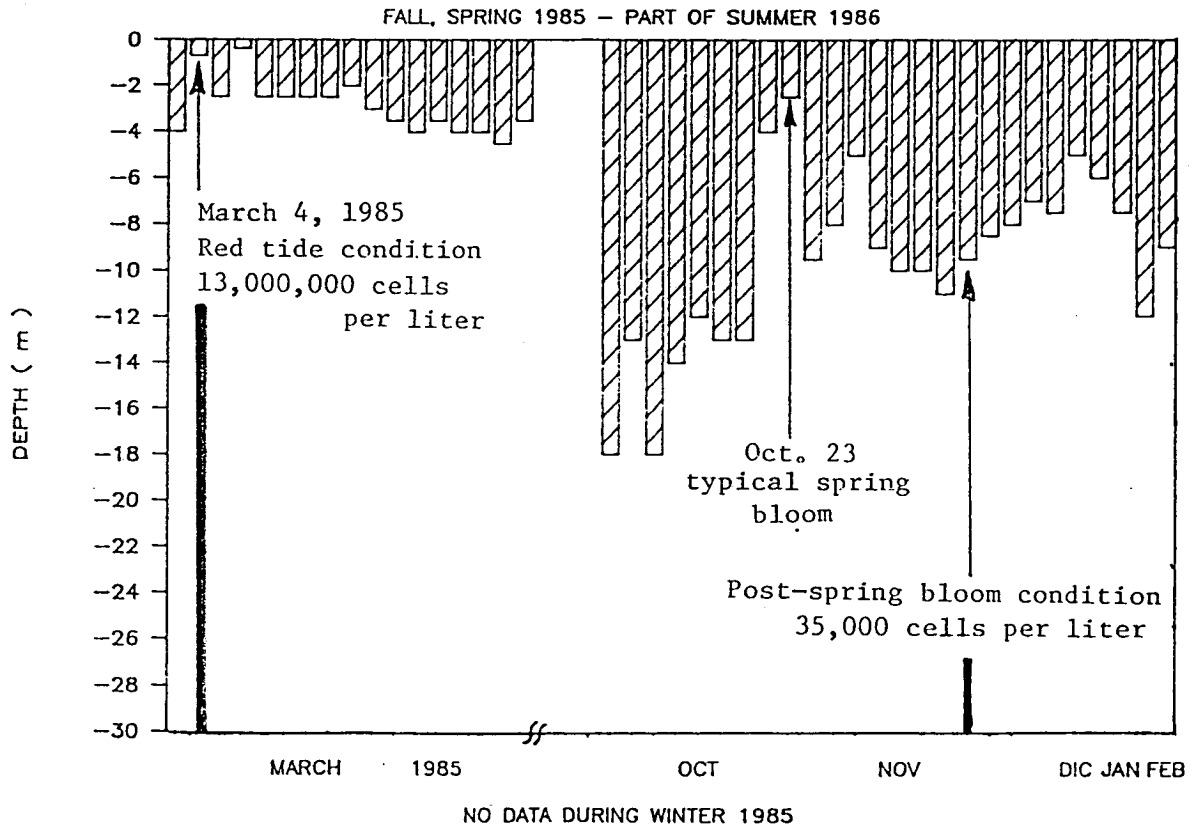

The inverse correlation between Secchi disk depth and phytoplankton cell abundance is quite clear in the above data, and suggests that **operators of cage culture activities** might keep a close watch on water visibility simply by measuring Secchi depths, a very inexpensive monitoring technology. The Oct. 23, 1985 Secchi data, 2.5 m (Fig. 26), represents the visibility level one can expect during a normal spring bloom. However, salmon farmed mortality has been reported at PNIS due to Chaetoceros convolutus at very low cell densities (Rensel, com. per 1988, Gaines and Taylor, 1986).

4.2.5. **Nutrient Distributions in the SAIC**

The vertical distribution of nutrient concentration in the SAIC (Fig 4, for stations) shows a low content in the upper 5 m (< 2 uM in nitrate; < 1 uM in phosphate). At deeper depths, concentrations increase rapidly up to high values at the level of 30 m (> 20 uM in nitrate; > 1.5 in phosphate [Fig. 27 to 30]).

The dissolved oxygen at the surface has values above 6.5 ml/l or above 100% of its saturation point. Below the upper 15 m it decreases to values around 4 ± 0.5 ml/l. Therefore, this deeper water has a relatively low oxygen content with around 60% of its saturation value.

Comparison of SAIC Nutrient Profiles: Open Ocean - Inlet Waters

The vertical distribution of nitrate and phosphate nutrients in the inlets waters, compared to the open ocean off Boca del

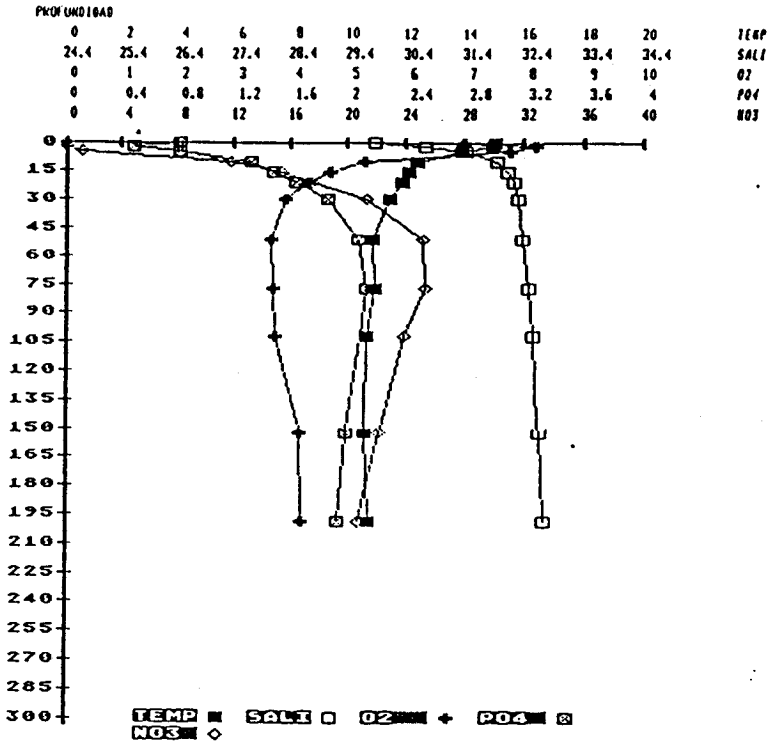

FIG. 27 : VERTICAL DISTRIBUTION OF TEMPERATURE, SALINITY, DISSOLVED OXYGEN and NITRATE AT STATION HUDSON 210 (march 28, 1970)

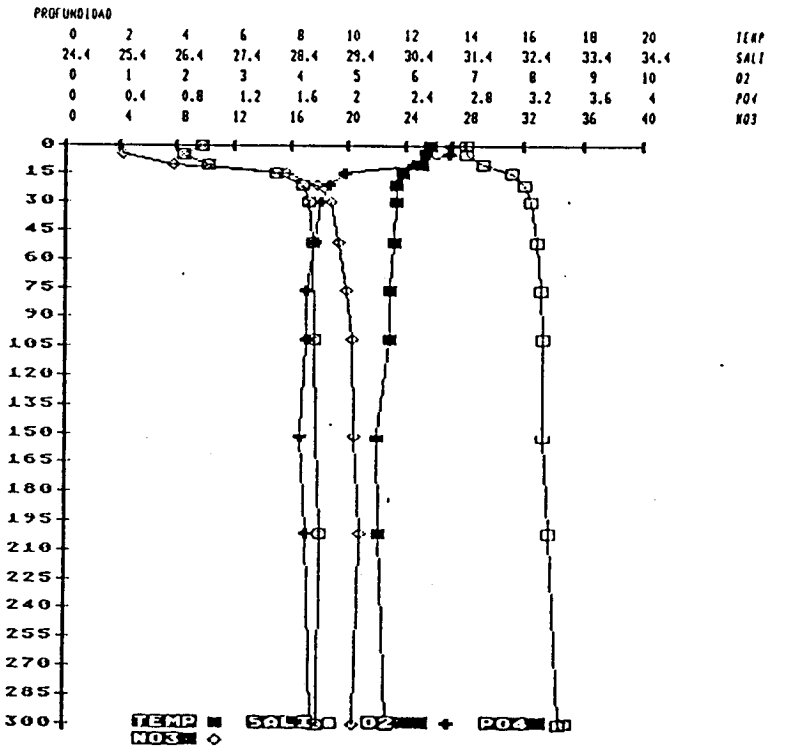

FIG. 28 : VERTICAL DISTRIBUTION OF TEMPERATURE, SALINITY, DISSOLVED OXYGEN and NITRATE AT STATION HUDSON 212 (march 28, 1970)

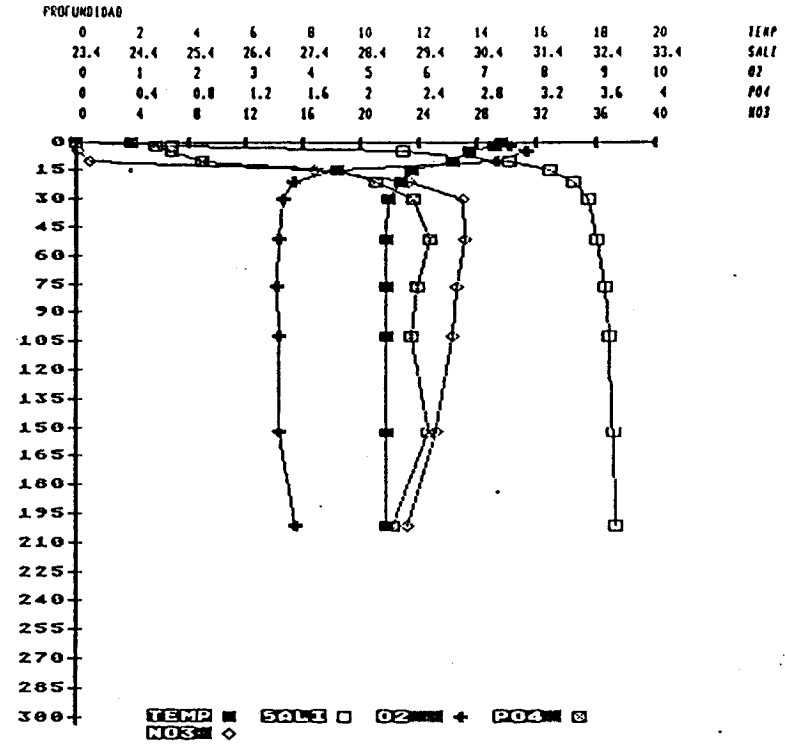

FIG. 29: VERTICAL DISTRIBUTION OF TEMPERATURE, SALINITY, DISSOLVED OXYGEN and NITRATE AT STATION HUDSON 218 (march 28, 1970)

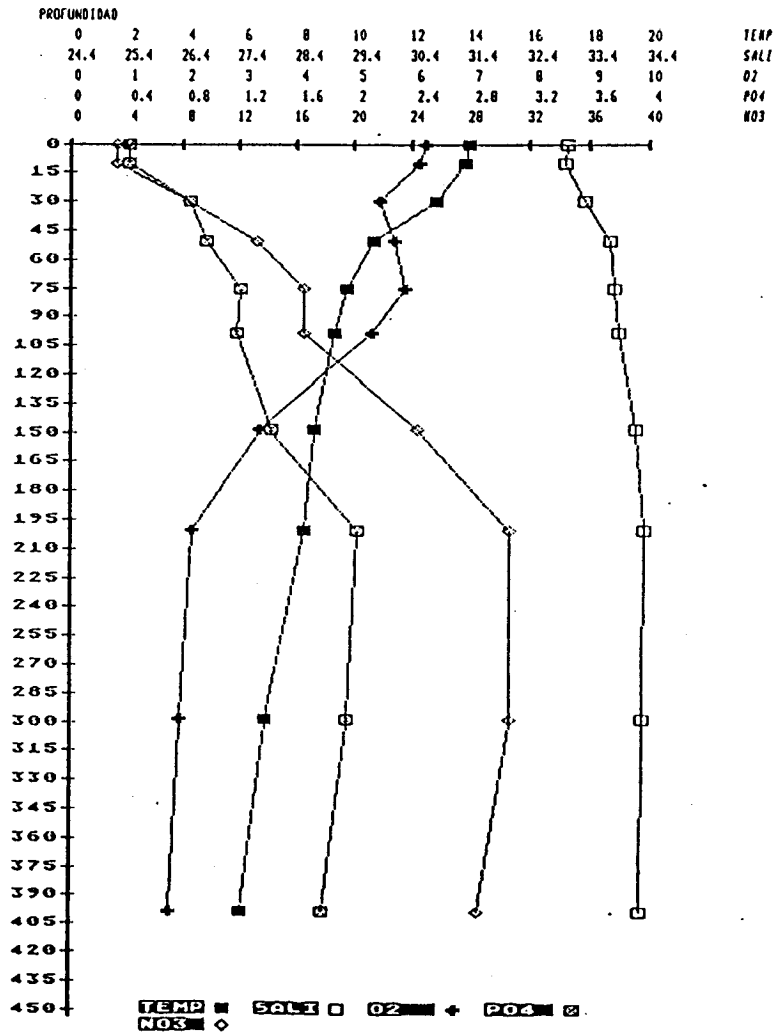

FIG. 30 VERTICAL DISTRIBUTION OF TEMPERATURE, SALINITY, DISSOLVED OXYGEN and NITRATE AT STATION HUDSON 193 (march 26, 1970)

Guafo, is fairly similar as far as the values of maximum concentration reached. However, an important difference is that the inlets waters reach their high values at much shallower depths, 15-20 m, versus 150 m for the open ocean case. A similar situation occurs when comparing the dissolved oxygen vertical distribution (Figs. 27 to 30). According to this, the inlets waters have a high nutritive potential. Nevertheless, any Ekman transport that may be favorable to upwelling will have to break through the stability before it can supply fertilization to the upper 10 m waters.

Nitrate - Phosphate Ratio

The N:P ratio found in the inlets waters is 1:14 which is fairly similar to the accepted Redfield ratio (Redfield, et al., 1963). The regression that associates these variables shows that the nitrate could be the limiting micronutrient (i.e. NO_3^- = -6.85 + 13.73 PO_4^{-3} for Hudson station number 210). In the nearby open waters the N:P ratio changes to 1:18 (station 193), which suggests that the outer waters are richer in nitrate than the inlets waters.

Several factors have been mentioned that affect the dynamics of the SAIC and their influence on phytoplankton blooms. Key factors might be freshwater runoff, light intensity, stratification and nutrients. Data collection and analysis should be carried out as a program to assess the coupling of these factors and phytoplankton biomass in this region.

4.2.6. **Noxious phytoplankton blooms and their effects on marine cage aquaculture:**

The earliest report of noxious phytoplankton blooms affecting marine cage aquaculture are from Japan and Northwestern Europe (In: Okaichi, et al in press, Beveridge, 1987). Salmon cage aquaculture throughout the world is expanding at a rapid rate (Table 1, Fig. 31a and b). Recently the industry worldwide has been seriously affected by phytoplankton blooms, and during this 1988-year Norway, Scotland and Chile suffered one of the largest economic losses (larger than $ 10 million) within world aquaculture (Table 2).

The causes of these blooms are apparently unknown, but it seems that they are related to mesoscale processes (Johannessen and Farrely, 1988). It cannot be stated that it has been enhanced by fish-farming environmental effects. However, there are some facts that need to be studied to explain the high frequency and magnitude of the blooms during this 1988 year. Future research needs to focus on nutrients inputs from sea-farms and how phytoplankton populations response to this new nutrient source. Fish feed is extremely rich in water soluble vitamins and there are several phytoplankton species (auxotrophs) that show increased growth rate from these compounds (Bonin et al 1980). The statement is not that the fish-farm effects are the cause of the recent blooms, but they are probably facilitating the selection and maintenance of species-specific phytoplankton populations.

TABLE 1. WORLD PRODUCTION OF FARMED SALMON, ATLANTIC AND PACIFIC SPECIES

COUNTRIES	1980	1981	1982	1983	1984	1985	1986	1987	TOTAL	1990
NORWAY	4200	8422	10266	17016	22300	28700	45000	55000	190904	80000-100000
U.K.	600	1333	2152	2536	3900	6900	9700	14000	41121	20000
IRELAND		80	103	256	300	700	1200	1600	4239	
ICELAND*		20	30	50	300	600	1300	2000	4300	5000-8000
FAROES IS.		100	130	160	400	700	1200	1800	4490	5000-10000
CANADA (BC)		176	200	220	100	200	577	849	2322	5000-25000
USA **		450	680	900	1000	1400	2000	2400	8830	3000
JAPAN	2000	1150	2122	2900	5000	7000	8000	12000	40172	8000-12000
CHILE		60	184	94	109	500	1144	1821	3912	3000-20000
TOTAL	6800	11791	15867	24132	33409	46700	70121	91470	300290	

* INCLUDE RANCHING ** INCLUDE PEN-SIZED FISHES.

SOURCES: Atkinson, C.E. 1987
Bjordnal, T. 1987
Hannesson, 1987
Lavin and Anderson, 1986
Ruckes, E. 1987
SERNAP, 1987.

TABLE 2

REPORTED MARINE PHYTOPLANKTON BLOOMS AFFECTING SALMON FARMING WORLDWIDE

COUNTRY	DATE	SPECIE	REFERENCE
NORWAY	1966	Gyrodinium aureolum	In: Tangen, 1977
	1976	G. aureolum	Tangen, 1977
	MAY 1988	Chrysochromulina polylepis	Wallentius, 1988
SCOTLAND	1980	Gyrodinium aureolum	Jones, et al 1982
	MAY 1988	Phytoflagellate	Red Tide Newsletter 3
	JULY 1988	Chaetoceros	Red Tide Newsletter 3
IRELAND	1978	Gyrodinium aureolum	In: Jones, et al 1982
CANADA (B.C.)	1986	Heterosigma akashiwo	Taylor, F.J.R. com. per.
	MAR.1987	Chaetoceros convolutus	Red Tide Newsletter 2
	OCT. 1987	Chaetoceros convolutus	Red Tide Newsletter 2
USA (Puget Sound)	NOV. 1987	Chaetoceros convolutus	NRAC workshop
CHILE (SAIC)	APR. 1983	Prorocentrum micans	Lembeye and Campodonico, 1984
	SEP. 1988	Phytoflagellate	Muñoz com. per.
FAROES IS. (DENMARK)	JUL.1984	Gonyaulax excavata (=Alexandrium excavatum)	Mortensen, 1985

Japan has been excluded, however they have serious problem with red tides events and massive fishkills (yellow tail).

FIG. 31 a) WORLD SALMON FARMING PRODUCTION

AND COUNTRIES PRODUCERS LEADER.

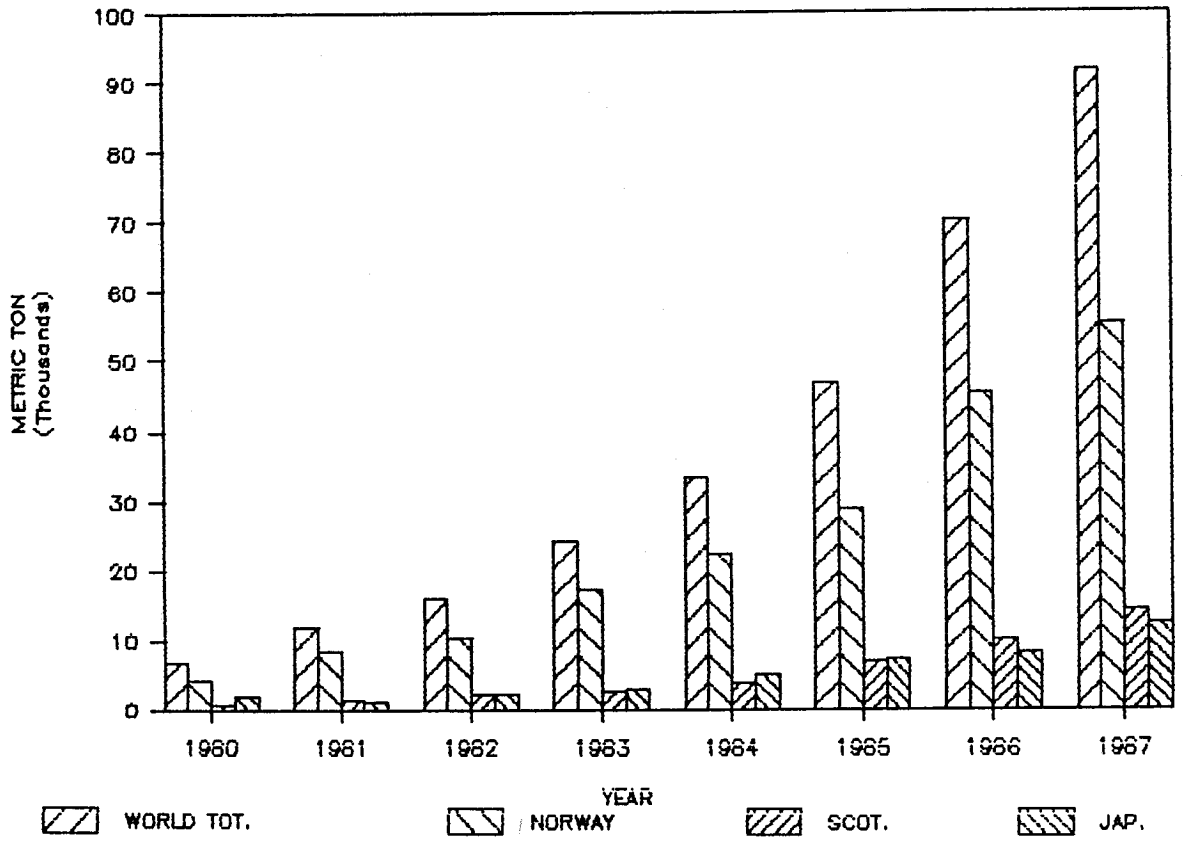

FIG. 31 b) FARMED SALMON PRODUCTION

BY OTHER IMPORTANT COUNTRIES.

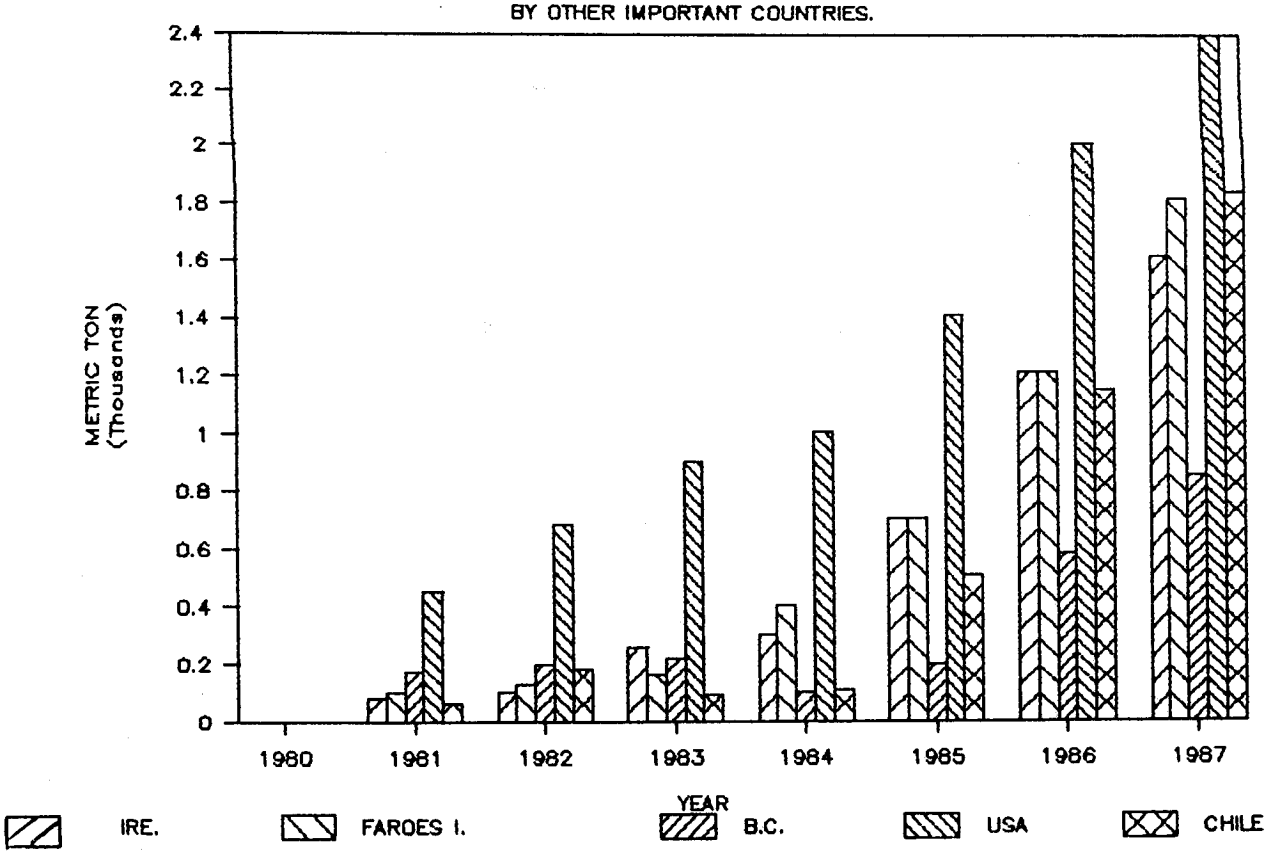

An extremely unusual phytoplankton bloom recently (Sept. 1988) ocurred in the SAIC (Muñoz and Alvial, 1988, Larrain com.per.) caused by a non-identified small phytoflagellate (< 5 u). This specie has never before been reported as an important component of the plankton (Avaria, 1970, Guzmán and Campodónico, 1975 and 1978, Hermosilla, 1979, Lembeye et al 1981, Rivera and Cox, 1982, Lembeye and Campodónico, 1984, Winter et al, 1984, Clément and Guzmán, 1988), probably due to its size and occasional sampling of the area. It seems that unusual winter-spring transition conditions were the key factors of the recent event.

Accordingly, key oceanographic and meteorological trends of Southern Chile , need to be studied as a base line of "normal" years or seasons, as well as their scales of variability.

To minimize the salmon mortality in Southern Chile due to noxious phytoplankton blooms it is neccessary to understand the basic physical and chemical conditions of the system that intensify the biological processes. Near real time reliable taxonomic identification of the species causing the blooms is a task that Chilean marine biologist need to challenge quickly. Then, we can significantly improve our management strategies.

4.3.REMOTE SENSING

Satellites ocean color is 10 years old this year. The Coastal Zone Color Scanner (CZCS) was launched on the Nimbus-7 satellite in October 1978, as a 1-year-proof-of-mission, however,

was turned off in 1986 with no plans for a replacement. Fig. 32a and b show the general description of the satellite and optical configuration of the sensor.

Several bio-optical studies were carried out before the launch of CZCS (Jerlov and Nielsen, 1974, Smith and Baker, 1978, Clark et al 1980, Austin, 1980). Descriptions of the systems, imagery and algorithms have been studied intensively during the last decade by different groups (Hovis, et al 1980, Gordon et al 1980, Smith and Wilson, 1981, Gordon et al 1983, Gordon and Morel, 1983, Guan et al 1985, Platt 1986).

Spatial and temporal variability of phytoplankton pigment concentrations have been studied for the North Pacific eastern boundary current (Abbott and Zion, 1987, Denman and Abbott, 1988, Pan, et al 1988, and Uribe and Neshyba 1983) for the South Pacific eastern boundary current. In general, these images show the complexity of the chlorophyll field and both eastern boundary currents show coastal upwelling, high pigment concentrations and eddies.

A spring bloom of the North Atlantic was studied by Brown et al (1985) using ship and satellites data, and phytoplankton pigments spatial distribution of the continental shelf waters off southeastern U.S. have been examined by Yoder et al (1987). Carder and Stewart (1985) have studied mathematical models that simulate the spectral curves of remote-sensing reflectance of dinoflagellate blooms, in the case 2 waters along west Florida shelf during high pigment concentration events.

a)

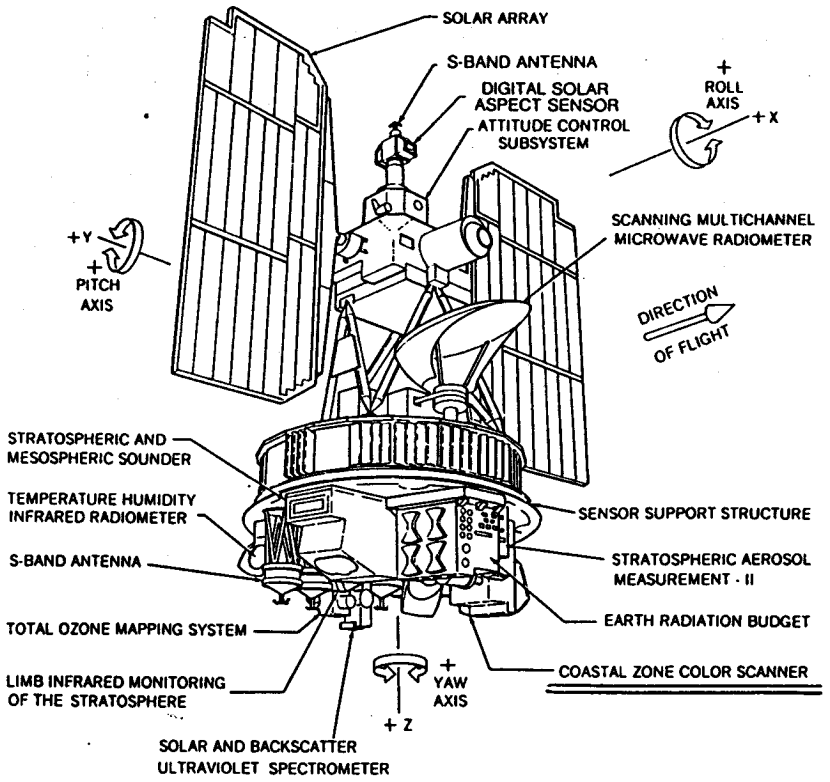

b)

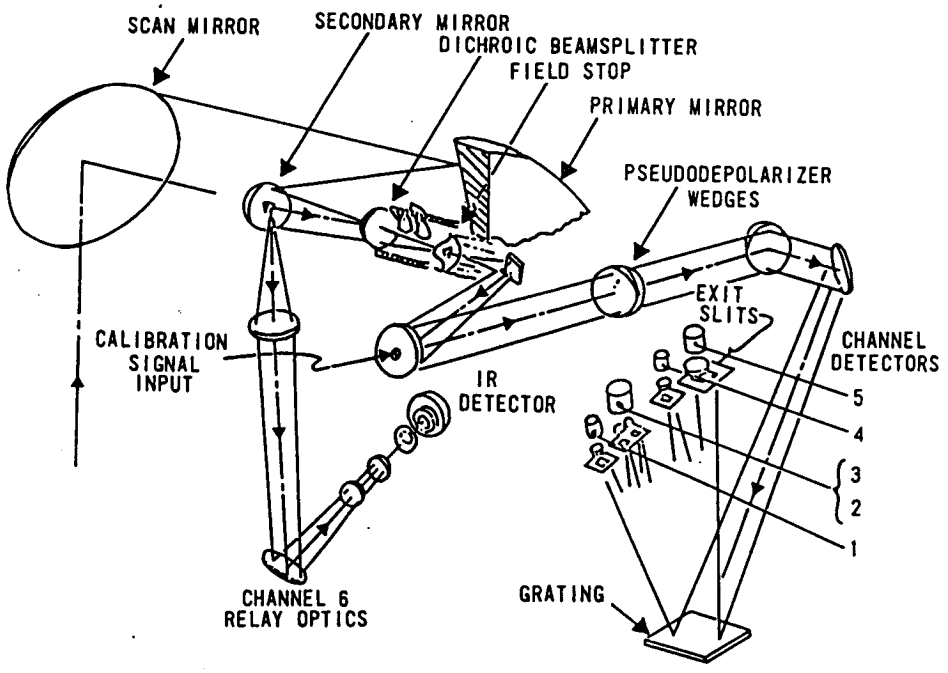

FIG. 32. NIMBUS-7 OBSERVATORY, NOTE COASTAL ZONE COLOR SCANNER SENSOR (CZCS) a) CZCS OPTICAL ARRENGEMENT b)
From NASA 1978, Madrid (ed.)

4.3.1. Simple Bio-optics basis for Estuarine Remote Sensing:

Chlorophyll and dissolved organic pigments (DOP) absorb strongly at blue and violet wavelengths (< 500 nm) and chlorophyll-a also absorbs red light at 670 nm (Fig. 33b). For sediments, absorption depends on several factors. Iron oxide compounds absorb blue and violet light much like DOP. Scattering tends to be achromatic when a mixture of sizes is present, with a slight decrease corresponding to increasing wavelength (In: Stumpf, 1987).

The strong absorption by water at long wavelengths means that clear water will have negligible reflectance in red and near-IR light (Fig. 33a). This is generally true in oceanic waters. This red absorption together with the strong scattering of blue light by very clear oceanic waters results in the characteristic blue of the open ocean. As DOP is relatively low and constant in concentration in the ocean and the only particulates are plant cells, chlorophyll can easily be detected because it reduces the blue light reflectance, turning the water a turquoise or mint green. Clear water has $b_b > a$ for blue light (a is the absorption and b_b is the backscatter coefficients respectively), whereas chlorophyll-bearing water has $a > b_b$. Morel and Prieur (1977) have develop a simple expression for irradiance reflectance

$$R(L,z) = E_u(L,z) / E_d(L,z)$$

$$= 0.33\, b_b(L,z) / a(L,z)$$

where R (L,z) is the spectral reflectance (irradiance ratio), Eu (L,z) is the upwelling irradiance (W m^{-2} nm^{-1}), and Ed (L,z) is the downwelling irradiance at depth z in the ocean and at L wavelength, in nanometers. R (L,0) is closely related to the spectral remote-sensing reflectance RRS (L):

$$R_{RS}(L) = L_w(L) / E_T(L)$$

where Lw (L) is the upwelling spectral radiance (W m^{-2} sr^{-1} nm^{-1}) that emanates from below the sea surface, and ET (L) is the total downwelling irradiance (solar + sky) at the sea surface.

Chlorophyll has a minimum effect on the green light reflectance, therefore a ratio of reflectance of blue light to green light will show the chlorophyll concentration. This behavior is the basis for CZCS chlorophyll algorithm (Gordon et al, 1983, Gordon and Morel, 1983).

$$C_S = a\,(R_{ij})^{b}$$

where

$$R_{ij} = L_w(L_i) / L_w(L_j)$$

For instance, the ratio R13 = Lw (443) / Lw (550) is the most common algorithm to estimate pigment concentration when Cs < 1.5 mg/m^3. However, coastal waters tend to have Cs ≥ 1.5 mg/m^3, therefore the algorithm switch to

$$R_{23} = L_w(520) / L_w(580)$$ (Gordon et al, 1983, Gordon et al, 1980).

In estuaries and near-coastal waters, the situation is much different. DOP and sediments with their iron content occur in much higher and more variable concentrations. Therefore a

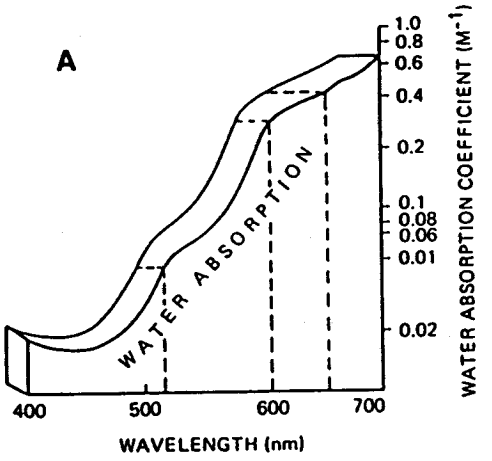

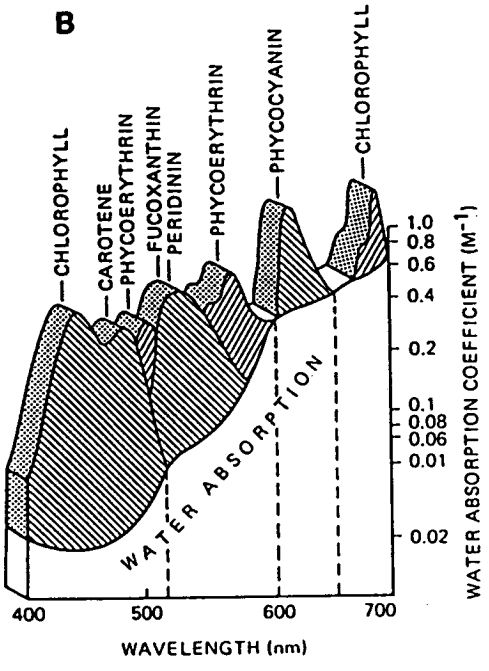

FIG. 33.

. Absorption of light: (a) by water absorption, (b) by different algal pigments in the windows of 'clarity' of water; the spectra for the pigments approximate those measured *in vivo*; fucoxanthin and peridinin are superimposed (Yentsch and Yentsch, 1984).

C) CZCS SPECTRAL RESPONSE

FOR CHANNELS 1 THROUGH 5

From NASA 1978, Madrid (ed.)

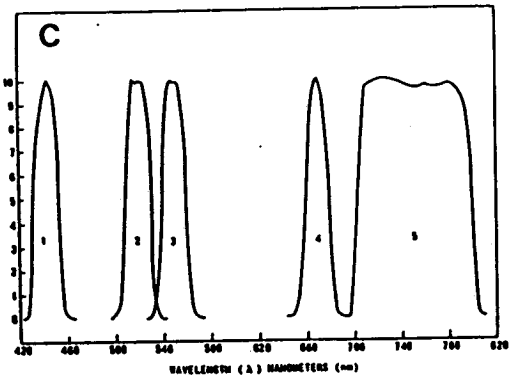

blue/green reflectance ratio is ineffective for measuring chlorophyll. The comparatively high and variable DOP and chlorophyll content and the potential iron component reduce the reflectance at shorter wavelengths, producing a maximum reflectance between 550-650 nm (yellow or orange light). In case of extremely high sediment loads (> 200 mg/l) the maximum reflectance maybe in the red (650-700 nm and near-IR > 700 nm) wavelengths. Hence sediment laden coastal waters have a milky brown appearance (Stumpf, 1987).

Within the SAIC the seasonal sediment loads might be less "noisy" for chlorophyll remote sensing sensors than in the above systems (i.e., Chesapeake Bay, Delaware Bay; plain estuaries). The SAIC is a fjordic-estuary system and the other systems are shallow estuaries. A deeper, larger and almost negligible anthropogenic input is an advantage from a remote sensing viewpoint. This could demonstrate that some gulfs (e.g. Golfo de Ancud) could be adequate targets, as well as the Juan de Fuca Strait for PNIS.

Application of different visible and near IR sensors to the La Plata River estuary (Argentina) have been summarized by Gagliardini et al (1984). Their results indicate that each sensor contributes a different kind of information that complements each other type and, if used as a set, will provide a better understanding of the estuaries.

Stumpf (1987) has studied AVHRR satellite data applied to sediment and chlorophyll in turbid coastal waters. His algorithms

include correction for atmospheric effects and calculation of reflectance, thereby allowing interscene comparison and even comparison of data collected with different sensors. Stumpf and Tyler (1988), found a technique to estimate chlorophyll content using the AVHRR and CZSC sensors on the Chesapeake Estuary, thereby having a potential to integrate the temporal resolution of the AVHRR with the spatial detail of others sensors, including those onboard of LANDSAT and SPOT. However, this will be to high cost effective. The following table illustrates a general comparison of sensor characteristics.

Table 3. Comparison of Sensor Characteristics

SATELLITE	NOAA-n	LANDSAT-n		SPOT	NIMBUS-7	MOS-1**
SENSOR	AVHRR	MSS	TM	HRV*	CZCS	MESSR
Resolution (km)	1.1	0.08	0.03	0.02	0.82	FOV (5°) altitude
Frequency (days)	0.5-1	16	16	26*	3-5	17 909 km
Scene width (km)	2000	180	180	60	1500	
# of bands						
reflected	2	4	4	3	5	
thermal	3	0	2	0	1	
Radiometric resolution per count						
red band	0.052	0.131	0.081	0.04	0.005	
near IR band	0.034	0.115	0.084	0.055	0.093	
($mW\text{-}cm^{-2}um^{-1}sr^{-1}$)						
Saturation radiance						
red band	50	17.9	20.4	10.2	2.9	
near-IR band	33	14.8	20.6	14	23.9	
($mW\text{-}cm^{-2}um^{-1}sr^{-1}$)						
Coastal general application	SST maps	coastal water mapping water sed. distr.		ocean color	coastal water mapping water sed. conc. turbid water mapping SST	

* The HRV sensor can be pointed upon request, therefore, an area can be image several times during a cycle.

** Recently launched Japanese sat. with three sensors on boaboard (VTIR and MSR), but limited to estearn world (Japan and Northern Australia)

Sources: Modified from Stumpf, 1987 and EOSAT. 2, 1987.

4.3.2. British Columbia Imagery Data:

The imagery data obtained from CZCS of B.C. water has been tabulated in table 4, according to the tiles tape labels, and filenames in MicroVAX and SUN systems respectively. Some images are shown on the Appendix.

Estimated pigments data from the three different regions of B.C. (Queen Charlotte Strait, Strait of Georgia, and Juan de Fuca Strait; Fig.3 and 7) have also been summarized in Tables 5, 6, and 7 according to date, percentage of pixels within the range (WCTS 1987), and the statistical parameters.

Despite the high standard deviation, which was expected due to the limitations of CZCS for inland marine waters, some results are useful for future analysis of the region using water-leaving irradiance.

Queen Charlotte Strait shows at its mouth, a high coefficient of variation of high pigment values (Fig. 34). The presence of "V" shape features are probably due to effects of shallow waters, and/or glacial runoff (see Appendix 3.2). Moreover, Queen Charlotte Strait ($\approx$ 51 ° N) has a more limited number of day of cloud-free. This may not be important because Queen Charlotte Strait only contains about 3.4 % of the salmon sea-farms in operation in B.C. (Anon.), whereas the concentration of farms are found in the Strait of Georgia area (Fig. 2)

Imagery data from the Juan de Fuca box has the lowest

TABLE 4

SELECTED TILES AND FILES FROM OSU OCEANOGRAPHY INVENTORY OF CZCS CHLOROPHYLL DATA. SELECTED FILES FOR DIGITAL IMAGE PROCESSING.

TAPE LABEL	MICROVAX II VMS (OSUVAX) FILENAME	SUN UNIX SYSTEM FILENAME	JULIAN	PERCENTAGE CLOUD-FREE
TC8108	C8118419C.RMG	81184C.DAT	81184	85
TC8109	C8125619C.RMG	81256C.DAT	81256	95
TC8109	C8125619F.RMG			86
TC8109	C8125619G.RMG	81256G.DAT	81256	84
TC8204	C8214419G.RMG	82144G.DAT	82144	80
TC8204	C8214719C.RMG	82147C.DAT	82147	99
TC8205	C8223018G.RMG	822308G.DAT	82230	79
TC8207	C8227219C.RMG	82272C.DAT	82272	80
TC8207	C8227219F.RMG			97
TC8207	C8227219G.RMG	82272G.DAT	82272	99
TC8207	C8227319F.RMG			77
TC8207	C8227319G.RMG			99
WTC306	C8313219C.RMG	3219C.DAT	83132	40
WTC306	C8313219G.RMG	3219G.DAT	83132	98
WTC308	C8314218C.RMG	4218C.DAT	83142	99
WTC308	C8314218G.RMG	4218G.DAT	83142	22
WTC307	C8321719F.RMG			50
WTC307	C8321719G.RMG	1719G.DAT	83217	96
WTC307	C8323019C.RMG	3019C.DAT	83230	81
WTC307	C8323019F.RMG			82
WTC307	C8323019G.RMG	3019G.DAT	83230	98
WTC310	C8326319C.RMG	6319C.DAT	83263	34
WTC310	C8326319F.RMG			93
WTC310	C8326319G.RMG	6319G.DAT	83263	99
WTC310	C8326419C.RMG	6419C.DAT	83264	51
WTC310	C8326419F.RMG			98
WTC310	C8326419G.RMG	6419G.DAT	83264	99
WTC310	C8327319F.RMG			59
WTC310	C8327319G.RMG	7319G.DAT	83273	99

BLANK SPACE MEANS DELETE FILES
G: COVER JUAN DE FUCA AND GEORGIA STRAITS
C: COVER QUEEN CHARLOTTE STRAIT AND SOUTH PART OF SOUND
F: COVER OFF-SHORE SOUTHERN VANCOUVER ISLAND

TABLE 5

STATISTICAL PARAMETERS OF PIGMENT CONCENTRATION OF CZCS FROM JUAN DE FUCA STRAIT

BOX COORDINATES (180,168,228,180) TOTAL PIXELS=637

DATE	JULIAN	COUNT RATIO	%	CHLOR (mg/m^3)	SD	C.V *100
SEP-13	81256	637/637	100	3.17	0.97	0.31
AUG-18	82230	634/637	99.5	4.42	1.02	0.23
SEP-29	82272	637/637	100	3.04	1.01	0.33
MAY-12	83132	631/637	99.0	1.90	0.58	0.30
MAY-22	83142	636/637	99.8	2.77	0.51	0.19
AUG-5	83217	535/637	83.9	0.91	0.40	0.44
AUG-18	83230	630/637	98.9	4.73	1.27	0.27
SEP-20	83263	636/637	99.8	3.40	1.06	0.31
SEP-21	83264	632/637	99.5	5.85	2.80	0.48
SEP-30	83273	632/637	99.2	2.37	0.85	0.36
GREAT MEAN				3.26		0.32
GREAT S.D				1.37		0.08

TABLE 6

STATISTICAL PARAMETERS OF PIGMENT CONCENTRATIONS OF CZCS FROM QUEEN CHARLOTTE STRAIT

BOX COORDINATES (156,384,228,420) TOTAL PIXELS=2701

DATE	JULIAN	COUNT RATIO	%	CHLOR (mg/m^3)	S.D.	C.V. *100
JUL-3	81184	1963/2701	72.6	1.86	2.17	1.17
SEP-13	81256	1145/2701	42.3	3.4	2.756	0.81
MAY-27	82147	2522/2701	93.3	3.62	2.63	0.73
SEP-29	82272	2555/2701	94.5	3.6	3.44	0.96
MAY-12	83132	523/2701	19.4	1.69	1.03	0.61
MAY-22	83142	153/2701	5.7	3.74	3.94	1.05
AUG-18	83230	2569/2701	95.0	4.73	2.36	0.50
SEP-20	83263	2221/2701	82.2	10.70	7.37	0.69
SEP-21	83264	2159/2701	79.9	12.31	8.25	0.67
GREAT MEAN				5.07		0.80
GREAT S.D.				3.57		0.21

TABLE 7

STATISTICAL PARAMETERS OF PIGMENT CONCENTRATIONS OF CZCS FROM STRAIT OF GEORGIA

BOX COORDINATES (96,73,160,85) TOTAL PIXELS=845

DATE	JULIAN	COUNT RATIO	%	CHLOR (mg/m^3)	SD	C.V*100
SEP-13	81256	556/845	65.8	3.22	3.18	0.99
MAY-24	82144	697/845	82.5	6.61	5.43	0.82
AUG-18	82230	765/845	90.5	7.01	4.54	0.65
SEP-29	82272	634/845	75.0	5.42	5.43	1.00
MAY-12	83132	767/845	90.0	3.06	2.50	0.82
MAY-22	83142	655/845	77.0	3.21	3.44	1.07
AUG-5	83217	443/845	52.4	1.22	1.34	1.10
AUG-18	83230	754/845	89.2	4.18	2.24	0.54
SEP-20	83263	765/845	90.5	3.76	3.39	0.90
SEP-21	83264	493/845	58.0	7.62	8.05	1.06
SEP-30	83273	668/845	79.1	4.29	2.80	0.65
GREAT MEAN			77.3	4.51		0.87
GREAT S.D			12.8	1.86		0.18

FIG. 34. PIGMENT CONCENTRATIONS AT QUEEN CH.STR.

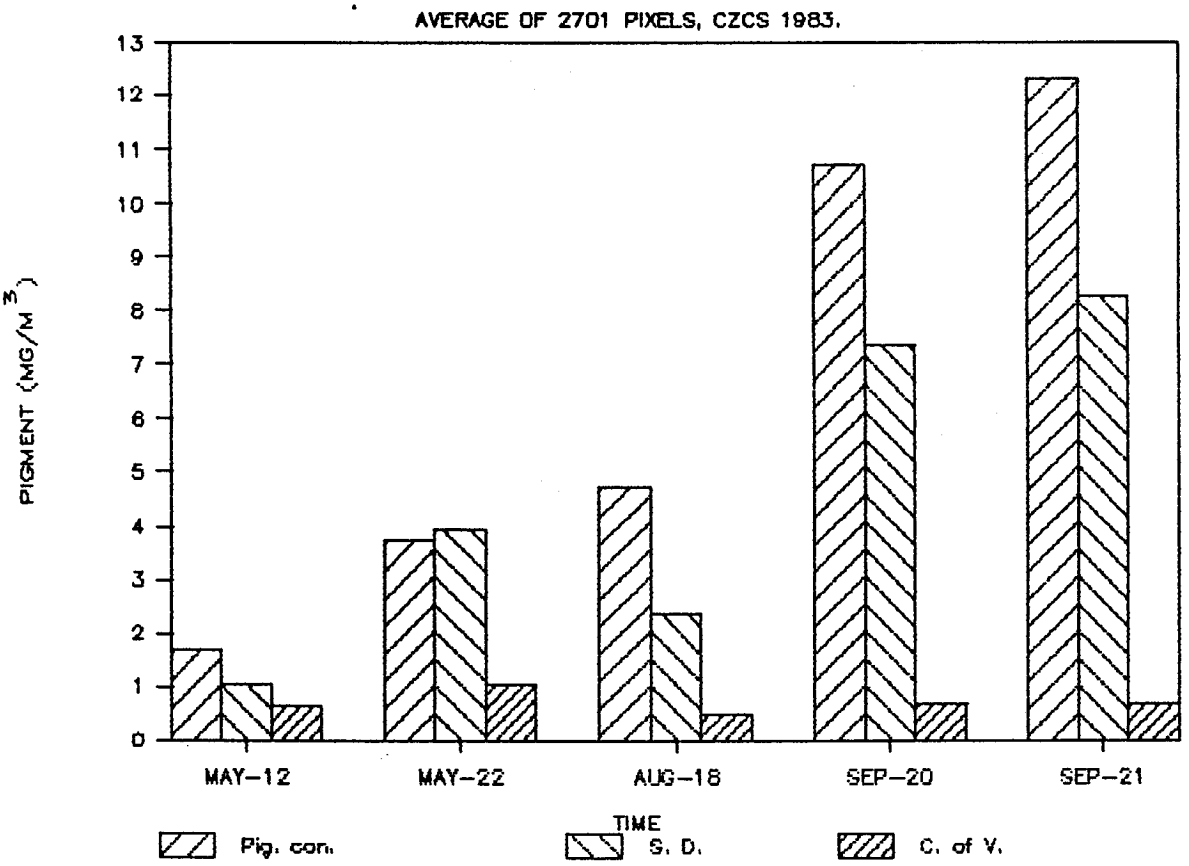

FIG. 35. PIGMENT CONCENTRATIONS AT JUAN DE FUCA

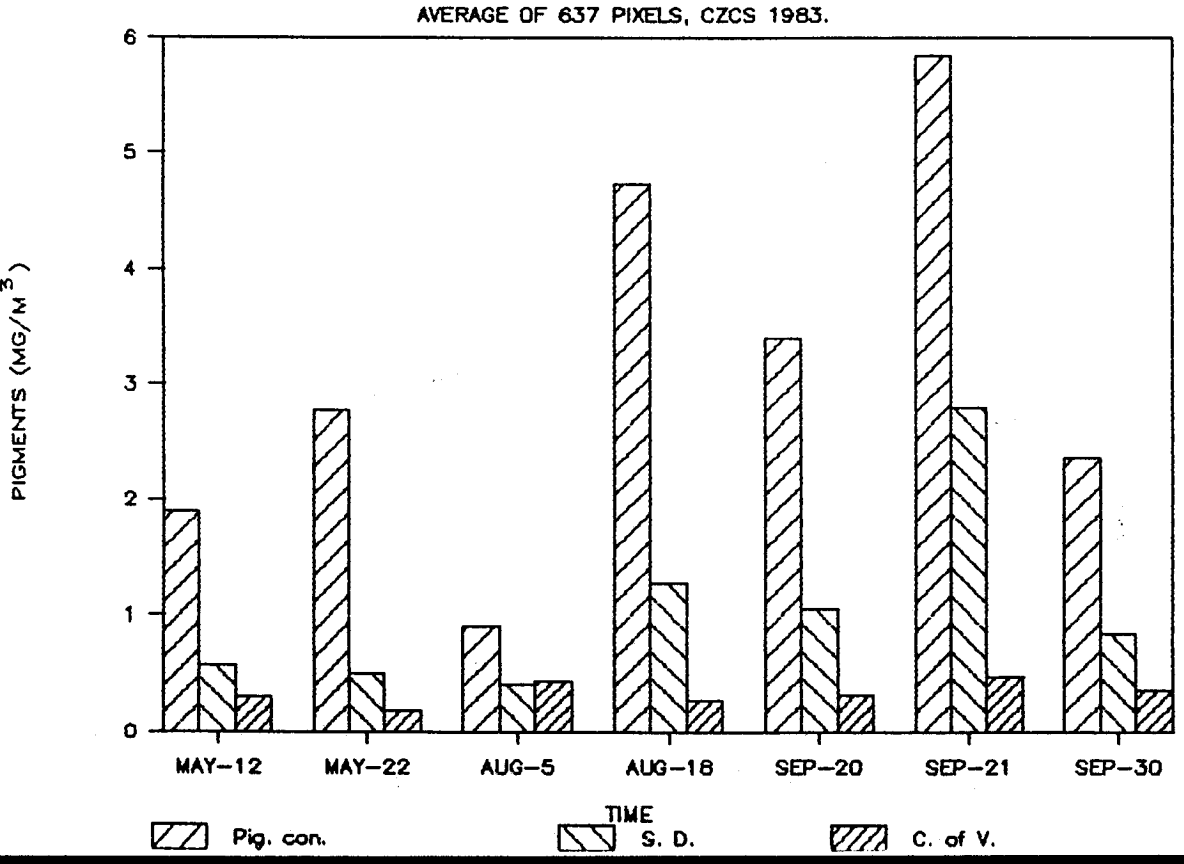

variability, with a coefficient of variation value (for each box) no larger than 48%, a great mean of 32% (the mean of the entire boxes available) and ranges from 19% to 48% (Table 5, Fig. 35).

The Strait of Georgia which is about 110 Km north of the Juan de Fuca Strait, is a more closed-system, with a deeper basin and with stronger reflectance effects due to the Fraser river constituents. All of its coefficient of variation values are larger than 50%, with a great mean of 87% and ranges from 54% to 110% (Table 7, Fig. 36).

The different radiance values of the CZCS sensor within a small region of this inland marine waters (PNIS) is important. Assuming, that the coefficient of variation of pigment concentrations is a reliable index to assess the relative response of the phytoplankton in the area, then it can be stated that **spatially** the Juan de Fuca Strait, is the more stable and presents less variability than the rest of the inland waters of the B.C. system. Therefore, it can be used as a target to understand the **temporal** pattern of phytoplankton using radiometer remote sensing sensors.

On the other hand, Fig. 37 shows the temporal variability within the area is enormous, but it is due to "noise" rather than real signal. Nevertheless, the summer images (August 18, see Appendix for images), for the entire imagery retrieved present the lowest coefficient of variation for the three regions simultaneously; Juan de Fuca Strait a 27%, Queen Charlotte Strait 50%, and Strait of Georgia 54 % (Figs. 33, 34, 35).

FIG. 36. PIGMENT CONCENTRATIONS AT ST.OF GEORGIA

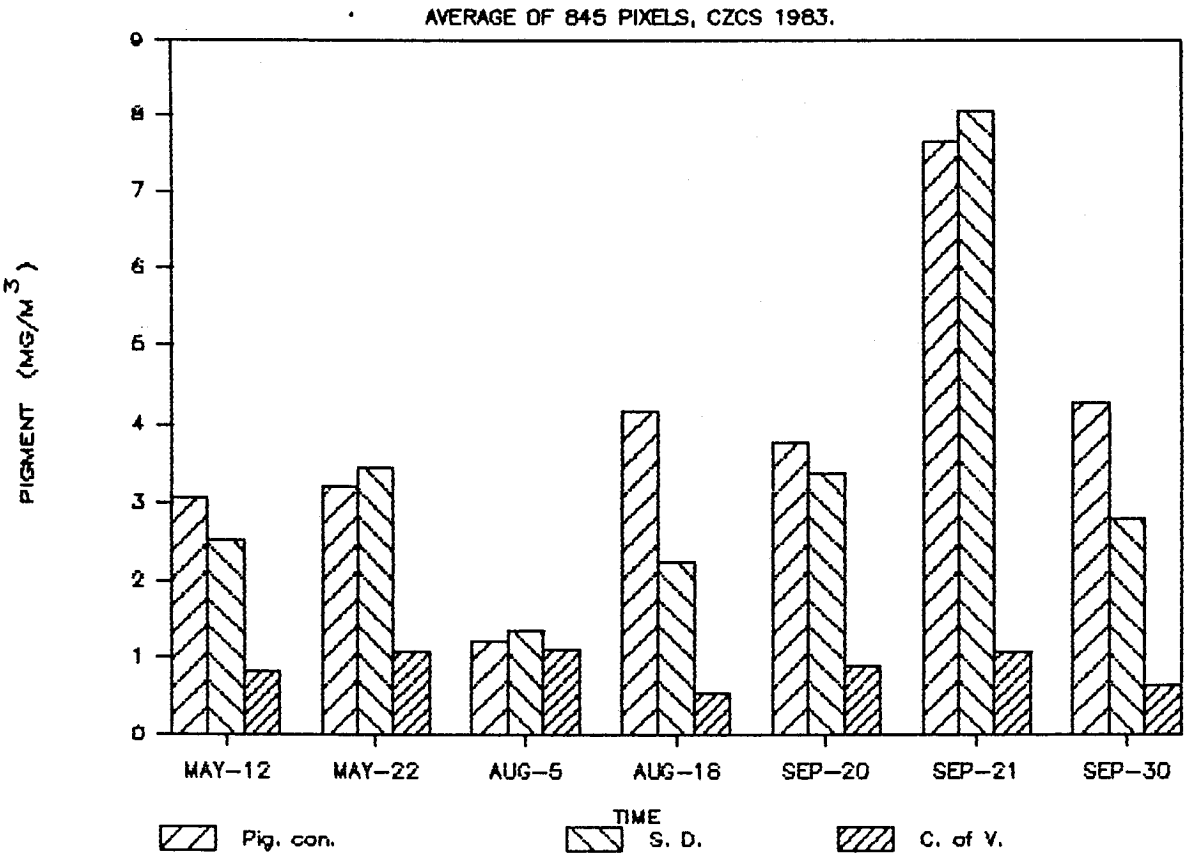

FIG. 37. PIGMENT CONCENTRATIONS IN B.C. FJORDS.

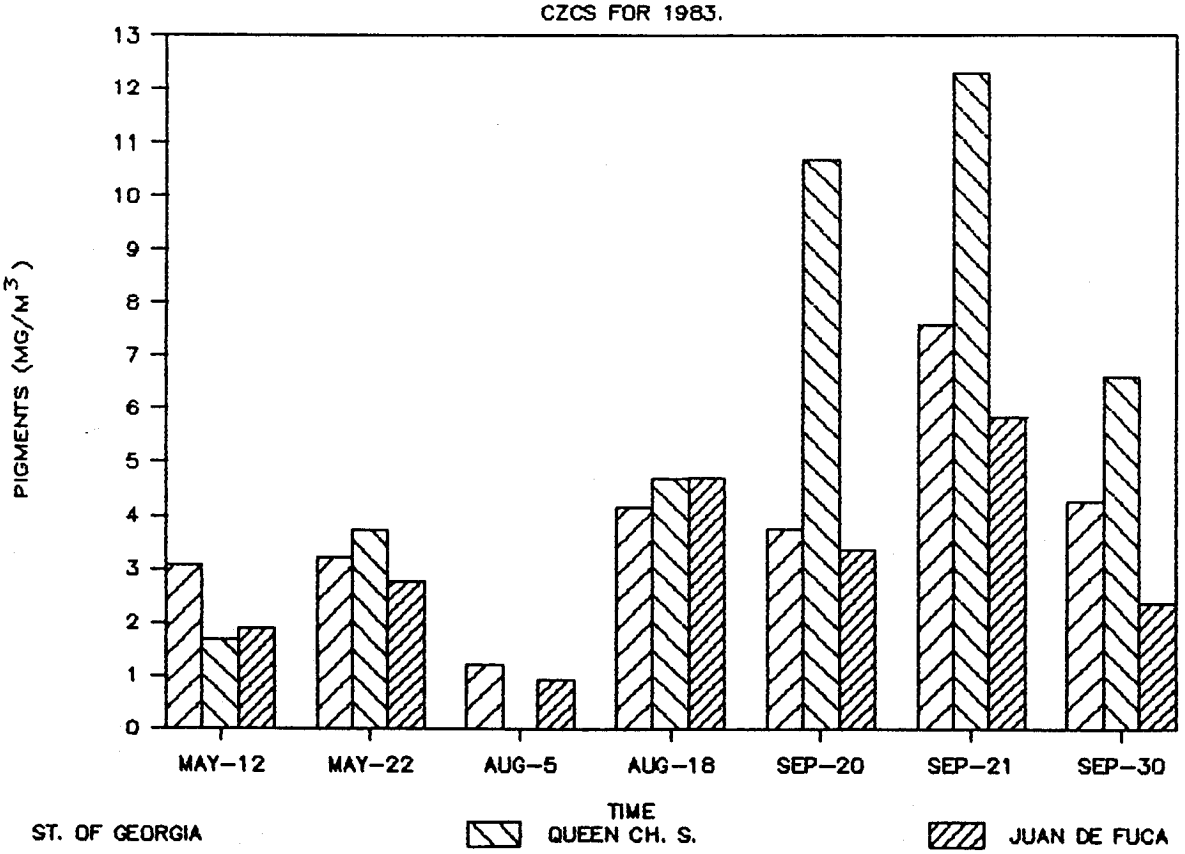

Therefore, during at least some days of summer, the small scale spatial distribution can be mapped. But, this is not enough for a program that requires more continuous tracking of phytoplankton spatial and temporal distributions near inlets/fjords at which salmon production has been concentrated (Appendix illustrated images).

4.3.3. Southern Chilean Imagery Data:

For the first time Chilean inland marine waters have been studied using the CZCS. It is know that absolute pigment values are not useful or reliable data sets, but some images-pictures show interesting flow patterns that can be used to understand more about circulation of the inland marine waters. The imagery data are summaries in Table 8.

Band 3 and the band 1/band 3 ratio of the images (pictures) from orbit 2039, located south of Golfo de Penas (≈ 48° S), illustrates the strong reflectance of glacial runoff and probably glacial silt in these fjords. Moreover, it shows a southward flow at the mouth of the inlets (Fig. 38). These glacial/river runoff effects are originated from the Campo de Hielos Patagonicos Norte (Northern Patagonia Ice Field), and Baker River which is one of largest in the country. For more information about the ice field itself can be found in Mercer, (1976) , Aniya and Enemoto, (1986). Pickard (1971), surveyed the Chilean fjord region in the same month, but 9 years before. He reports extremely low salinities and secchi disk depth values (mean for entire area 2.1

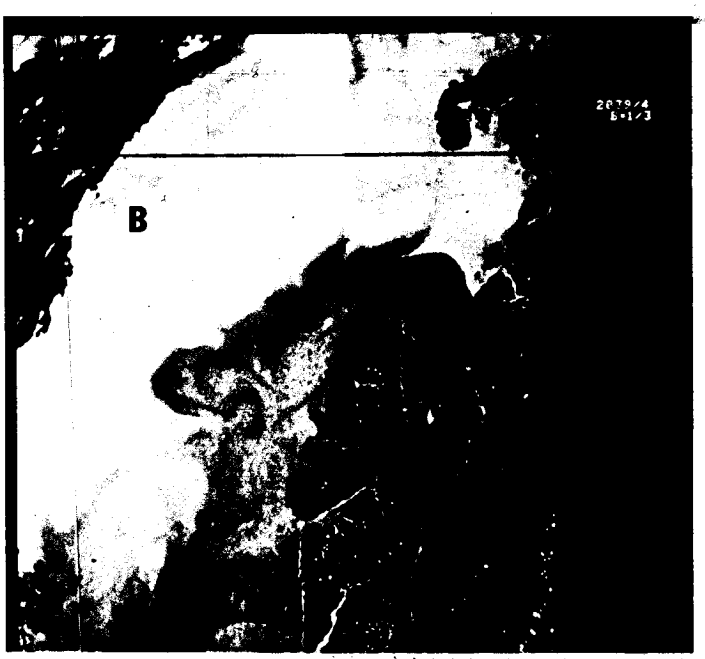

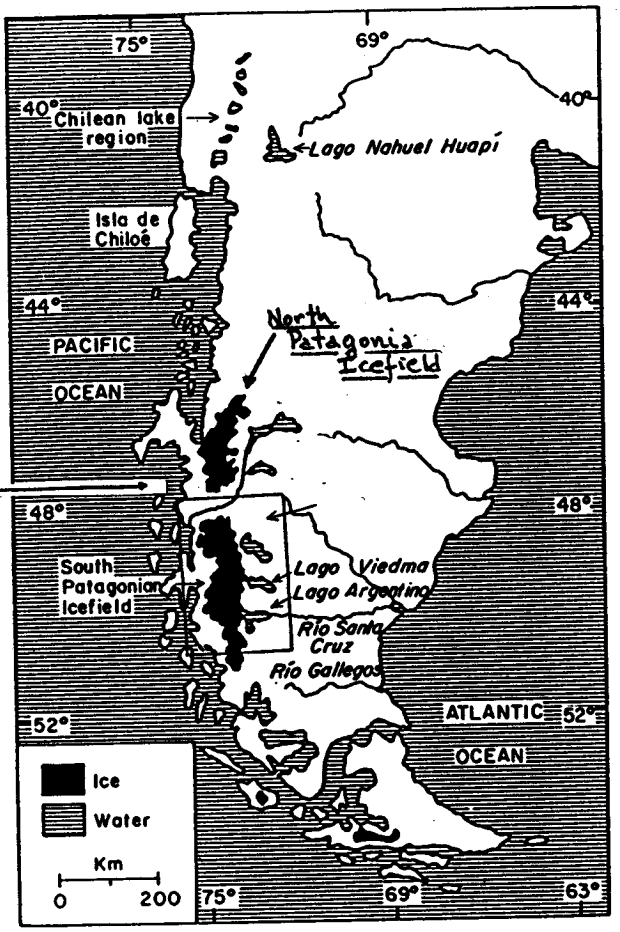

C Location map.

FIG. 38. IMAGE OF ORBIT 2039 OF NIMBUS-7 CZCS SHOWING A HIGH REFLECTANCE (PROBABLY DUE TO GLACIAL/RIVER RUNOFF), AND A SOUTHWARD FLOW. BAND 3 a) BAND 1/3 b) LOCATION MAP c).

m; see page 1096) for Baker region (South of Peninsula de Taitao).

The image of orbit 4747 (Band 1/Band 3) illustrates a southward tidal flow from Reloncavi Fjord into the Seno Reloncavi (Fig. 39). This demonstrates the importance of tidal surface currents and also the fjord-basin influence in the surface circulation of the southeastern Seno Reloncavi. Even though the tide was not at its maximum amplitude (e.g. spring tide, Fig. 22 a and b), it was an ebb tide as could be expected from the southward flow seen. In addition, during spring, freshwater discharge is large and increases the net outflow of the Reloncavi Fjord. A recent AVHRR image shows a very similar low SST pattern in the same area (Muñoz and Alvial, 1988). Several toxic red tide outbreaks had been reported in this fjord (Lembeye et al, 1981), therefore, it is a potential source of exported phytoplankton cells for regions near the sea-farms.

Images from orbit 2232 show interesting off-shore features in band 3, and the band 1 to band 3 ratio. A narrow pigment concentrations and hammerhead (eddy) off-shore Chiloé Island are clearly seen (Fig. 40). The image (band 3) west of Canal de Chacao shows a large area of pigment distribution or reflectance that might be exported pigment from inland marine waters, despite the low transport rates through this channel.

Maybe Canal de Chacao is playing an important role upon phytoplankton pigment distributions in the northwest part of SAIC. Coincidently, salmon sea farms are concentrated there and

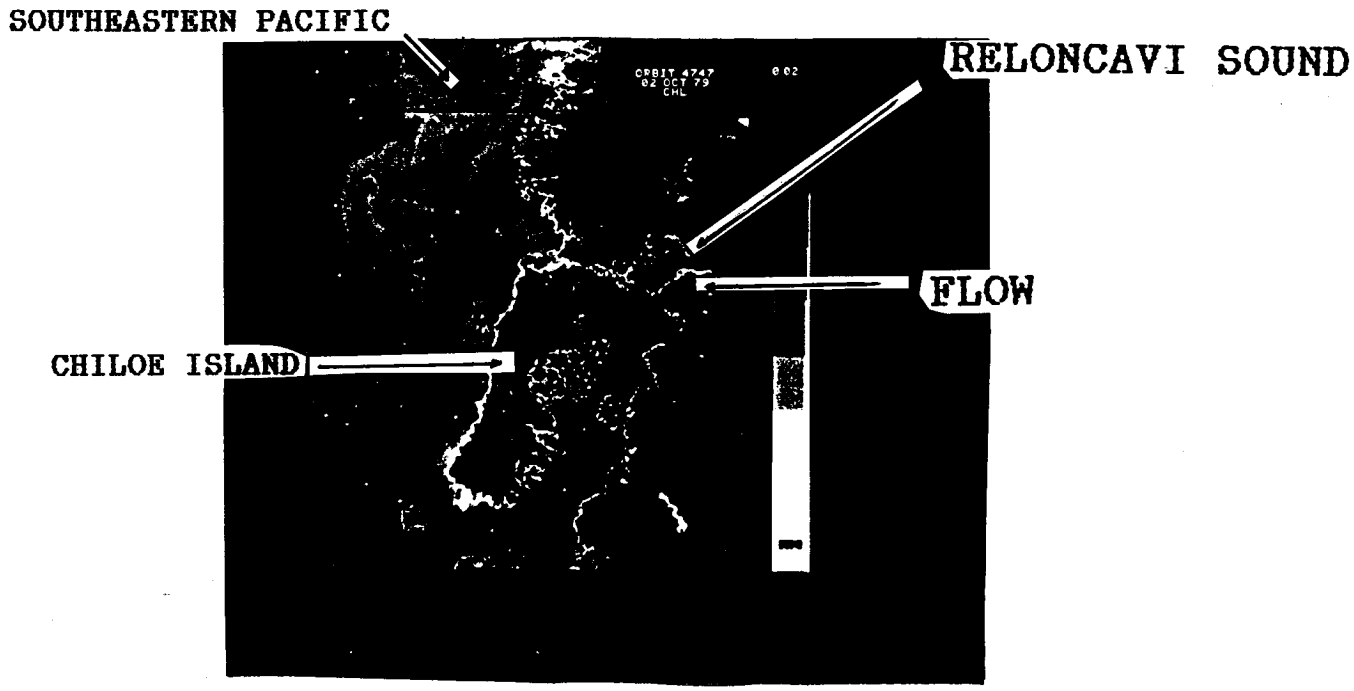

FIG. 39. CZCS IMAGE (ORBIT 4747) SHOWING DIFFERENT PIGMENT PATTERNS AND A SOUTHWARD FLOW IN SENO RELONCAVI, 2 OCT. 1979. (SEE FIGURE 22 a AND b FOR TIDE CONDITION).

they suffered severe impact during the last phytoplankton bloom.

In general, the ratio (R1/3) of above image illustrated larger pigment values within Golfo de Ancud than Golfo Corcovado. It seems that the Apio-Desertores Constriction is an important barrier for chlorophyll horizontal distribution in the SAIC.

The image from orbit 23212, late fall (May 30, 1983) shows a moderate concentration of pigment off-shore Chiloé Island, probably due to coastal upwelling (Fig. 41). The salmon sea-farms are concentrated on opposite eastern shore of Chiloé Archipelago. Their estuaries are affected by two channels of oceanic sub-antarctic waters (Silva and Neshyba, 1977). A survey of the chlorophyll field along the Pacific coast off Chiloé Island would be very useful to understand the origin of patches. These patches could originate within the inland marine waters or off-shore or even from both systems. To determine this, one could need to used ocean color sensors and compute the Bakun upwelling index at least weekly.

No satellite ocean color sensors are on orbit at present time, but during the early 90's Sea-WiFS onboard LANDSAT-6 will be launched and near real time data will be available. Table 9 summarizes the future situation of satellite ocean color sensor before the end of century.

FIG. 40. CZCS IMAGE (ORBIT 2232) SHOWING A HAMMERHEAD FEATURE OFF-SHORE CHILOE ISLAND. ALSO HIGH REFLECTANCE WEST OF CANAL DE CHACAO. BAND 1/3 a) BAND 3 b) (COURTESY, S. NESHYBA).

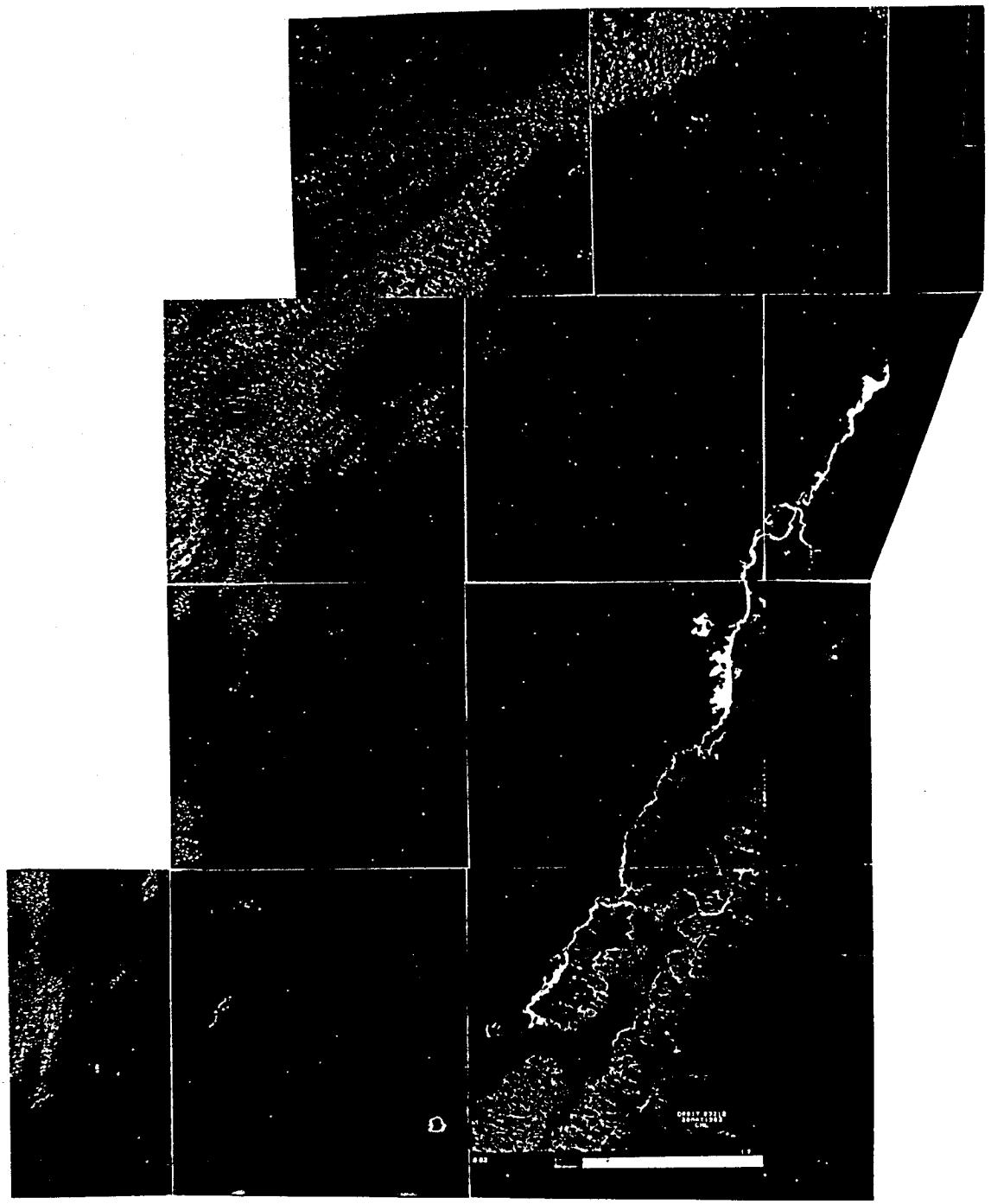

FIG 41 A CZCS MOSAIC IMAGE ALONG THE SOUTH COAST OF CHILE. THE BRIGHT STRIP (HIGH RADIANCE BAND 1/3) CORRESPOND TO COASTAL UPWELLING, 30 MAY 1983.

TABLE 8
CZCS IMAGERY FROM SOUTHERN CHILE. SEE MAPS FOR LOCATIONS

ORBIT	DATE	BANDS	LOCATION
2039	20/MAR/79	3 1/3	MOSAIC, SOUTH OF TAITAO PENINSULA
2232	3/APR/79	3 1/3	OFF-SHORE CHILOE (SAIC)
4747	2/OCT/79	1/3	SENO RELONCAVI SYSTEM (SAIC)
23212	30/MAY/83	1/3	OFF-SHORE CHILOE ISLAND (SAIC)

TABLE 9. FUTURE SENSORS FOR OCEAN COLOR MAPPING

SATELLITE	SENSOR	LAUNCH	SPECTRAL CHARACTERISTIC
LANDSAT-6 (USA)	Sea-WiFS*	1991	7 bands in the visible/near IR plus a 860 nm band, bandwidth of 20 nm.
ADEOS (JAPAN)	OCTS	1994	Probably as Sea-WiFS, visible including two additionals (410-415 nm) and several TIR, to separate phytoplankton from detritus
NASA (USA)	MODIS-(N,T)	>1995	N=Nadir. Containing those bands with no requirements for off-nadir pointing, including all IR viewing. T=Tilt. Containing visible and near IR bands requiring fore and aft nadir viewing.
	HIRIS	>1995	It will have 192 spectral bands, and 30 m of spatial resolution
SPOT-3 (FRANCE)	OCI	?	Eight spectral bands, bandwidth of 20 nm
NOAA-K (USA)	OCI	?	Idem as Spot-3.

Sources: Abbott, M. com per, 1988. EOSAT, 1987. NASA, 1986, 1987.
JOI, 1985. Yoder et al, 1988.
* See Appendix for recent up-date of Sea-WiFS

Limitations of Satellite Visible Imagery for Fjordic Estuaries Systems:

In summary, CZCS data sets for coastal and inland marine waters have more limitations rather than advantages to the study of temporal and spatial distribution of phytoplankton blooms affecting the cage salmon industry, even more if we considered particularly the worldwide latitudinal distribution of marine fish-farms.

Therefore the limitations have been summarized as follows:

1. **Nonlinear biological effects.**

   The presence of constituents or biological materials that influences the total attenuation coefficient and do not covary with chlorophyll (Smith and Baker, 1978, Gordon and Morel, 1983).

2. **Non-chlorophyll suspended particulate.**

   Certain coastal areas (mayor estuaries, embayments and fjords) are expected to deviate from a linear relationship between suspended particulate matter and pigments (chlorophyll and phaeopigments), due to supply of inorganic material from river or glacial runoff, bottom resuspension, large anthropogenic sources, or inorganic mineral precipitation (Clark, et al 1980).

3. **Mid-latitude regions and atmospheric corrections**

   Most of the salmon cage farms are in mid-latitude regions of the world (> 42° and < 62° Lat.). For a satellite remote

sensing the disadvantages are due to:

a) Rayleigh scattering algorithm and atmospheric correction:

Especially during the non-summer seasons. Moreover, new algorithms for CZCS chlorophyll estimates are now possible for latitude which fall between 60° N and 60° S (In: Yoder et al, 1988).

b) Low percentage of days cloud-free:

Using LANDSAT-1 data of Southern Chile, as an example, it takes 18 days for the orbit pattern to progress westward to point coverage repetition, thus, the satellite has the capability of covering about 20 times per year the same point. Hence, with a cloud coverage of at least 60%, which is a conservative estimate based upon LANDSAT-1 data of Southern Chile, and using simple probability calculations it could retrieve 8 images cloud-free per year. However, the actual number of images available for 1972-1973 year was less than the estimated value. This demonstrated limitations of Earth Resources Satellites, and maybe even in the near-future it can not be entirely used as remote sensing device to forecasts or at least to map marine phytoplankton pigments within short-term scales (< 15 days).

4. **Spatial Resolution.**

Low coverage frequency (in days) of NIMBUS-7, NOAA-n is more desirable than a better spatial resolution. Spring bloom and red tide events currently cover areas larger than

the spatial resolution limits (≈ 1 Km), wherefore the limitations arise for only site specific sea-farms.

5. **Radiance saturation of Sensors.**

Despite the high radiometric sensibility of CZCS sensor it seems that this effect is much more important due to clouds rather than land, especially for the B.C. inland water images, where land is mostly cover by vegetation. (see images on Appendix).

6. **Attenuation depth.**

It will depend on the depth of photic zone and attenuation coefficient for downwelling irradiance and bottom depth. If the photic zone depth is larger than the bottom depth; strong radiance reflection may occur from the bottom.

8. **High pigment concentrations.**

High pigment concentrations (the pattern of concern), increases the upwelling radiance near the red (670 nm), causing problems to the atmospheric corrections algorithm (Carder and Stewart, 1985).

9. **Non species composition data.**

Satellite pigment maps represent only chlorophyll a plus phaeopigments, therefore the information regards only to biomass, but not as species composition which is an important parameter for a marine aquaculture management strategy. Coccolithophorids are the exception.

10. **Satisfactory sea-truth data.**

The SAIC does not have a satisfactory data set that could be

use as ground truth.

11. **Image processing facilities and real time data.**

Image processing facilities are expensive and actual real time data would not be available unless a specific ocean color ground station is develop. This possibility could be carried out through NASA and Universidad de Chile or if file/image would be in a compatible format for microcomputers.

5. CONCLUDING REMARKS

5.1. THE REMOTE SENSING SITUATION

Near real-time ocean color images are not available to study phytoplankton pigment distributions, additionally their limitations for inland marine waters have been mentioned above. However, AVHRR data and algorithms have been used to explain indirectly pigment variability at the mouth of Juan de Fuca Strait, but requires ship data (Thomas, com per) and directly for estuarine waters, in Chesapeake Bay (Stumpf, 1987).

Unfortunately, not until 1991 will the second ocean satellite sensor Sea-WiFS launched onboard Landsat-6 and in 1994 a Japanese mission with OCTS sensor be available. Therefore, large gulfs of the SAIC (Ancud and Corcovado, Fig. 4) can be used as targets. Coastal conditions could be digitally studied using CZCS archive data to find out which are the major weakness that could be improved for future sensors algorithms for the region.

But, sea truth data is required or at least an adequate data set of temporal and spatial distributions of suspended particulate matter and phytoplankton pigments within the SAIC. Thus, part of this management strategy should consider phytoplankton information applied to remote sensing.

5.2. A MANAGEMENT STRATEGY

The first approach of a management strategy dealing with environmental processes and their effects on natural resources as well as on society is the scientific knowledge of the problem itself. Then we can develop management policies.

Valuable meteorological, oceanographic and remote sensing data has been presented to understand the dynamics of phytoplankton blooms and/or red tide events in fjordic estuaries.

The proposed management strategy assumes that some environmental processes have been studied, therefore it would expect similar patterns during comparable time scales. Otherwise, data collection would be necessary.

This contingency plan points out an efficient approach that will minimize cage salmon mortality due to noxious phytoplankton blooms. This management strategy has been conceptually draw in flow diagrams (Fig. 42 and 43), which they illustrate the different inputs and outputs of information.

The inputs have been classified under a) meteorological and other physical factors, b) oceanographic factors and c) remote

FIG. 42. GENERAL FLOW DIAGRAM OF MANAGEMENT STRATEGY.

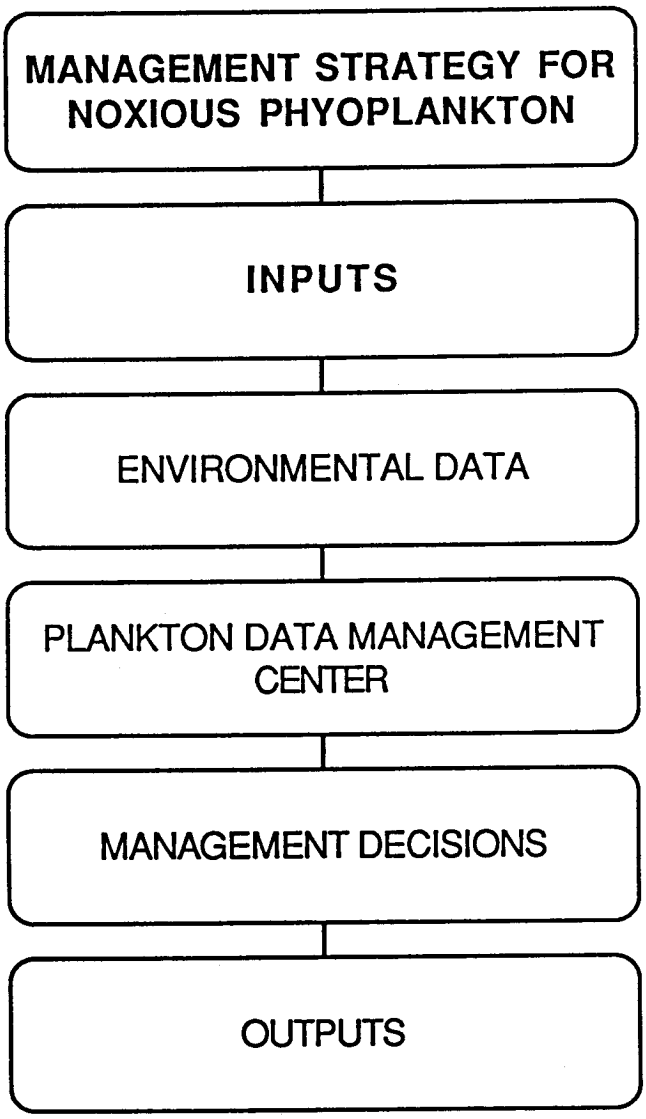

sensing data, which have been discussed in the present project.

All the information has to be centralized in a Plankton Data Management Center which generates the outputs for:

a) short term management decisions, within a time period of days to weeks. This is the most critical and important decision-making process step. As we know, phytoplankton distributions can change rapidly. Therefore it will be wise to have different approaches in function of these phytoplankton blooms and/or red tides' characteristics. For instance, observation of plankton cells will determine if they have night vertical migration behavior or not and measurements of oxygen consumption will allow the fish manager to apply appropriate mitigation techniques to the cages in the vertical axes (Z). Other examples are nutrient concentrations, light intensity, wind pattern, tide cycle and zooplankton predation. All of them will provide a basis for a forecast of the horizontal distribution (X, Y) of patches and probable decay of the event.

b) long term management decisions. This is referred to as a planning program within 5 years. One of the these programs will be the evaluation of the effectiveness of mitigation techniques (Fig. 43).

c) scientific goals. It has been included as output according to which are the scientific priorities to be solved in relation with phytoplankton distributions and their impact on marine aquaculture.

The budget to carried out such program should come from the salmon industry, local government, national and international research funds. The management strategy success will depend on the amount of money, technical team and salmon fish managers.

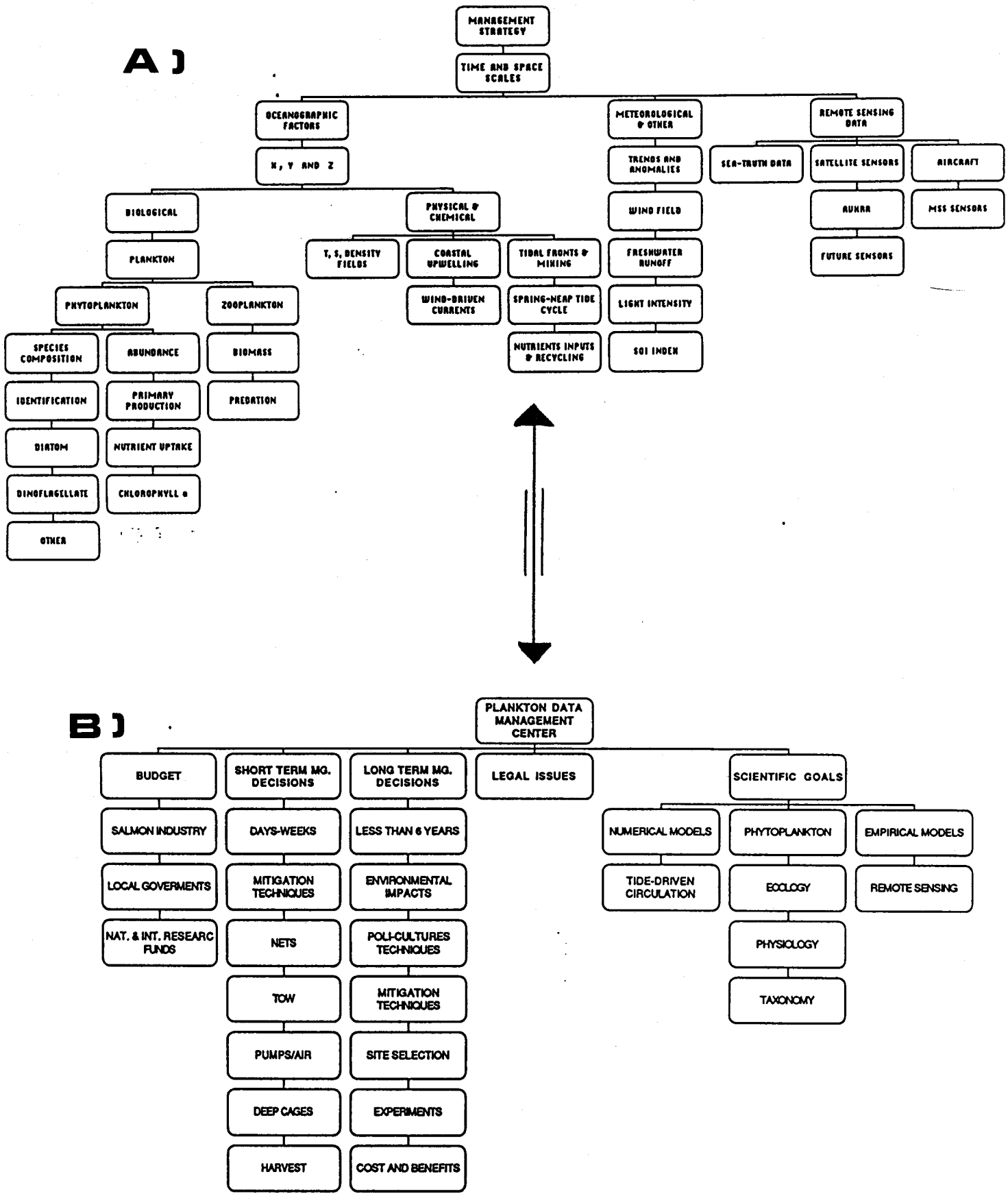

FIG. 43. FLOW DIAGRAM OF SPECIFIC inputs A) AND SPECIFIC outputs B) OF MANAGEMENT STRATEGY. THE INFORMATION IS CENTRALIZE IN THE PLANKTON DATA MANAGEMENT CENTER.

6. SUMMARY

The increase of cage salmon aquaculture throughout Northwestern Europe, North America and Southern Chile has raised major management issues. One of these is the importance to the industry of minimizing the salmon mortality caused by noxious phytoplankton blooms and/or red tide events. In order to be effective in this capacity we have to gain more knowledge about phytoplankton dynamics in the systems involved.

The solution seems to be complex. An approach is to understand mesoscale processes by assessing key meteorological and oceanographic factors that will enable prediction of blooms.

Meteorological and climatic factors such as wind field, precipitation and air temperature could show long term anomalies that have effects on phytoplankton dynamics.

The oceanographic factors of fjordic estuarine-type systems that affect phytoplankton blooms have high time-space variability. Even so generalizations can be made about some physical-biological processes; the presence of either tidal fronts or stratification along with high nutrient concentrations increase phytoplankton abundance, and physical forces also can influence the germination of benthic resting cysts that will initiate a bloom.

Remote sensing data either from satellite or aircraft is useful support information for mapping horizontal chlorophyll distribution. However management decisions can not be made with this data alone because of the limitations of the available techniques. Data obtained from the ocean color sensors, Sea-WiFS and OCTS on satellites due to be launched in the near future and/or real time data obtained from aircraft should be part of management strategy to minimize salmon mortality in fjordic estuarine systems.

A management strategy is proposed to organize a data collection regime that would generate the necessary environmental information on which to base management decisions. This information would be analyzed and then used to advise fish managers who are responsible for applying the appropriate mitigation technique.

7. REFERENCES

-**Abbott, M.R. and P.M. Zion,** 1987. Spatial and Temporal Variability of Phytoplankton Pigments off Northern California During Coastal Ocean Dynamics Experiment, Experiment 1. J. of Geophysical Res. vol. 92. N C2, 1745-1755.

-**Anderson, D.M. and B.A. Keafer.** 1985. Dinoflagellate cyst dynamics in coastal and estuarine waters. In: Anderson et al Toxic Dinoflagellates. Elsevier. pp. 219-224.

-**Aniya, M., and H. Enemoto,** 1986. Glacier variations and their causes in the Northern Patagonia Icefield, Chile, since 1944. Arctic and Alpine Res. vol. 18, N 3. 307-316.

-**Anonymous**, MS 1971. Chile 70 Cruise, 1970. Inst. Oceanogr. University of British Columbia Data Report, Rep. 31. 45 pag.

-**Anonymous**. Aquaculture Information. Bull. N 18A. Province of B.C. Ministry of Agriculture and Fisheries. Canada.

-**Atkinson, C.E.** 1987. The Fisheries and Market of Japan with special reference to salmon. Perspectivas de la Salmonicultura en Chile. Seminario Internacional. Fundación Chile. Santiago, Chile.

-**Austin, R.W.** 1980. Gulf of Mexico, Ocean-color surface-truth Measurements. Boundary-Layer Meteorology, 18, 269-285.

-**Avaria, S.** 1970. Fitoplancton de la Expedición "Doña Berta" en la zona de Puerto Montt- Aysen. Rev. Biol. Mar. Valparaiso, Chile. 14: 1-17.

-**Beveridge, M.** 1987. Cage Aquaculture. Fishing News Books Ltd. England. pp. 352.

-**Bjordnal, T.** 1987. Industrial Structure and Cost of Production in the Norwegian Aquaculture Industry. N. 31. Institute of Fisheries Economics, Norwegian School of Economics and Business Administration. Bergen-Sandviken, Norway.

-**Bonin, D.J., S. Maestrini, and J. Leftley.** 1981. The role of hormones and vitamins in species succession of phytoplankton. In: Platt, T (ed.) Physiological bases of Phytoplankton Ecology. Can. Bull. Fish. Aquat. Sci. 210. 310-322.

-**Brattström, H and E. Dahl**. 1951-1952. General Account. List of

Stations. Hydrography. Reports of the Lund University, Chile Expedition 1948-1949. Lund University, Arsskr., N.F., Avd. 2, Bd. 46. Nr. 8. 1-86.

-**Brown D. B. et al** 1985. Phytoplankton blooming off the U.S. east coast: A satellite description. Science, 229, 163.

-**Brunson, B.A. and W.P. Elliot,** 1974. Steric contribution to the seasonal oscillation of sea level off Oregon. J. Phys. Ocean. 4 (3): 304-9.

-**Carder K. and R. Stewart,** 1985. A remote-sensing reflectance model of a red-tide dinoflagellate off west Florida. Limnol. Oceanogr. 30 (2), 286-298.

-**Clark, D.K. et al** 1980. Upwelled Spectral Radiance Distribution in Relation to Particulate Matter in Seawater. Boundary-Layer Meteorology. 18, 287-298.

-**Clément, A., S. Neshyba, T. Fonseca, and N. Silva.** 1988. Oceanographic and Meteorological Factors Affecting the Cage Salmon Industry in Southern Chile. In: Perspectivas de Cultivo y Manejo del Salmon: Desarrollo Recientes. Tomo I. Fundación Chile. Santiago, Chile.

-**Clément, A.** 1988. Mortalidad de Peces en el Fiordo Reloncaví, Chile. vol. 4: 79-84. Biota. Chile.

-**Clément, A. and L. Guzmán.** Red Tides in Chilean Fjords. (in press). In: T.Okaichi, D.M. Anderson, and T. Nemoto [eds.], Red Tides: Biology, Environmental Science and Toxicology. Elsevier, New York. pp. 121-124

-**Crean, P.B.** 1978. A numerical model of barotropic mixed tides between Vancouver Island and the Mainland and it relation to studies of the estuarine circulation. In: Nihoul (ed.) Hydrodynamics of Estuaries and Fjords. Elsevier Scientific Publishing Company. Amsterdam.

-**Denman, K and M. Abbott,** 1988. Time evolution of surface chlorophyll patterns from cross-spectrum analysis of satellite

color images. J. of Geophysical Res. vol. 93. N C6. 6789-6798.

-**EOSAT**, 1987. Sea-WiFS System Concept Announced. vol.2. 3.

-**Eppley, R.W. and B.J. Peterson**, 1979. Particulate organic matter flux and planktonic new production in the deep ocean. Nature, Lond. 282: 677-680.

-**Espinoza, F.** 1984. Sea Surface Water Motion off Chile Latitudes 18°S-40°S, Revealed from Satellite Images of Chlorophyll and Temperature Distribution. Oregon State University. MRM Research Project. Corvallis, USA.

-**Farmer, D.M. and H.J. Freeland.** 1983. The Physical Oceanography of Fjords. Prog. Oceanog. Vol. 12, pp. 147-220.

-**Freeland, H., D.M. Farmer, and C. Levings (eds).** Fjord Oceanography, NATO Conferences Series IV Marine Series, vol.14 Plenum Press.

-**Gaines, G. and F.J.R. Taylor**, 1986. A Mariculturist's Guide To Potentially Harmful Marine Phytoplankton of the Pacific Coast of North America. Province of B.C. Ministry of Environment, Marine Resource Section. Report 10. pp. 53.

-**Gagliardini, D.A. et al**, 1984. Application of LANDSAT MSS, NOAA/TIROS AVHRR, and NIMBUS CZCS to study the La Plata River and Its Interaction with the Ocean. Remote Sensing Environm. 15: 21-36.

-**Gordon, H.R. et al** 1980. Phytoplankton Pigments from the Nimbus-7 CZCS: Comparisons with surface measurements. Science. vol. 210. pp. 63-66.

-**Gordon, H.R. et al** 1983. Phytoplankton pigment concentrations in the Middle Atlantic Bight: Comparisons of ship determinations and

satellites estimates. Appl. Optics. 22, 20.

-**Gordon, H.R. and A. Morel.** 1983. Remote Assessment of Ocean Color for Interpretation of Satellite Visible Imagery. A Review. Lectures Notes on Coastal and Estuarine Studies. Springer-Verlag. pp. 114.

-**Guan, I. et al**, 1985. The atmospheric correction and measurement of chlorophyll concentration using the CZCS. Limnol. Oceangr. 30 (2), 273- 285.

-**Guzmán, L and I. Campodónico.** 1975. Marea Roja en la Región de Magallanes. Instituto de la Patagonia. (Punta Arenas, Chile) Series Monógraficas, 9, 44 pp.

-**Guzmán, L and I. Campodónico.** 1978. Mareas Rojas en Chile. Interciencia. vol. 3, 3 Mayo-Junio.

-**Hannesson, R.** 1987. Salmon farming catches on. Infofish Int. 6, 18-20.

-**Hermosilla, J.** 1979. Variación estacional de los dinoflagelados tecados y tintinidos del Estero de Castro, Chiloé. Acta Zoologica Lilloana, XXXV.

-**Hovis, W.A. et al** 1980. Nimbus-7 Coastal Zone Color Scanner: System Description and Initial Imagery. Science, vol. 210. pp.60-63.

-**ICC-CONIC,** 1987. Etapa: Trabajos de Terreno - Estudios Maritimo-Ambientales. Tomo I. Estudio para el mejoramiento Integral del alcantarillado de Puerto Montt.

-**I.H.A.** 1988. Tablas de Marea de la Costa de Chile. Inst. Hidrografíco de la Armada, Pub. 3009.

-**Jerlov, N. G., and E. S. Nielsen, (eds.),** 1974. Optical Aspects

of Oceanography. Academic Press. pp. 494.

-**Johannessen, J. and B. Farrely,** 1988. (Abstract). Remote Sensing and Model Simulation Studies of the Norwegian Coastal Current During the Algal Bloom. EOS. Transactions. AGU. vol. 69. N 44. pp. 1118.

-**JOI.,** 1985. Oceanography from Space. A Research Strategy for the Decade 1985-1995. Part 2: Proposed Measurements and Missions. Joint Oceanographic Institucions Incorporated. Washington D.C.

-**Jones, K.J., et al.** 1982. A red tide of Gyrodinium aureolum in sea lochs of the firth of clyde and associated mortality of pond-reared salmon. J. mar. biol. Ass. UK. 62, 771-782.

-**Keala, B.A.L.** 1965. Table of Sigma-t with Intervals of 0.1 for Temperature and Salinity. Special Scientific Report-Fisheries # 506. United States Department of the Interior.

-**Lavin, P. and J.L. Anderson,** 1986. The Status of Atlantic Salmon Aquaculture. NOAA/Sea Grant. Marine Tech. Report 92.

-**Lembeye, G. and I. Campodónico,** 1984. First recorded bloom of the dinoflagellate Prorocentrum micans Ehr. in South Central Chile. Botanica Marina, 17: 491-493.

-**Lembeye, G. et al,** 1981. Intoxicaciones por consumo de mariscos del Estero Reloncaví (X Región), Chile (1970-1980). Resumen, Jorns. Cs. del Mar. Montemar.

-**Malone, T.C. et al** 1988. Influences of river flow on the dynamics of phytoplankton production in a partially stratified estuary. Mar. Ecol.-Prog. Ser. Vol. 48: 235-249.

-**MCDW.** Monthly Climatic Data for the World. Volumes from 1977 to 1987. NOAA. USA.

-**Mercer, J.H.,** 1976. Glacial History of Southernmost South America. Quaternary Research 6, 125-166.

-**Mendez, R.** 1988. El Estado de la Norma que Regula el Cultivo Comercial del Salmón en Chile. In: Perspectivas de Cultivo y Manejo del Salmon: Desarrollo Recientes. Tomo II. Fundación

Chile. Santiago, Chile.
-**Morel, A. and L. Prieur,** 1977. Analysis of variation in ocean color. Limnol. and Oceanogr. 22. 709-722.
-Mortensen, 1985. In: Anderson et al (eds.). Toxic Dinoflagellates. Elsevier, New York.
-**Muñoz, P and A. Alvial.** 1988. Proliferación de Microalgas. Origen, dinámica e impactos en pisciculturas. In: Perspectivas de Cultivo y Manejo del Salmon: Desarrollo Recientes. Tomo II. Fundación Chile. Santiago, Chile.
-**NASA,** 1986. MODIS, Moderate-Resolution Imaging Spectrometer, EOS. Instrument Panel Report. vol. IIb.
-**NASA,** 1987. HIRIS, High-Resolution Imaging Spectrometer: Science Opportunities for the 1990s. EOS vol. IIc, Instrumental Panel Report. pp. 74.
-**Neshyba, S.** 1987. Oceanography, Perspectives on a Fluid Earth. John Wiley and Sons. 506 pp.
-**Pan, D., F.J.R. Gower, and G.A. Borstad.** 1988. Seasonal variation of surface chlorophyll distribution along British Columbia coast as shown by CZCS satellite imagery. Limnol. Oceanogr. 33 (2), 227-244.
-**Parsons T.R., M. Takahashi, and B. Hargrave.** 1977. Biological Oceanographic Processes. Second Edition. Pergamon Press. pp. 323.
-**Pickard, G. L.** 1971. Some Physical Oceanographic Features of Inlets of Chile. J. Fish. Res. Bd. Canada 28: 1077-1106.
-**Pingree, G. et al.** 1975. Summer phytoplankton blooms and red tides along tidal fronts in the approaches to English Channel. Nature. Vol. 258, 5537, 672-677.
-**Pingree, G., P.M. Holligan and G.T. Mardell.** 1978. The effects of vertical stability on phytoplankton distributions in the summer on the northwest European shelf. Deep Sea Research vol. 25, 11, 1011-1028.
-**Pittock, H.L., et al.** 1982. Observations of sea level, wind and atmospheric pressure at Newport, Oregon 1967-1980. Data Report

98. School of Oceanography. Oregon State University. USA.

-**Platt, T,** 1986. Primary production of the ocean water column as a function of surface light intensity: algorithms for remote sensing. Deep-Sea Research. vol. 33, No 22, pp. 149-163.

-**Red Tide Newsletter.** 1988. vol 1. Numbers 2 (April) and 3 (July). A Sherkin Island Marine Station Publication. Ireland.

-**Redfield, A.C., B.H. Ketchum and F.A. Richards.** 1963. The influence of organism on the composition of sea water. IN: The Sea, M.N.Hill Interscience, New York. Vol. 2, 26-77.

-**Rivera, P. and P. Cox,** 1982. Contributions to the Diatom Flora of Chile II. 7th Diatom Symposium.

-**Ruckes, E.,** 1987. World Production and Salmon Markets and Overview. Perspectivas de la Salmonicultura en Chile. Seminario Internacional. Fundación Chile. Santiago, Chile

-**SERNAP,** 1987. Anuario Estadístico de Pesca. Ministerio de Economía, Fomento y Reconstrucción. Chile.

-**Silva, N. and S. Neshyba,** 1977. Corrientes superficiales frente a la costa austral de Chile. CONA, 3: 37-42.

-**Smith, R.C. and K.S. Baker,** 1978. The bio-optical state of ocean waters and remote sensing. Limnol. Oceanog. V.23 (2), 247-259.

-**Smith, R.C. and W. Wilson,** 1981. Shipand satellite bio-optical research in the California Bight. In: J.F.R. Gower (ed). Oceanography from Space. Plenum Press, New York. 281-294.

-**Stumpf, R.P.** 1987. Application of AVHRR satellite data to the study of sediment and chlorophyll in turbid coastal water. NOAA Tech. Memorandum, NESDIC AISC 7. US Department of Commerce.

-**Stumpf R.P., and M.A. Tyler,** 1988. Satellite Detection of Bloom and Pigment Distributions in Estuaries. Remote Sensing of Environment. 24: 385-404.

-**Sverdrup, H.U.** 1953. On conditions for the vernal blooming of phytoplankton. J. du Conseil pour l´Exploration de la Mer, 18, 287-295.

-**Tangen, K.** 1977. Blooms of Gyrodinium aureolum in North European waters, accompanied by mortalities of marine organisms. Sarsia, 63, 123-133.

-**Thomson, R.E.** 1981. Oceanography of the British Columbia Coast. Can. Spec. Publ. Fish. Aquat. Sci. 56: 291 p.

-**Townsend, D. W. and R.W. Spinrad.** 1986. Early spring phytoplankton blooms in the Gulf of Maine. Continental Shelf Research. Vol. 6, 4, pp. 515-529.

-**Uribe, E. and S. Neshyba.** 1983. Phytoplankton Pigments from the Nimbus-7 Coastal Zone Color Scanner: Coastal Waters of Chile from 18° to 40° S. In: Arana, P. (ed). Marine Resources of the Pacific. US Inter. Sea Grant and Univ. Cat. de Valparaiso, Chile.

-**Vidal, J. and S. Andrade.** 1984. Proyecto de Desarrollo de la Oceanografia Biotecnológica en las Regiones Australes de Chile. Manuscrito. S.U.N.Y. New York.

-**Wallentinus, I.** 1988. Announcement. Limnology and Oceanography. Vol. 33. 4. Part I. pp. 648

-**WCTS,** 1987. West Coast Time Series. User Guide. NASA and Jet Propulsion Lab (JPL).

-**Winter, J. et al,** 1984. Recent Developments, Status and Prospects of Molluscan Aquaculture on the Pacific Coast of South America. Aquaculture, 39, 95-134.

-**Yentsch, C.M., and C.S. Yentsch.** 1984. Emergence of optical instrumentation for measuring biological parameters. Mar. Bio. Ann. Rev., 22, 55.

-**Yoder, J. et al,** 1987. Spatial scales in CZCS-chlorophyll imagery of southeastern US continental shelf. Limnol. Oceanogr. 32 (4), 929-941.

-**Yoder, J. et al,** 1988. Satallite Ocean Color-Status Report. Oceanography Magazine. July, vol. 1.No 1, pp. 18-20.

APPENDIX

Program SHO (originally on UBC Oceanography's VAX750)
MODIFIED to work on a SUN colour workstation by Bill Meyers (Jan,88 - ?)
INSTALLED at OSU Oceanography by Andy Thomas (Jan-Jun 88)
SUN documentation by Andy Thomas 88.jun.28
DISCLAIMER not all commands are implimented on the SUN,
and not all commands are well described here.

OVERVIEW

Sho displays specially formatted images on a SUN workstation.
You can then interactively change the displayed image in a variety
of ways, and then SAVE the result to a disk file. The program assumes
your image (or whatever data you intend to display) is byte data
stored as a 2 dimensional array. If the data is an image, it needs
to be already geometrically corrected for the display to look
like a proper projection. A common use of the program is to
change the relation between data value and brightness
(=colour) displayed to "enhance" the image.

==========TABLE OF CONTENTS==========

AVAILABILITY: Sho is written in the language C, and runs on the SUN
system using the SUNTOOLS library,
under the UNIX operating system. The executable file is in /usr/lib
The source is managed by Andrew Thomas who will let users know
about updates and changes as they occur (the SUN version of SHO
is very much in the research/developement stage).

TO USE: 1) log onto SUN colour monitor
2) be sure /usr/lib is in your path name
3) run SUNTOOLS
4) in the bottom window, type in "sho"

DATA FORMAT: The images to be shown may have up to 512 pixels per line,
and up to 512 lines.
The data matrix is loaded L to R, top to bottom ie. the 1,1
array member ends up in the top,left corner. The byte data should
have values between 0 and 255; the display has 8 bit resolution.
If you have a map in the same format, it can be overlaid as a
binary 'overlay'. Sho will not create such maps.

CAPABILITY: SHO will let you open a number of image planes (windows)
each with a different image in them of a size determined by the
data (set by user). The windows can be moved, stretched,
(standard SUNTOOLS functions) or modified, blanked, destroyed
or saved (SHO commands). Separate windows are
used to display the data histogram, the colour palette, and the
current enhancement function.

ACTION: upon starting sho...

SHO clears the screen, displays a window in the bottom left where
all commands must be typed in.
**NOTE the cursor must be within this box
for typed commands to entered.
SHO prints a header message identifying the latest version.
SHO creates a command bar across the top of commonly used commands which can
be accessed by clicking with the LEFT mouse button ie through SUNTOOLS).
SHO gives a prompt "_"

Enter commands at keyboard one at a time (wait for prompt), or
click the left mouse button to execute corresponding commands.

To STOP : enter <ctrl-d> (while holding down the CTRL key, press d).

1. DESCRIPTION OF SHO COMMANDS.

This will put you back in UNIX, still in the SUNTOOLS environment.
(To get out of SUNTOOLS, click the RIGHT mouse button to OPEN the
options window, then select EXIT SUNTOOLS, and follow directions.)

*** EXAMPLE: a typical sequence of commands: get an image, enhance it, exit sho.

_sho 1
_get 1
file? "directory/file where image is located"
  Image fills screen.
  (Premature end of file causes rest of screen to be filled with black.)
_sho all
The data-to-brightness function and the histogram for this file are displayed.
_enhance (apply function to display)
  (no change apears at this stage as the default function (a straight line)
   is applied to the image)
_linear
  sho will change the prompt to a > to indicate a subprocess
  Move cursor to 'enhancement filter' window, and click on a position.
  Function is drawn through crosshairs. Image is enhanced.
  at the prompt > type in 3 (means quit linear change mode)
_slide (and move cursor horizontally)
  again sho will give you a > prompt to indicate a subprocess
  Enhancement function moves.
  grey scale/pixel value changes.
  type 3 (to stop changing function)
_ <ctrl-d> to stop and exit sho.

********* SUMMARY of COMMANDS

1 inspect	2 pan	3 exit	4 draw	5 crop	6 flip	7 flop	
8 status	9 fit	10 section	11 linear	12 ramp	13 get	14 destroy	
15 repeat	16 unzoom	17 colour	18 slide	19 trace	20 hide	21 save	
22 quit	23 zoom	24 enhance	25 integrate	26 roll	27 show	28 iconify	

NOTATION: <something> means: substitute a something (without <>)
  << >> means the arguement is optional

Options for the commands below are:
  <window number> 1-3 (size >256), 1-4 (size <=256), pseudocolour,
    rainbow, function, histogram, graphics (f.+h.), map ,or all
  <colour wanted> black, red, green, yellow, blue, magenta, cyan, white .
  <operation> copy, add, sub, or, xor, and, conditionnal .

Abbreviations OK if unambiguous. Rejected options or commands are answered
by a list of alternatives, so ? can be used to display valid options.

Commands by category: they can be typed from the work window, or activated
  by clicking the appropriate area on the command window.
  Those marked with "T" toggle on/off,
  some will give you a list of options, some just operate
  with no further arguments.

DISPLAYING:
  size <bytes/line>
  get <window number>
  show <window number>
  blank <window number>
  zoomin (at cursor position)
  unzoom
  destroy <window number>
  pan (at cursor position)
  inspect (at cursor position)

  MODIFY:

```
   legend  <<filename>>
   filter  <<filename>>
   copy <fromwindow number> <towindow number>
   palette
   font  <<type>>  <<size>>
   set  <xleft/ytop/bars/width> <value>
   text  <string>
   enhance <on/off>  T
   color  T
   reroute <window number>
   fill <value>
   draw T
   grid  <size>
   dash  <value>
   plot  <filename>
   paint overlay <colour desired>

 ENHANCE:
  mix <color>T
  linear T
  ramp   T
  trace
  integrate
  roll T
  slide  T

                          MISCELLANEOUS:
 CURSOR:                    help <<command number>>
   x <number>
   y <number>               define <button>
   store                  T repeat <button>
 FILE OUTPUT:               quit
   map <file>               status
   save <window number>     verbose {on|off|full}
                            wait   <seconds*30>
 UNIX:                      reset
   !<unix-command>          source  <filename> (aka "<")
```

DEFINITIONS

****** DISPLAY , CURSOR , DEFINE

DISPLAY: Commands which are reversible, changing only what is shown.

size <bytes/line> : Should be issued before GET to specify length of lines in file. Default value is 512.

show <window number> : add image,function,histogram or map to display.
<window number> is 1-3 (size >256) or 1-9 (size <=256)
,rainbow (test pattern, pixel value 0-255)
,function (in graphics window)
,histogram (in bottom half : only that for last file read)
,graphics (function + histogram, no image)
,map (generated by commands grid, get map, and text)
,all (display all windows)
,pseudocolour (3 images control 1 colour each: 1R 2G 3B.
If size <=256, combinations are 123 / 456 / 789).
,overlay (displays text / drawing / map on top of image window)

blank <window number> : un-show, but without destroying.
get it back by typing sho <window number>

zoomin : Expand image around cursor (x2 at each application to limit).

unzoom : Shrink image to original size.

pan : Shift image about crosshair. For continuous

```
                pan, see REPEAT command. BUGS: Wraparound past edge can easily
                happen, or overlap into adjacent image. SEEMS FLAKEY

inspect         : Print coordinates and value of pixel at crosshair.
                Image coord: UL = (0,0), mid=(256,256), LR=(511,511).
                CF MAP command in section on file output.
                In function design mode, Y displayed is that of function.
                Function coord: LL=(0,0), UR=(255,255).
CURSOR: commands to manipulate cursor. NOT YET IMPLIMENTED

X <number>      : leaving Y unchanged, set X-value of cursor.
                This is done by shifting the origin on the digitizing tablet.
                "x -1" , or "reset" return the origin to (0,0).
Y <number>      : like X .
X  (alone)      : shuttle between X values of last 2 store commands.
Y  (alone)      :    "       "    Y    "

store           : Store X, Y at current point for later use by
                X, Y command. Only latest 2 pairs are stored.
                "get <image> implicitly does a "store" command at each
                end of the histogram.
DEFINING MACROS,      EXAMPLE : ANIMATION  ---SEEMS FLAKEY
Here I use "/" to mean "new line" to save paper.

define 'command number'  (needs to be a number > 25)
sho 1  / wait 30  / sho 2  / wait 30  / sho 3  / wait 30  /  /
repeat 25
quit

*****  MODIFY: change the contents of image, overlays.

attach <filename>       : Specify filename for all future "get" and "save".
        If no <filename> (i.e. "attach"), "get" and "save" will ask
        for filename from keyboard (not "source" file ).
        To access tape, file name is /dev/smt0 or /dev/smt1.
get <window number> or <operation>      : Read from file. If "attach" not used,
        sho will ask for file name; command may then be aborted by blank line.
        If it can't find the file (bad path), it says so.

    In particular,
        get <window number#> : read image, not necessarily currently displayed.
        get rainbow     : read colour look-up table (cf. save).
        get map         : read overlay. 0=transparent, 1=opaque. (cf reroute)
                          NB : old map is not erased.
        get function    : read function (cf. save).
        get histogram   : read histogram (cf save).

<operation> <from-window number> <to-window number> : Ex: "copy 1 2" .
        <operation> is one of copy, add, sub, or, xor, and, conditionnal.
        Pixel-by-pixel combination of <from-image> and <to-image>, modifying
         <to-image>.

destroy <window number> : permanently erase <window number> (cf. blank )

text  <string>  : string is drawn on map overlay starting
                          at crosshair. See FONT for size and angle .
text                    : Multiple lines are stored, then copied to screen
                            when empty line entered.

font <character size> : Cf text. defines size of text on image          3

font  :with no arguement lists available fonts. to use one, type font <name>

erase  <#characters>    : Fill a rectangle with 0's (black). Size of rectangle
                          is according to character size as specified in
                          "font". Angle is horizontal.
```

```
grid  <size>              : draw square grid in map overlay, using bit
                            pattern selected by dash. Default <size> 16.
dash  <number>  : -1 is solid line (default). 12345 is interesting.

save  <window number#>  : copy image memory to a file, as modified by
                  enhancement function (if ON) or any text or drawing
                  that you have done. Maps cannot be saved.
                  May be aborted with CTL-C.  At present SAVE is flakey
                  and to save an image you have written onto (cf reroute, text)
                  you need to go "sho # / rer # / sho overlays / save #"
                  to actually get it to save an image.

save <function/rainbow/histogram> : copy to file for later "get" command.

legend <filename> : Writes 2 vertical stripes in UL corner of current image.
                      image. Edge band has 256 horizontal segments with values
                     0-255 . Inner band has a segment for each data value
                      which, after passing through function, shows as a
                      distinct colour. Re-do after change in function.
                      If <filename> is specified, inner band is labelled
                      according to contents of that file. Format is :
                      <pixel-value> <label>

set <xleft,ytop,bands,size> <value> : options for position, size of legend.
                Defaults: xleft=0 , ytop=0 (UL) , bands=1, size=16 .

reroute <window number> : for text, grid, draw, erase, plot, and "get map"
                          commands. Select plane to draw on. Default is map
                          'overlay'.
reroute <window number> <value> : Draw on <image> with pixel value <value> .
                       Default = 254 (white) . NOT YET IMPLIMENTED!!

fill             : Starting from cursor, fill current image with value 254,
                   spreading to boundary (cf reroute, plot,draw) defined
                   by an unbroken line with the value 255 on the same image.

fill <value>     : For all points with same value as current point, replace
                   with <value> . Stop at boundary defined by an unbroken
                   line of points with value different from current point.
                   NOT YET IMPL.

map <filename>   : For later use by "plot" : redefines mouse buttons 1-3 (L-R).
                   [1] = append crosshair coordinates to file, button=1 (move)
                   [2] = same as 1, button=2 (draw).    [3] = stop
                   Format 3A2 (LSByte first): <button>,<x>,<y>  .
                   First button should ALWAYS be 1.

plot <filename> :  Read file generated by "map" and draw on the map plane
                   in white. Cf "reroute" .
                   Special case : if "map" in progress, and <filename> not
                   specified, draw all points inspected so far.

crop             : Define a write enabled window, protecting all outside it.
                   Buttons 1-3 redefined :
                   [1] = set LL.  [2] = set UR. [3] = stop .
                   Should be done immediately before get/draw/plot , since
                   show and other commands reset it to entire screen.
                   NB in the case of "get" , origin is not moved: data outside
                   the window are just thrown away. (DOESN"T SEEM TO WORK)

draw             : Toggle on/off drawing on current text plane a line following
                   crosshair. Cf "map" , "reroute". Drawn as a value of 254.
                   Press left mouse button to draw. Don't forget to toggle OFF.

nudge            : Destructively shifts current image by distance between fixed
```

and moving crosshair everytime button [1] is pressed.
Button [2] repositions fixed crosshair. Button [3] to STOP.
'nudge <fromimage>' : all copying is done from the original
to the current image .
Ex: NUDGE / Move xhair to recognizable feature on image /
Press [2] / Xhair to same feature on map / Press [1] /
If satisfied, press [3] to stop.
Everytime [2] or [1] is pressed, nudge reports on the
cumulative distance (+,+)=(right,down) moved since 'nudge'
command was issued.
WARNINGS : Cumulative motion is zeroed at every start of
'nudge', but not when image is changed by 'get' , 'copy'...

filter <filename> : Specify a file, generated by "save function", to be used to transform data for future "get image" commands. If <filename> blank, turns filter off.

****** ENHANCE: design an enhancement function.

All 6 design commands have the following in common:

"Sho all" should be done to make function and histogram visible.
"Enhance" should be ON for function to operate on display.
Prompt is "+" in 'standby' mode, else the name of active operation.
1st call to any design command starts a "standby" mode : 2 crosshairs are displayed, one fixed, the other follows cursor around. Crosshairs are restricted to the upper half.
Anytime during function design ("continue" mode) :
type 3, or command "reset" , stops function design. (ie resets you back to sho.)
type 1: go back to standby mode. Alternately force y-value to be function value / follow cursor.
type 2: go back to standby mode. Move fixed crosshair to moving crosshair position.
type 4 ... (function design commands) : immediately execute that command. Exception: executing one of the continuous functions (all but integrate) twice in a row returns the program to "standby" mode.

linear: Draw "infinite" line through 2 crosshairs, clipping at 0,255. Always changes whole function. Continuously updated.

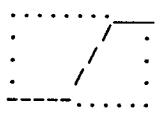

ramp: Like linear, but clipped at crosshair y-values. Continuously updated.

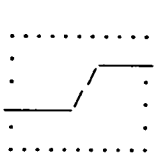

trace: Draw line between fixed, moving crosshair, then follow moving crosshair. Best used with X, Y commands,and/or frequent return to standby mode via button 2. Continuously updated.

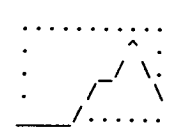

integrate: Draw a line whose slope is proportional to histogram frequency, scaled to fit between crosshairs. Executed just once.

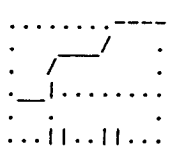

```
roll:   Shift function left-right. Wraparound at x=0,255
        Continuously updated by clicking left mouse button.

slide:  like roll, but no wraparound.

mix <colour>    : copy <colour> part of rainbow into "function", thus allowing
                  use of function design commands to modify colours.
                  Side effect: destroys function. Cf. "save function".
                  "mix" to stop mixing (check "status") .

****MISCELLANEOUS

?               : print list of commands

<command> ? ?   : print options for that command.

help            : print all commands assigned to buttons.

help <button#>  : print commands for that button.

define <button#>: Enter commands, 1 per line, to be executed when
                  <button#> is pressed. No prompt is given.
                  Enter and empty line to stop.
<button#>       : Execute sequence of commands defined for that button.

repeat <button#>: sho will "push" <button#> as often as possible.

repeat <button#>: stop repeat

quit            : stop all repeating commands, exit function design
                  or other "continue" modes.

status          : display parameters: size, enhancement, colour,
                  , any continuous function, and all repeating functions.

wait  <frames>  : 1 frame waits 1/60'th second. Default 20 minutes !!!

source <filename> : reroute command input from keyboard to file <filename>.
                    "<" is a synonym.

#               : Comment: ignore rest of line. For files used with "source".
                  Must be at beginning of line.

cd  <directory> : Change default directory (for filenames not
                  beginning with  "/" ). NB: "!cd" does nothing.

pwd             : Print <directory> from last successful "cd" command.

!<unixcommand>  : A typed-in line whose first character is ! is
                  passed on to a shell (command interpreter) to
                  be executed as a unix command, then return to sho.
                  It is ok to run a program which put an image on the raster.
```

```
c              CHLOROPHYLL CONCENTRATION
c           BY RODRIGO NUNEZ AND ALEX CLEMENT AUGUST-1988
c       this program calculates the average concentration of chlorophyll
c       using a file of 512X512. You have to choose a small rectangle inside
c       the geographic area that you are studying and then with the coordinates
c       of each corner you can calculate the average, the standard deviation
c       and count the pixels with value less than 245(partial counter) and
c       the total number of pixels(total counter).
c        Example: 45%=45 percent of the pixels are less than 245

      dimension image(512,512),chlo(512,512)
      dimension imagen(512,512),image1(512,512)
      integer xmin,xmax,ymin,ymax,imax
      integer sum3
      real ratio,sum1,c
      real aver,mean,chlosd,chlovar,sum2
      character*1 ch(512)
      character*35 title
      print*,'Enter name of file to read values from'
      read (*,50) title
 50   format(a35)
      write(*,*)'Enter ymin'
      read (*,*) ymin
      write(*,*)'Enter ymax'
      read (*,*) ymax
      write(*,*)'Enter xmin'
      read (*,*) xmin
      write(*,*)'Enter xmax'
      read (*,*) xmax
      open(unit=12,file=title,status='old',form=
     & 'unformatted',recl=512,access='direct')
      open(unit=31,file='image',status='unknown',form=
     & 'unformatted',recl=512,access='direct')
      open(unit=1,file='chlor.con',status='unknown')
      imax=512
      do 44 i=1,imax
         read(12,rec=i) (ch(kk),kk=1,512)
         write(31,rec=i) (ch(kk),kk=1,512)
 44   continue
      close(unit=31)
      open(unit=32,file='image',status='old',form=
     & 'unformatted',recl=512,access='direct')

      do 88 k=1,512
         read(32,rec=k) (ch(kk),kk=1,512)
         do 89 kk=1,512
            image(kk,k)=ichar(ch(kk))
            image(kk,k)=(-image(kk,k))
 89      continue
 88   continue

      aver=0
      c=0
      sum1=0
      sum2=0
      sum3=0
      do 78 i=xmin+1,xmax+1
      do 79 j=ymin+1,ymax+1
      if(image(i,j).lt.0) then
      imagen(i,j)=-image(i,j)
      goto 179
      endif
      imagen(i,j)=256-image(i,j)
 179  write(1,*)'image(i,j)=',imagen(i,j),'x=',i-1,'y=',j-1
      if(abs(imagen(i,j)).lt.245) then
      chlo(i,j)=10**((imagen(i,j)*0.012)-1.4)
      aver=aver+chlo(i,j)
      sum1=sum1 + 1
      endif

 79   continue
 78   continue
      mean=aver/sum1

      do 188 i=xmin+1,xmax+1
      do 189 j=ymin+1,ymax+1
      if(image(i,j).lt.0) then
      image1(i,j)=-image(i,j)
      goto 156
      endif
      image1(i,j)=256-image(i,j)
 156  if(abs(image1(i,j)).lt.245) then
      chlo(i,j)=10**((image1(i,j)*0.012)-1.4)
      sum2=sum2+(chlo(i,j)-mean)**2
      sum3=sum3+1
      endif
      c=c+1
 189  continue
 188  continue
      chlovar=sum2/sum3
      chlosd=sqrt(chlovar)
      ratio=100*(sum1/c)
      write(*,*)'partial counter=',sum1
      write(*,*)'total   counter=',c
      write(*,*)'THE MEAN CONCENTRATION OF CHLOROPHYLL IS=',mean
      write(*,*)'THE STANDARD DEVIATION OF CHLOROPHYLL IS=',chlosd
      write(*,*)'THE RATIO BETWEEN PARTIAL/TOTAL COUNTER IS=',ratio
      write(1,*)'partial counter=',sum1
      write(1,*)'total   counter=',c
      write(1,*)'THE MEAN CONCENTRATION OF CHLOROPHYLL IS=',mean
      write(1,*)'THE STANDARD DEVIATION OF CHLOROPHYLL IS=',chlosd
      write(1,*)'THE RATIO BETWEEN PARTIAL/TOTAL COUNTER IS=',ratio

 99   close(unit=12)
      close(unit=1)
      close(unit=32)
      stop
      end
```

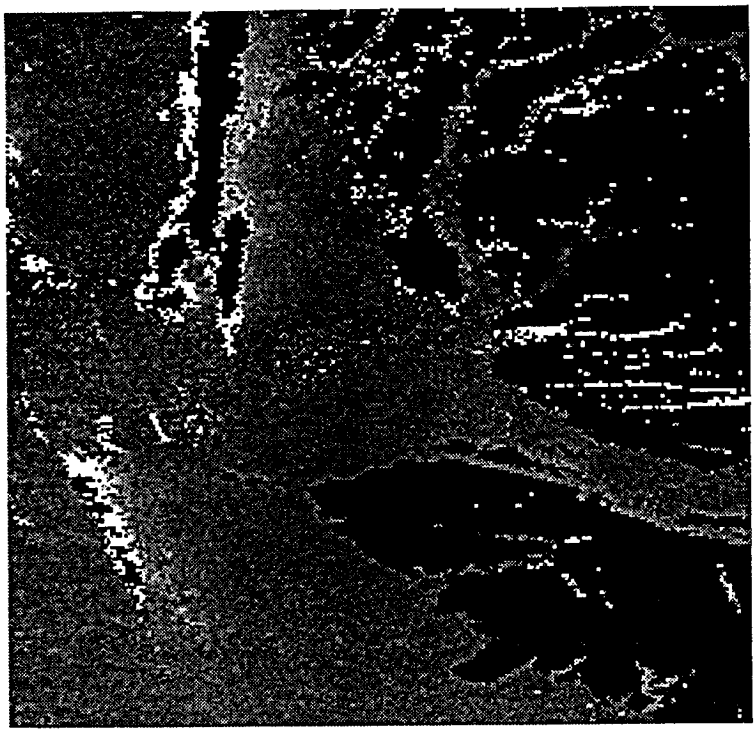

a) Clouds saturation effect.

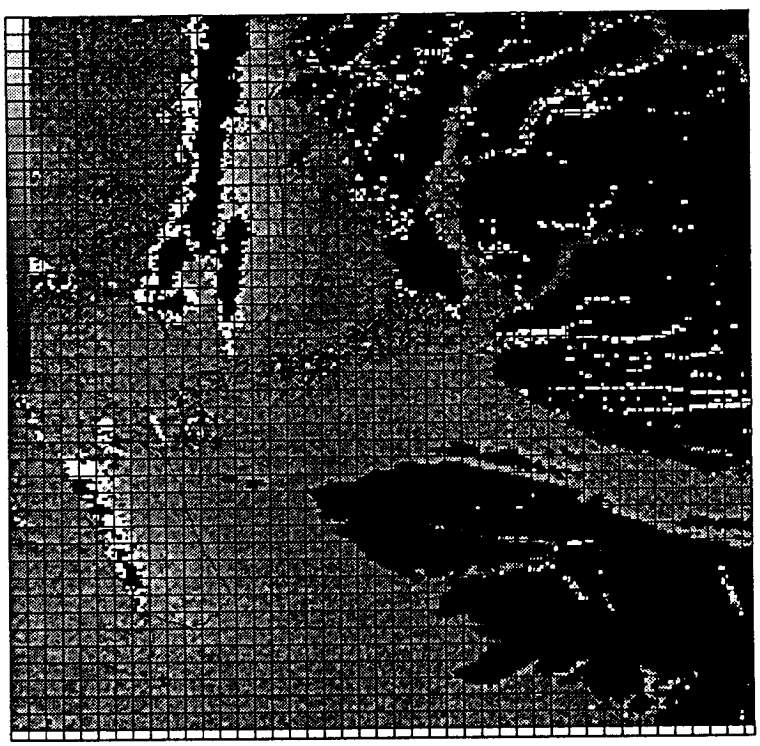

b) SHO commands example.
Map-Grid-Legend

3.5. QUEEN CHARLOTTE STRAIT.

Posted: Fri Nov 4, 1988 12:49 PM EST Msg: HGII-3803-3902
From: R.KIRK
To: wifs.tech
CC: color.group, [wifs/gsfcmail]gsfc
Subj: SeaWiFS baseline status

We are near completion of the baseline for the way we contract with EOSAT for SeaWiFS, and operate the Project in NASA. Below are the instrument performance specifications, with the modifications which came out of the SWG meeting last month (please verify), and the way we intend to get the data from the satellite. There is no provision in the Project for support of scientific LAC data collection stations at either NASA or Academia. NASA HQ will try to tap funding for them outside the Project funding line. The processing archiving and delivery baseline remains the same. That is, NASA will collect and process through Level 3 all the recorded GAC data

SeaWiFS Performance Specifications:

SeaWiFS instrument performance shall be as specified in the NASA-EOSAT Joint Working Group Report of August 1987, except as modified herein.

Spectral Bands:

Band	Spectral Range	Saturation Radiance	Min SNR (all angles)	
Vis/NIR				
1	402-422nm	11.3	424	
2	433-453	11.3	424	
3	480-500	11.3	493	
2	510-530	8.3	493	
3	555-575	5.7	350	
4	655-675	3.1	285	
5	745-785	2.2	280	Notched between 760-770
6	843-887	1.5	280	

Spatial Resolution	Approx 1 km LAC and 4 km GAC
Radiometric Accuracy	5% each band
Relative Precision	< 1%
Between Band Precision	< 1%
Polarization Sensitivity	< 2% (worst case)
Dynamic Range	10 bits quantization; gains (.8, 1, 1.25, 1.5, 2) adjustable on board
Bright Target Recovery	< 10 samples
Scan Plane Tilt	+20, 0, -20 degrees
Swath Width	> 2200 km
Location accuracy	<1 km
Equator Crossing Time	Between 10:30am and 2:30pm
Mission Life	Three years or more

4. RECENT Sea-WiFS PERFORMANCE SPECIFICATIONS.
(Courtesy, Mark Abbott)